Copyright Warning & Restrictions

The copyright law of the United States (Title 17, United States Code) governs the making of photocopies or other reproductions of copyrighted material.

Under certain conditions specified in the law, libraries and archives are authorized to furnish a photocopy or other reproduction. One of these specified conditions is that the photocopy or reproduction is not to be "used for any purpose other than private study, scholarship, or research." If a, user makes a request for, or later uses, a photocopy or reproduction for purposes in excess of "fair use" that user may be liable for copyright infringement,

This institution reserves the right to refuse to accept a copying order if, in its judgment, fulfillment of the order would involve violation of copyright law.

Please Note: The author retains the copyright while the New Jersey Institute of Technology reserves the right to distribute this thesis or dissertation

Printing note: If you do not wish to print this page, then select "Pages from: first page # to: last page #" on the print dialog screen

ABSTRACT

DESALINATION OF BRINE AND PRODUCED WATER BY MEMBRANE DISTILLATION AT LOWER AS WELL AS HIGHER TEMPERATURES AND PRESSURES

by
Dhananjay Singh

Direct contact membrane distillation (DCMD)-based desalination process is a thermally-driven separation process where a hydrophobic microporous membrane separates a hot brine feed and a cold distillate which condenses the water vapor from the hot brine passing through the membrane pores. So far, DCMD has been explored for hot brines and other aqueous solutions below 100^{o}C. For feed solutions above 100^{o}C, DCMD has an extra advantage over other conventional separation processes like reverse osmosis (RO) which requires cooling of the feed solution costing additional energy; further, RO can not utilize the heat available in the feed solution. Produced water obtained from steam assisted gravity drainage (SAGD) process is one such example where DCMD can potentially be a very useful process. In this dissertation, the DCMD technique is explored in the range of 80-130^{o}C for brine solutions containing 10000 ppm sodium chloride with porous flat sheet polytetrafluoroethylene (PTFE) membranes. The pressure of solution went up to 2-3 atm. The performance of this membrane has also been explored with a saline feed containing 3000 ppm NaCl, 45 ppm phenol, 45 ppm cresol and 10 ppm naphthenic acid, simulating the composition of hot produced water obtained from the SAGD process. There was no leakage of salt under any conditions. The highest water vapor flux achieved was 195 L/m^2-hr, which is a few times larger than that for seawater RO process. The water generated by the DCMD process may be used for steam

generation in the SAGD process. Different types of hollow fiber modules were fabricated and explored with 1% NaCl solution and produced water at lower as well as higher temperatures.

Desalination by air gap membrane distillation (AGMD) combines in one device the processes of evaporation of water from hot brine through a porous hydrophobic membrane, condensation of the water vapor so generated on a cold condenser surface and recovery of heat in the condenser cooling liquid which may be the cold/cooled brine. Existing devices for AGMD are bulky due to the condenser arrangements adopted, even though evaporation from brine may be carried out with porous hydrophobic hollow fibers. In this research a two-hollow fiber-set based compact device was developed where all such functions are combined in a compact device. The first fiber set consists of porous hydrophobic hollow fibers of either polypropylene (PP) or polyvinylidene fluoride (PVDF). The second set of hollow fibers is of solid PP through the bore of each such hollow fiber the cooling liquid is passed and on the outside surface of which water vapor condensation takes place. A number of modules having different packing densities of hollow fibers have been studied for desalination of brine containing 1% NaCl. The performance of such modules have been investigated for a range of feed brine temperatures as well as the flow rates of the two liquid streams, hot brine and the cooling liquid. Enhanced water vapor productivity was achieved in small laboratory devices suggesting potential for scale up.

DESALINATION OF BRINE AND PRODUCED WATER BY MEMBRANE DISTILLATION AT LOWER AS WELL AS HIGHER TEMPERATURES AND PRESSURES

by
Dhananjay Singh

A Dissertation
Submitted to the Faculty of
New Jersey Institute of Technology
in Partial Fulfillment of the Requirements for the Degree of
Doctor of Philosophy in Chemical Engineering

Otto H. York Department of
Chemical, Biological and Pharmaceutical Engineering

May 2012

.

APPROVAL PAGE

DESALINATION OF BRINE AND PRODUCED WATER BY MEMBRANE DISTILLATION AT LOWER AS WELL AS HIGHER TEMPERATURES AND PRESSURES

Dhananjay Singh

Dr. Kamalesh K. Sirkar, Dissertation Advisor Date
Distinguished Professor of Chemical, Biological & Pharmaceutical Engineering, NJIT

Dr. Zafar Iqbal, Committee Member Date
Research Professor of Chemistry and Environmental Science, NJIT

Dr. Boris Khusid, Committee Member Date
Professor of Chemical, Biological & Pharmaceutical Engineering, NJIT

Dr. Somenath Mitra, Committee Member Date
Distinguished Professor of Chemistry and Environmental Science, NJIT

Dr. Xianqin Wang, Committee Member Date
Assistant Professor of Chemical, Biological & Pharmaceutical Engineering, NJIT

BIOGRAPHICAL SKETCH

Author: Dhananjay Singh

Degree: Doctor of Philosophy

Date: May 2012

Undergraduate and Graduate Education:

- Doctor of Philosophy in Chemical Engineering,
  New Jersey Institute of Technology, Newark, NJ, 2012

- Master of Science in Material Science,
  Indian Institute of Technology, Kanpur, (IIT Kanpur), India, 2007

- Bachelor of Science in Chemical Engineering,
  Institute of Technology, BHU, (IT- BHU), Varanasi, India, 1998

Major: Chemical Engineering

Presentations and Publications:

D. Singh, K.K. Sirkar, Desalination of brine and produced water by direct contact membrane distillation at high temperatures and pressures, J. Membr. Sci. 389 (2012) 380-388.

D. Singh, K.K.Sirkar, High temperature and high pressure DCMD based desalination, AIChE Annual Meeting, Minneapolis, USA, 2011.

K. K. Sirkar, D. Singh, Direct contact membrane distillation-based desalination: membranes, modules, scaling, cascades, operating conditions, International Workshop on Membrane Distillation and Related Technologies, Ravello, Italy, 2011.

D. Singh, K. K. Sirkar, Desalination of brine and produced water by direct contact membrane distillation at lower as well as higher temperatures and pressures, NAMS Annual Meeting, New Orleans, LA, June 9-13, 2012 (accepted).

K. N. Rai, D. Singh, Impact resistance behavior of polymer nanocomposite transparent panel, J. Comp. Mat. 43 (2009) 139-151.

D. Singh, T. Jayasimha, K. N. Rai, A. Kumar, Preparation and characterization of polymer nanocomposite using PMMA, styrene and nanoalumina, J. Nanosci. & Nanotech. 8 (2008) 1-12.

D. Singh, R. Kumar, A. Kumar, K. N. Rai, Synthesis and characterization of rice husk silica, silica-carbon composite and H_3PO_4 Activated Silica, Cerâmica 54 (2008) 203-212.

D. Singh, T. Jayasimha, K. N. Rai, A. Kumar, Preparation of PMMA nanocomposite with superior impact strength, J. App. Poly. Sci. 105 (2007) 3183-3194.

D. Singh, T. Jayasimha, K. N. Rai, A. Kumar, Synthesis and characterization of nanoalumina-styrene acrylonitrile high impact composite as a plausible civilian armour material, J. Comp. Mat. 41 (2007) 2785-2805.

D. Singh, A. Kumar, K. N. Rai, Nanosil strengthening of PMMA composite panels, J. Thermo. Comp. Mat. (doi 0892705711412648).

D. Singh, S. Dalvi, R. N. Dave, Precipitation of ultra-fine particles of fenofibrate with controlled size distribution by RESOLV: rapid expansion Vs stabilizer concentrations, presented in session "03A06 Particle formation in supercritical fluids for food and pharmaceuticals" of 2008 AIChE annual meeting.

D. Singh, T. Jayasimha, K. N. Rai, A. Kumar, Preparation and characterization of polymer nanocomposite using PMMA, styrene and nanoalumina, 3rd International Conference on Advanced Nano Material (ANM-2007), Indian Institute of Technology, Bombay (IIT Bombay).

Dhananjay Singh, Kamalesh K Sirkar, Desalination by air gap membrane distillation using a two hollow fiber set membrane module, (under preparation).

‘To my beloved mother and families’

ACKNOWLEDGMENT

I would like to express my deepest appreciation to Dr. Kamalesh K. Sirkar, who not only served as my dissertation advisor, providing valuable and countless resources, but also made my graduate study possible. I want to say a special thanks to Dr. Zafar Iqbal, Dr. Boris Khusid, Dr. Somenath Mitra and Dr. Xianqin Wang for actively participating in my committee.

I want to acknowledge Membrane Science, Engineering & Technology (MAST) Center and National Science Foundation (NSF) for financial support. I wish to thank Drs. Kay K. Bjornen, Xiaoyi Gong, Bruce Randolph, Raul J. Barriga and William Mickols from ConocoPhillips for their suggestions and financial support. I thank Clifton Ngan, Uwe Beuscher, Walter Kosar (Arkema) Zibigniew Twardowski (Hyflux-Filtech) and Rob German for providing the membranes. I am thankul to Dr. Gordana Obuskovic, Dr. Fei He, Dr. Jie Xingming and Dr. Sagar Roy for their assistance and suggestions. I want to give my special thanks to George Barnes for his valuable technical assistance during setup for my experiments. I am also grateful to many of my fellow students; John Chau, John Tang, Tripura Mulukutala, Joe Sousa, Dengue Chen, Yu Qin and Lin Li for providing workable environment in the lab. I want to thank all of my friends with whom I spend wonderful time in USA. Special thanks to Anagha Bhakay not only for her close friendship but also for her moral support during critical phase of my life without which it was impossible to achieve this milestone

Finally, deepest thanks to my family, especially my sister, for keeping me inspired and motivated.

TABLE OF CONTENTS

TABLE OF CONTENTS
(Continued)

Chapter **Page**

TABLE OF CONTENTS
(Continued)

Chapter **Page**

TABLE OF CONTENTS
(Continued)

LIST OF TABLES

LIST OF TABLES
(Continued)

LIST OF FIGURES

LIST OF FIGURES
(Continued)

LIST OF FIGURES
(Continued)

Figure **Page**

LIST OF FIGURES
(Continued)

Figure **Page**

LIST OF FIGURES
(Continued)

Figure **Page**

LIST OF FIGURES
(Continued)

Figure **Page**

LIST OF FIGURES
(Continued)

Figure **Page**

LIST OF SYMBOLS

A_t	Total permeation area (m^2)
Å	Angstrom (10^{-10} meters)
c_p	Specific heat (kJ/kg)
C	Constant (kg m^{-2} s^{-1} Pa^{-1})
D_{wa}	Diffusion coefficient of water vapor in air (m^2s^{-1})
ΔH_V	Heat of evaporation (kJ/kg)
I_o	Intercept
J_i	Gas permeation flux (mol m^{-2} Pa^{-1} S^{-1})
k_B	Boltzmann constant (1.38 x 10^{-23} Joule/K)
K_n	Knudsen number
L_p	Effective pore length (m)
M_w	Molecular weights of water vapor
M_a	Molecular weights of air
$N_{t,i}$	Gas permeation rate (mol s^{-1})
N_v	Water vapor flux (kg m^{-2} h^{-1})
P	Vapor pressure (Pa)
P_f	Feed side vapor pressure (Pa)
P_p	Permeate side vapor pressure (Pa)
$\bar{p}$	Mean pressure (Pa)

LIST OF SYMBOLS
(Continued)

Δp	Transmembrane pressure difference (Pa)
r	Mean pore radius of membrane (m)
R	Gas constant (8.3144 m^3 Pa mol^{-1} K^{-1})
S_o	Slope
T	Absolute temperature (K)
T_m	Temperature at membrane surface
ΔT_p	Temperature rise on permeate side
ΔT_f	Temperature drop on feed side
$\dot{V}_{distillate}$	Volumetric flow rate of distillate (ml/min)
$\dot{V}_{feed}$	Volumetric flow rate of feed (ml/min)
V	Water vapor mean molecular speed (m/sec)
ε	Surface porosity
μ_i	Viscosity of gas (Pa s)
$\lambda_{w\text{-}a}$	Mean free path of water vapor in air
σ_w	Collision diameter of water vapor molecules
σ_a	Collision diameter of air molecules
Σ	Collision cross-section
T	Pore tortuosity
δ_m	Thickness of the membrane

CHAPTER 1

INTRODUCTION

Membrane distillation (MD) is a non-isothermal process involving the evaporation of volatile components from the feed solution through a porous hydrophobic membrane. The existence of membrane distillation has been known since late 1960s. The first patent on membrane distillation was filed in 1963 by Bodell [1]; the first publication appeared in 1967 by Findley [2]. However, membrane distillation processes did not receive much attention from industry till early 1980s. The major barriers for its acceptance were better membrane availability, module design, pore wetting, low permeate flow rate, flux decay with time, energetic and economic cost. As can be seen from Figure 1.1, membrane processes were explored further after 1980 when better membranes and modules became available [3].

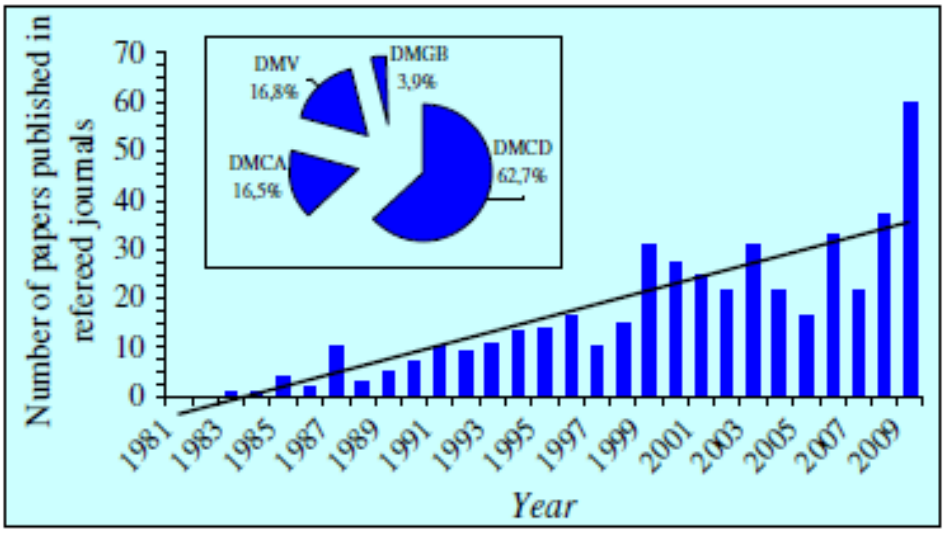

Figure 1.1 Number of papers published for membrane distillation in refereed journals per year (Taken from [3]).

In MD processes, the liquid feed to be treated is at around atmospheric pressure and in direct contact with one side of the hydrophobic membrane; the condition on the permeate side of the membrane depends upon the mode of the operation (Figure 1.2). In direct contact membrane distillation (DCMD) based desalination process [4], cold distilled water is in direct contact with the permeate side of the membrane. The driving force in DCMD for water vapor transport is the water vapor partial pressure difference across the membrane resulting from the difference in the liquid temperatures of the feed side and the permeate side. In vacuum membrane distillation (VMD) process [5], vacuum is applied on the permeate side of the membrane by a vacuum pump and water evaporation takes place due to the partial pressure difference between the saturation vapor pressure on the feed side and the applied vacuum pressure on the permeate side. The water vapor is condensed in a separate condenser. In air gap membrane distillation (AGMD) process [6], a stagnant air gap is maintained between the porous membrane and a condensation surface. In this case volatile molecules condense directly over the cold surface near the other side of the membrane. There is an additional MD technique called the sweep gas membrane distillation (SGMD) process [7]; here one can have a sweep air stream on the other side of the membrane prior to condensation of the vapor in a separate condenser. Each mode of membrane distillation process has its own advantages and disadvantages. In all cases, the feed brine temperature varies between 30-93^{o} C.

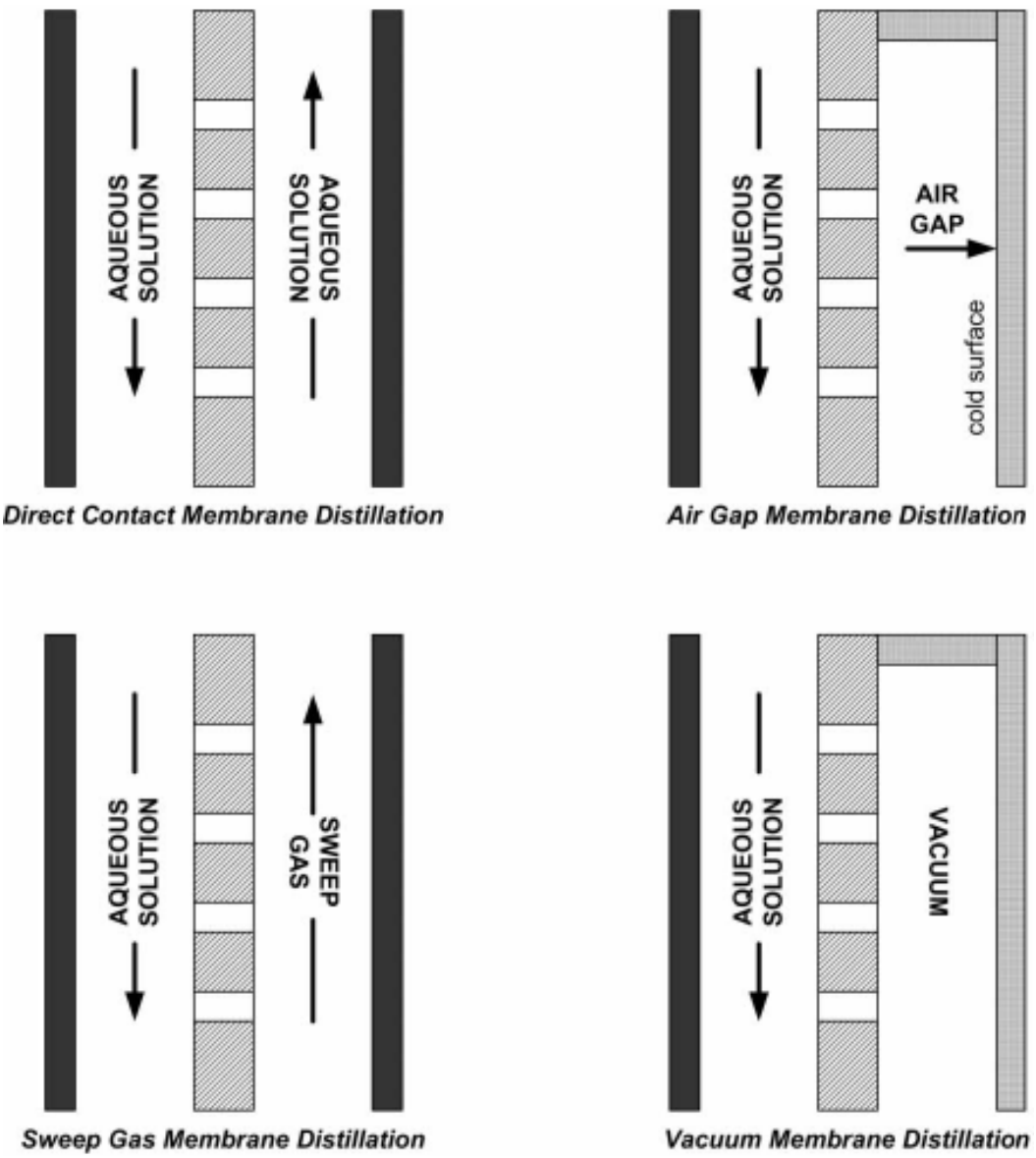

Figure 1.2 Different configurations of membrane distillation process (Taken from [8]).

The membrane should have following characteristics before use in membrane distillation process:

(i) At least one side of the membrane should be hydrophobic or one layer should be hydrophobic if membrane has multilayer. The hydrophobic nature of the membrane prevents mass transfer in liquid phase and only volatile compounds pass through the pores of the membrane and condensed/removed on the opposite side (permeate or distillate) of the system (Figure 1.3).

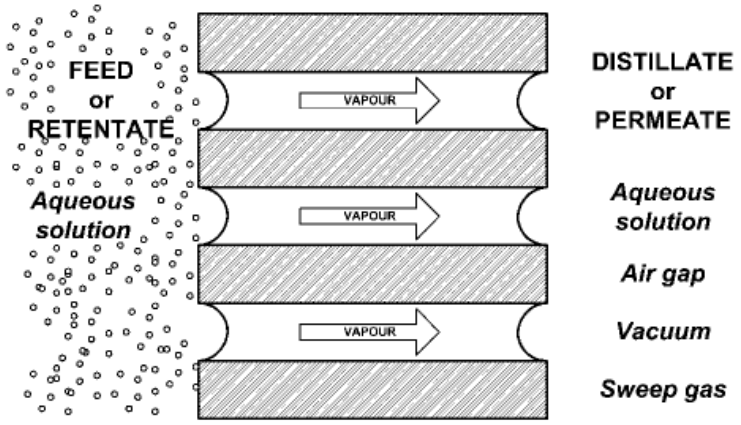

Figure 1.3 Schematic diagram of membrane distillation process (Taken from [8]).

(ii) Membrane should be porous in nature and pore size may vary from nanometers to few micrometers. The pore size distribution should be as narrow as possible.

(iii) Liquid entry pressure (LEP) which is defined as the minimum transmembrane pressure required for water or other feed solutions to enter into the pore, should be as high as possible. LEP depends on each membrane and decreases with the increase of the maximum pore size and/or the decrease of the contact angle of the feed solution.

(iv) The tortuosity factor is the measure of the deviation of the pore structure from straight cylindrical pores. It should be small and close to one, but a value of 2 is frequently assumed for theoretical prediction of transmembrane flux.

(v) The porosity which is defined as the void volume fraction open to membrane distillation vapor flux, should be as high as possible.

(vi) Heat loss through the membrane by conduction should be minimized by keeping the thermal conductivity of the membrane material as low as possible.

(vii) Although fouling in membrane distillation may not be a serious problem but still membrane surface can be modified with thin coating of fouling resistant material to avoid any possible fouling of the surface.

(viii) Membrane should be chemically resistant and should have a long life for stable membrane distillation performance.

CHAPTER 2

DESALINATION OF BRINE AND PRODUCED WATER BY DIRECT CONTACT MEMBRANE DISTILLATION

2.1 Introduction

In the MD processes, the liquid feed to be treated is at around atmospheric pressure and in direct contact with one side of the hydrophobic membrane; the condition on the permeate side of the membrane depends upon the mode of the operation. In direct contact membrane distillation (DCMD) based desalination process [4], cold distilled water is in direct contact with the permeate side of the membrane as shown in Figure 2.1. The driving force in DCMD for water vapor transport is the water vapor partial pressure difference across the membrane resulting from the difference in the liquid temperatures of the feed side and the permeate side. DCMD process has been investigated extensively by a number of groups [9-15]. First publication in area of MD was published by Findley in 1967 using DCMD configuration. Findley used various types of coated and uncoated membrane materials such as paper hot cup, gum wood, aluminum foil, glass fibers, paper plate, nylon, etc. Membranes were hydrophobized by providing a coating of Silicon and Teflon [2]. He calculated economical performance, especially at high temperatures considering high temperature, long life and low cost membrane are available. In the same year, first patent on desalination by DCMD was published by Weyl [16] and claimed an improve method and apparatus for recovery of demineralized water from saline water.

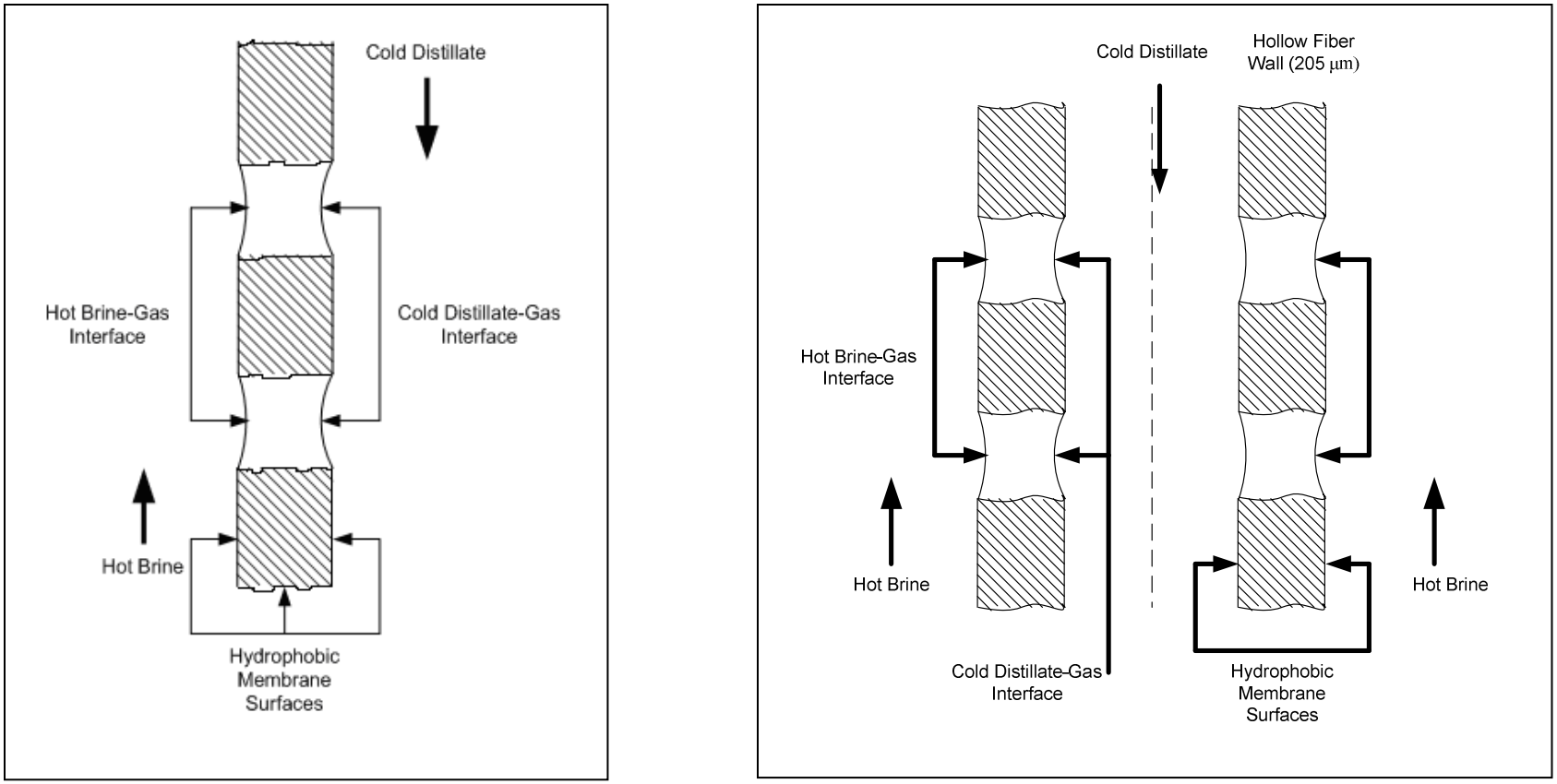

Figure 2.1 Direct Contact Membrane Distillation (DCMD) process in (a) Flat sheet membrane (b) hollow fiber membrane.

In DCMD, condensation step is carried out inside the module leading to the simplest mode of membrane distillation process. Because of its simplicity, more than 60 % of the research in membrane distillation area was focused on DCMD (Figure 2.2).

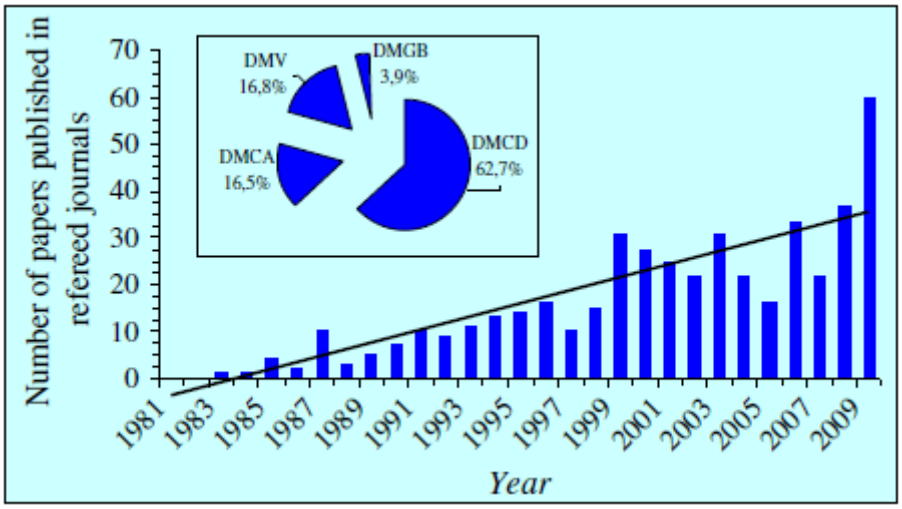

Figure 2.2 Research activity taken place in different MD configurations (Taken from [3]).

In DCMD process, mass transfer inefficiency due to air entrapped within the membrane pores and heat transfer inefficiency due to heat loss by conduction is high compared to the other MD configurations. Most of the investigations on DCMD were focused on the theoretical models and experimental studies dealing with operating conditions. Very few authors have paid attention towards new membrane development and new membrane module design. Membrane development is a key for commercialization of DCMD process. Membrane used in DCMD can be a single hydrophobic layer, a composite bilayer of hydrophobic/hydrophobic, a composite bilayer hydrophobic/hydrophilic membrane or a composite trilayer hydrophilic/hydrophobic/hydrophilic or hydrophobic/hydrophilic/hydrophobic porous membranes. In DCMD process, membranes act only as a barrier to hold the liquid-vapor

interface at the entrance of the membrane pores and is not involved in the transport phenomenon [11]. The separation performance is predominantly determined by the vapor-liquid equilibrium (VLE) principle and membrane is not necessary to be selective as required in other membrane processes [17]. It was also studied to see the effect of membrane and the properties of polymers used for preparation of fine porous hollow-fiber membrane on the DCMD selectivity [18, 19].

Various studies were done on development of single hydrophobic flat sheet membranes. Asymmetric PVDF flat sheet membranes were fabricated by phase inversion technique from different concentration of PVDF polymer in dimethyl acetamide (DMAc) or in dimethyl formamide (DMF) [20]. This membrane was tested in DCMD and permeate flux was lower than those of the commercial membranes. Another PVDF flat sheet membrane was prepared by using DMAC or DMF solvent and LiCl additive [21]. It was observed that DCMD flux increased with increase of LiCl concentration from 0 to 3 wt.%

A number of studies were carried out to develop copolymer flat sheet membranes for DCMD using the phase inversion technique. Copolymer PVDF-TFE membranes have been developed using phase inversion technique [22, 23]. These membranes prepared with the addition of LiCl in the casting solution exhibited better mechanical strength, higher hydrophobicity and lower DCMD fluxes than PVDF membrane. Low fluxes were consequence of its smaller pore size and lower porosity than PVDF membranes. When LiCl was replaced with lithium perchlorate trihydrate $LiClO_4.3H_2O$/trimethyl phosphate (TMP) as pore forming additive, the properties of the PVDF-TFE membranes such as pore size, porosity and DCMD fluxes were higher than those prepared with LiCl.

Another asymmetric flat sheet membrane was developed by the phase inversion technique using the copolymer PVDF-HFP [24]. The membrane prepared under the following conditions; 19.1 wt.% PVDF-HFP, 4.99 wt. % PEG, 35^{o} C coagulation temperature and 102 second solvent evaporation time, showed the highest salt rejection of 99.95 % with a permeate flux of 4.41 L/h m^2.

The first composite membranes for membrane distillation were developed by Cheng [25]. During last few years, many groups came up with new hydrophilic/hydrophobic type membrane and successfully tested it for DCMD. Partially hydrophilic dense fluoro-carbon composite membrane was successfully tested for DCMD [26]. The fluxes were of magnitude similar to those achieved in porous hydrophobic membrane but it was found that thermal efficiency for this membrane was superior to those of silicone membrane. Tri-layer membrane was prepared with a hydrophilic layer sandwiched between two hydrophobic layers and tested in DCMD with 0.3-0.5 M NaCl feed aqueous solutions [27]. Recently, porous composite hydrophobic/hydrophilic flat sheet membranes for DCMD were prepared by phase inversion method using fluorinated surface modifying macromolecules (SMMs) [28]. Hydrophobic side of the membrane was brought into contact with hot feed solution, while hydrophilic layer of the membrane was brought in contact with cold water. Water penetrates into the pores of the hydrophilic layer. The composite membranes have a low conductive heat loss through the membrane attributed to thicker hydrophilic layer. Apart from this low resistance to mass flux makes these membranes as very promising for desalination by DCMD. The SMMs used in these membranes were oligomeric fluoropolymers synthesized by polyurethane chemistry and tailored with fluorinated end-groups.

Hollow fiber membrane were also developed and explored for DCMD by various research groups. Porous hollow fiber membranes from PVDF in dimethyl sulfoxide (DMSO) were developed by dry/wet spinning technique [18]. The pore sizes of fibers were smaller than those of microfiltration membranes. It was reported that the water vapor flux and ethanol flux with those fibers were of 0.239-0.64 kg/m^{2}h and 0.878-2.314 kg/m^2 h respectively. Hollow fiber membranes of polypropylene (PP) and polyethylene (PE) were prepared using melt-extruded/cold-stretching method for DCMD application [29]. Because of larger pore size of the PE membranes, higher water vapor fluxes have been observed in PE hollow fiber membrane. Another type of PVDF hollow fiber membrane for DCMD was prepared using NMP solvent and ethylene glycol as a non-solvent additive by dry/jet wet spinning method. Those fibers exhibited very narrow pore size distribution. A water vapor flux of 41.5 kg/m^{2}h in DCMD was achieved as for 3.5 wt % aqueous salt solution at a temperature of 79.3^o C.

Co-extrusion method was used for fabrication of macrovoid-free PVDF hollow fiber membranes of high porosities [30]. Compared to other fibers developed by standard dry/wet spinning technique, the co-extruded hollow fiber membranes exhibited higher DCMD performance. Water vapor flux as high as 67 kg/m^{2}h was reported in DCMD for 3.5 wt. % NaCl solution with a very high salt rejection (> 99.9%). Mixed matrix PVDF/Cloisite clay hollow fiber membranes have been fabricated by the same group [31]. It was claimed that the clay particles in PVDF matrix not only enhanced the mechanical strength of the fibers but also improved their long-term stability. When these fibers were tested with 3.5 wt. % NaCl aqueous solution in DCMD, water vapor fluxes as high as 79.2 kg/m^2 h were achieved with 100 % salt rejection.

Porous hydrophobic hollow fiber membranes for DCMD using copolymer PVDF-HFP were fabricated by dry/wet spinning technique [32]. They used DMAc as a solvent and PEG as a non-solvent additive. The morphological properties of the PVDF-HFP hollow fiber membranes vis-à-vis copolymer concentration were studied by AFM; from Figure 2.3 it is clear that at high PVDF-HFP concentrations, the hollow fiber membranes exhibit a single sponge like structure, whereas at low copolymer concentrations the cross section of the hollow fiber membranes shows different layers of finger like structure.

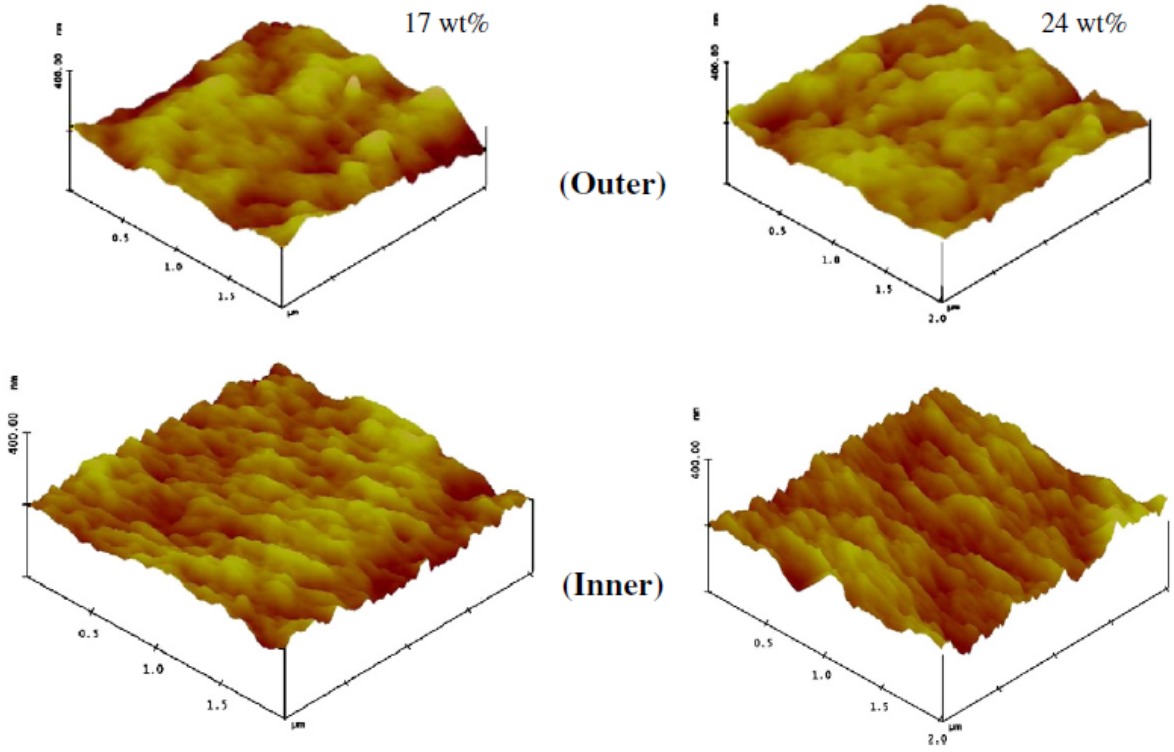

Figure 2.3 AFM images of the internal and external surfaces of PVDF-HFP hollow fiber membranes with different copolymer concentrations (Taken from [11]).

In DCMD experiments, two types of membrane configurations have been popularly tested so far: (i) flat sheet membrane (ii) hollow fiber membranes. Flat sheet membranes were explored either in Lewis test cells or plate -and-frame modules working

under tangential flows [33-35]. The main advantages with these cells are that the membranes can be easily replaced, changed or cleaned. But membranes in plate-and-frame module require support to hold the membrane, which cause a drop in temperature on membrane surface resulting into reduction of temperature or vapor pressure driving force across the membrane. On the other hand, hollow fiber membranes do not require any support but are an integral part of the module and can not be replaced or cleaned easily like flat sheet membranes. In case of hollow fiber membrane modules, if the pores are wetted by the liquid solutions, module becomes useless and can not be used further for the experiments. From commercial point of view tubular membrane modules as in hollow fibers are more attractive because in tubular membrane modules, much higher surface area to module volume can be achieved compared to plate and frame modules.

A new type of membrane module was assembled having the hollow fibers in plate-and-frame module in cross-flow mode for VMD/DCMD applications to reduce the temperature polarization effect by increasing the heat transfer coefficients [5, 12-14]. Later these modules were used to investigate scaling in DCMD process [36-38]. The fluid entrance on the shell side to the rectangular module had a well-designed diverging section; the exit similarly had a converging section. These allowed the fluid to flow uniformly in cross flow outside of and perpendicular to the fibers in the modules. The diverging section and the converging section were two boxes having a curved shape. Two face plates, with a wide size distribution of open holes, were made from two flat plastic sheets. The design mentioned above ensured a uniform flow of the feed solution through the shell side of the fibers. The material used for the face boxes and face plates was clear cast acrylic plastic having a reasonable thickness and heat transfer resistance. Two face

boxes and face plates were assembled with a rectangular membrane module channel to constitute the complete device (Figure 2.4).

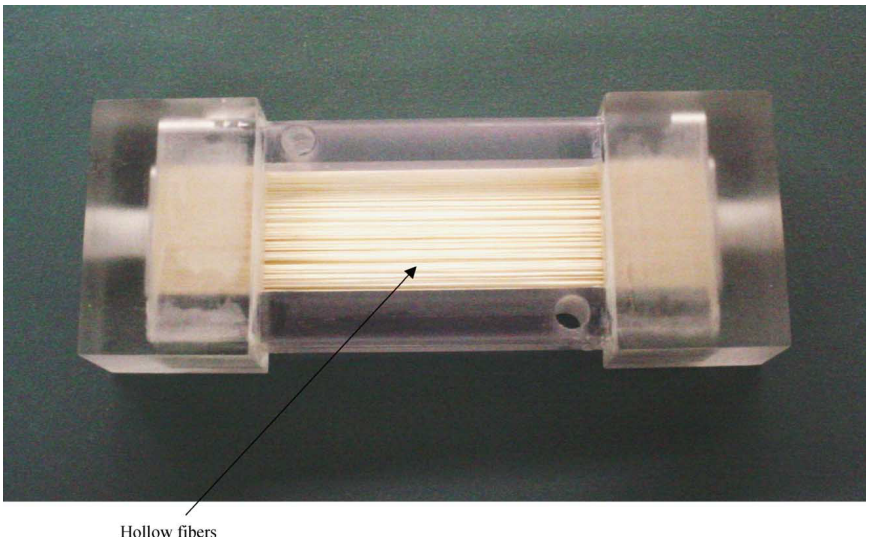

(a)

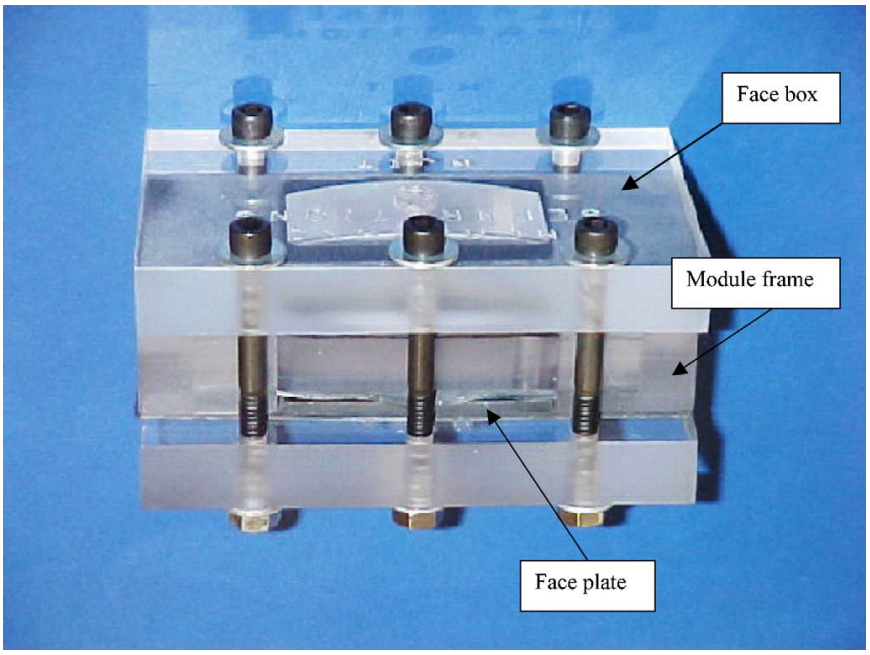

(b)

Figure 2.4 Phtographs showing (a) rectangular cross flow test module without face plates (b) rectangular cross flow test module with face boxes, face plates and assembly (Taken from [5]).

The DCMD process is currently confined to laboratory scale but recently some pilot plant studies have been done [14, 39, 40]. A small pilot plant was employed for DCMD (Figure 2.5) based desalination; it was run for 3 months [14]. The operations employed hot brine at the temperature of 64-93^{o}C and distillate at 20-54^{o}C. The hot brine was either, city water containing salt at the level of 3.5, 6 or 10% or seawater trucked in from Long Island Sound, CT.

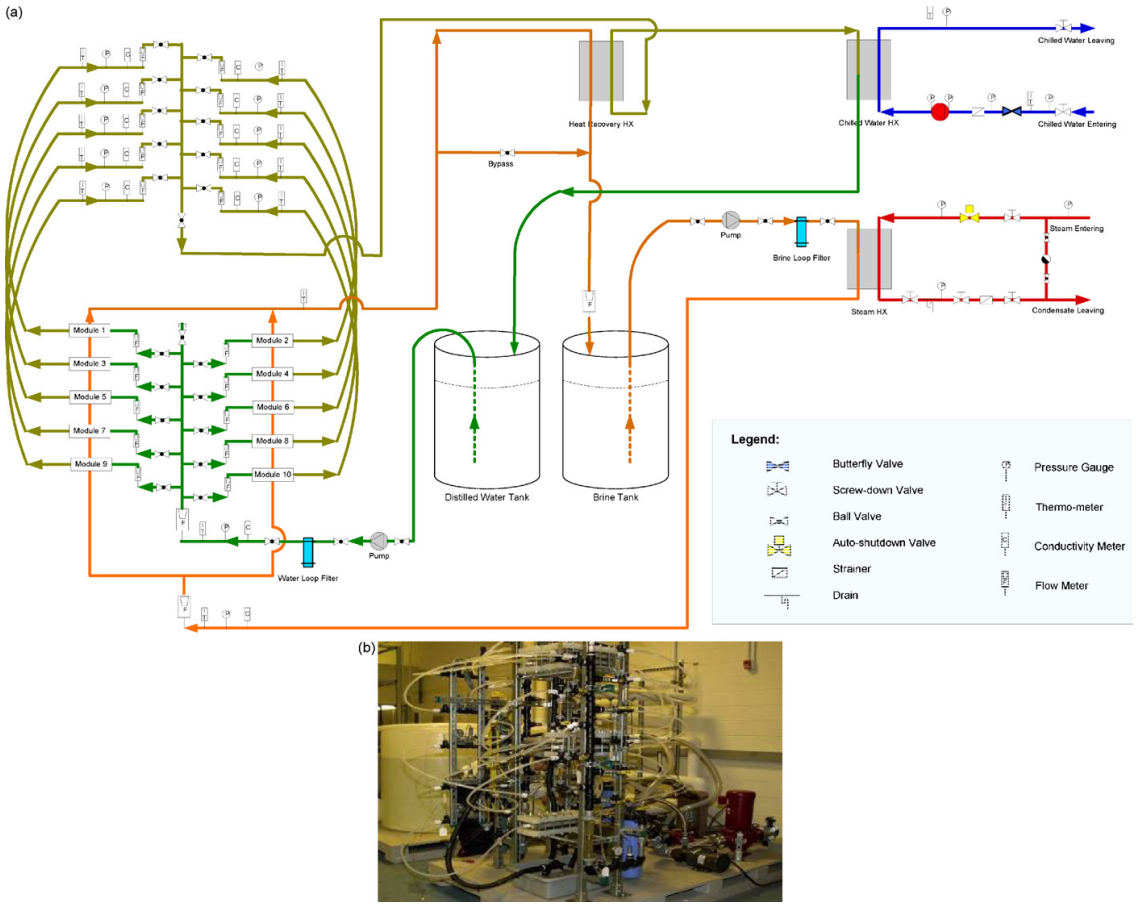

Figure 2.5 (a) Schematic of DCMD pilot plant (b) Photograph of part of pilot plant (Taken from [14]).

2.2 Transport Models

Mass transfer mechanism in DCMD process depends on the value of Knudsen number which is defined as the ratio of the mean free path (λ) of the gas molecule to the pore diameter (d) of the membrane i.e. $K_n = \lambda/d$. The mean free path of water vapor molecule in air medium is evaluated as follows [41, 42]:

$$\lambda_{w-a} = \frac{k_B T_m}{\pi \left(\frac{(\sigma_w + \sigma_a)}{2} \right)^2 P_T \sqrt{1 + \frac{M_w}{M_a}}} \tag{2.1}$$

Here T_m is the average membrane temperature; k_B is the Boltzmann constant (1.38 x 10^{-23} Joule/K); P_T is the total pressure, σ_w and σ_a represent the collision diameters of water vapor molecules and air molecules and their values are 2.64 x 10^{-10} m and 3.711 x 10^{-10} m respectively [43, 44]; M_w and M_a are respectively, the molecular weights of water vapor and air. In general, mean free path increases with an increase in temperature and a decrease in pressure. But for higher temperature and higher pressure DCMD experiments, both parameters will affect the mean free path in opposite direction and accordingly the value of Knudsen number will also vary.

According to the Schofield model [9], if the mean free path is greater than the pore diameter i.e., Knudsen number (K_n) > 1, the transport mode of water vapor through the pores of the membrane is dominated by Knudsen diffusion and water vapor flux through the membrane is given by

$$N_k = 1.064 \frac{r\varepsilon}{\tau\delta_m}\left(\frac{M_w}{RT}\right)^{0.5}\left(P_1 - P_0\right) \tag{2.2}$$

Here N_k is the mass flux in kg/m^2-sec, r is the pore radius of the membrane, ε is the porosity of the membrane, τ is the pore tortuosity, M_w is molecular weight of the water vapor, R is gas constant, T is average temperature at membrane surface, δ_m is the thickness of the membrane and P_1 and P_o are the water vapor pressures on the feed side and distillate side, respectively.

If the mean free path is less than the pore diameter of the membrane i.e., Knudsen number (K_n) < 1, the transport mechanism for water vapor through the pores of the membrane will be dominated by the Poiseuille flow model and water vapor flux N_P (kg/m^2-sec) is given by the following expression in terms of mass flux:

$$N_P = 0.125 \frac{r^2 \varepsilon M_w P_m}{\tau\delta_m \eta RT}\left(P_1 - P_0\right) \tag{2.3}$$

The water vapor pressure across the membrane can be evaluated by Antoine equation:

$$P = \exp\left(23.238 - \frac{3841}{T_m - 45}\right) \tag{2.4}$$

Here T_m is the average temperature of the membrane.

In equations (2.2) and (2.3), the tortuosity factor was introduced to take into the account the fact that gas molecules through the membrane travel a distance longer than

the thickness of the membrane; it is defined as the ratio of actual pore length to the thickness of the membrane. In membrane distillation studies, tortuosity factor is frequently assumed to be 2.0 to predict the water vapor flux [9]. Mackie and Meares [45] developed an empirical correlation to measure the tortuosity for membrane systems and it is given as follows:

$$\frac{\tau}{\varepsilon} = \frac{\left(2-\varepsilon\right)^2}{\varepsilon^2} \tag{2.5}$$

Another correlation for tortuosity factor of polymer structures of random cluster was predicted by fractal theory of random walks [46] and is given by

$$\tau = \frac{1}{\varepsilon} \tag{2.6}$$

Iversen et al. [47] have found the experimental tortuosity values for some of the membranes were similar to the values obtained from correlation (2.5) and some of them for example, Goretex membranes were very close to the tourtuosity values calculated from correlation (2.6).

There are several models for the transport in transition region between Knudsen and viscous flows. Schofield's proposed a general water vapor flux equation combining Knudsen diffusion, viscous flows and ordinary diffusion [48] which is given by

$$N = -\left(\frac{1}{a(1-b) + ab\left(P_{avg} / P_{ref}\right)} + \frac{P_{aM} RT\delta}{K_1 D_{wa} P_T M} \right)^{-1} \Delta P_w \tag{2.7}$$

Where ΔP_w is the water vapor pressure difference across the membrane, P_{aM} the logarithmic mean pressure of air, P_T the total pressure. D_{wa} is the ordinary diffusion coefficient which is replaced by an effective diffusion coefficient $K_1 D_{wa}$, where K_1 is a constant depending on membrane geometry. Assuming cylindrical and non-interconnected pores, K_1 is calculated as follows [49]

$$K_1 = \frac{\varepsilon}{\tau} \tag{2.8}$$

The constants a and b in equation 2.7, are related to another constants A and B as follows

$$A = \frac{a\delta}{Mv}(1-b) \tag{2.9}$$

$$B = \frac{ab\delta k_B T}{\sqrt{2}\sigma\ MvP_{ref}} \tag{2.10}$$

Where δ is the membrane thickness, M the molar mass of water vapor, k_B the Boltzmann constant, T the thermodynamic temperature, σ is the collision cross-section and v is the water vapor mean molecular speed given by

$$v = \sqrt{\frac{8RT}{\pi M}} \tag{2.11}$$

Assuming cylindrical pores of radius r in a porous membrane, the constants A and B from kinetic theory are given by

$$A = \frac{2r\varepsilon}{3\tau RT} \tag{2.12}$$

$$B = \frac{\pi r^2 \varepsilon}{32\tau RT} \tag{2.13}$$

The diffusion coefficient for water vapor in air can be described by [50]

$$D_{wa} = k_1 T^{k_2} \frac{P_o}{P} \tag{2.14}$$

Where D_{wa} is the diffusion coefficient at absolute temperature T and pressure P and P_o is one normal atmosphere. The value of k_1 and k_2 for water vapor are 0.187 x 10^{-9} m^2 sec^{-1} and 1.724 respectively [51].

2.3 Experimental

2.3.1. Materials and Chemicals

The following materials and chemicals were used: Sodium chloride (Sigma Aldrich), Phenol (Sigma Aldrich), Cresol (Sigma Aldrich), o-Phosphoric Acid (HPLC grade from Fischer Scientific), Methanol (HPLC grade from Fischer Scientific), Naphthenic Acid (Sigma Aldrich) and N-methyl-N-(tert.-butyldimethylsilyl) trifluoroacetamide which contains 1% t-BDMS-chloride (MTBSTFA, Regis, Morton Grove, IL), chloroform (Sigma Aldrich), dichloromethane (Fischer Scientific) and hydrochloric acid (Fischer Scientific).

2.3.2 Membranes Explored

Membranes of different materials and in various shapes were explored in DCMD as well as in AGMD experiments. Ceramic disk and tubules were procured from outside; they were hydrophobized for DCMD experiments. Hydrophobic polymeric membranes available either in flat sheet or hollow fiber, were obtained from various corporations for the experiments. Flat sheet membranes at lower temperatures were explored in a small stainless steel test cell having an effective area of 9 cm^2 (Figure 2.6 (a)). All higher temperature experiments with flat sheet membrane were performed in a large cell (Figure 2.6(b)) having 6 mm thick porous stainless steel disc to support the PTFE membrane. This large cell was originally used as a pervaporation cell (model PTC-6, Carbone Lorraine, Salem, VA) and obtained from GFT (Neunkirchen-Heinitz, Germany). Hollow fibers were potted in a stainless steel/PFA tubing with an appropriate epoxy. The details of membranes explored in the experiments are given in Table 2.1.

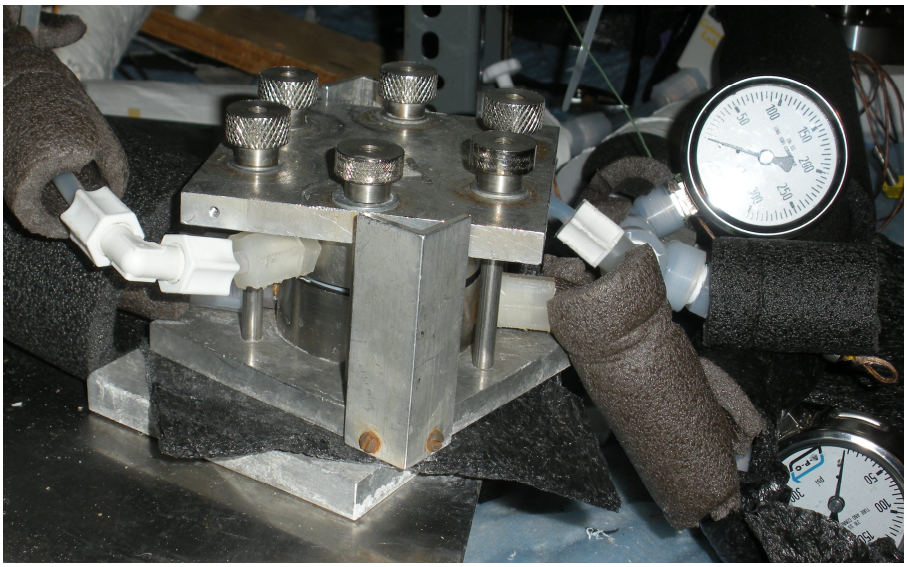

(a)

(b)

Figure 2.6 Photographs showing (a) small stainless steel test cell, (b) two small stainless steel test cells in series.

Table 2.1 Details of Membranes Explored in the Experiments

Membrane	Form	Pore Size	Porosity	Thickness
Ceramic (alumina 86%,SiO2 10%)	Disc	1.0 μm	0.4-0.5	10 mm, support included
Ceramic	Tubule	50 Å	0.4-0.5	1150 μm
PTFE	Flat Sheet	0.03 μm	0.65	24 μm
PVDF	Flat Sheet	0.1 μm	0.75	125 μm
PMP	Hollow Fiber	4.3-5 Å Dense skin	0.30	40 μm
PVDF 'H'	Hollow Fiber	0.62 μm	0.50	350 μm
PVDF 'E'	Hollow Fiber	0.2 μm	0.54	117
PTFE M	Hollow Fiber	0.24 μm	0.50	205 μm (I.D.=1.53 mm)
PTFE N	Hollow Fiber	0.27 μm	0.47	205 μm (I.D.=1.51 mm)
PTFE P	Hollow Fiber	-	-	275 μm (I.D.=0.53 mm)
PEEK	Hollow Fiber	-	-	80 μm (I.D.=0.29 mm)

2.3.3 Fabrication of Hollow Fiber Membrane Modules

Most of the modules fabricated at NJIT were built either in a stainless steel hose or in a polytetrafluroethylene (PTFE) tubing acting as a shell. Both ends of the tubing were fitted with male run tees. The size of male run tees was 1/4" or 1/2", depending upon the number of fibers and the diameter of shell. The length of the fibers was kept at least 2-3 cm longer than required.

Hollow fibers were potted in a stainless steel/PFA tubing using an appropriate epoxy depending upon the material of fiber. Before potting the fibers, inside of the fittings were made rough for better adhesion. For making modules with PP, PVDF and PMP, the fibers were potted first with medical grade adhesive M-21HP (Henkel Loctite Corporation, Rocky Hill, CT) due to its viscous nature. After curing for 12 hours, another epoxy mixture was made with C4 resin and D activator (Beacon Chemicals, Mt. Vernon, NY) in the weight ratio of 4/1. This epoxy mixture was applied to one end of the module and the module was clamped in a rotating spinneret to make sure that epoxy entered into blank space between the fibers. Once it was cured for 2 days, same potting procedure was followed at the other end of the module.

Potting of PTFE hollow fibers in stainless steel/PFA tubing was very difficult with C4 resin and D activator because of poor adhesive property of PTFE surface. Initially, few modules were fabricated using urethane based adhesive (Loctite U-09LV, Henkel Loctite Corporation, Rocky Hill, CT) according to same procedure adopted for the PVDF fibers. Later, modules were fabricated with cynoacrylate adhesive (Loctite 4205, Henkel Loctite Corporation, Rocky Hill, CT) for higher temperature DCMD experiments.

Surfaces of PMP hollow fibers were treated using chromic acid solution and then it was potted in stainless steel tubing in exactly the same fashion followed for PVDF hollow fiber's potting. Figure 2.7 shows the photograph of a hollow fiber membrane module in stainless steel tubing.

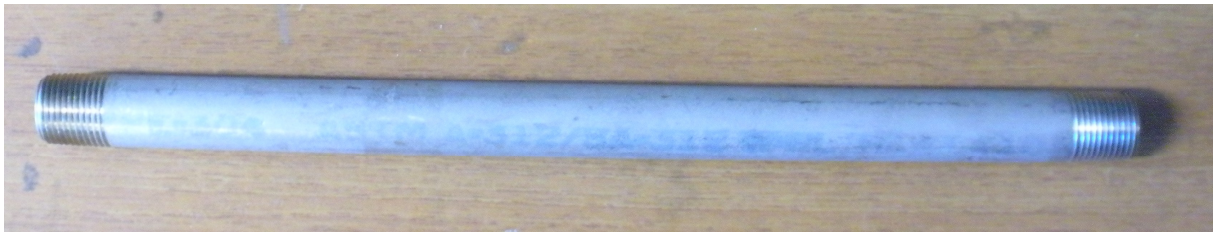

(a)

(b)

(c)

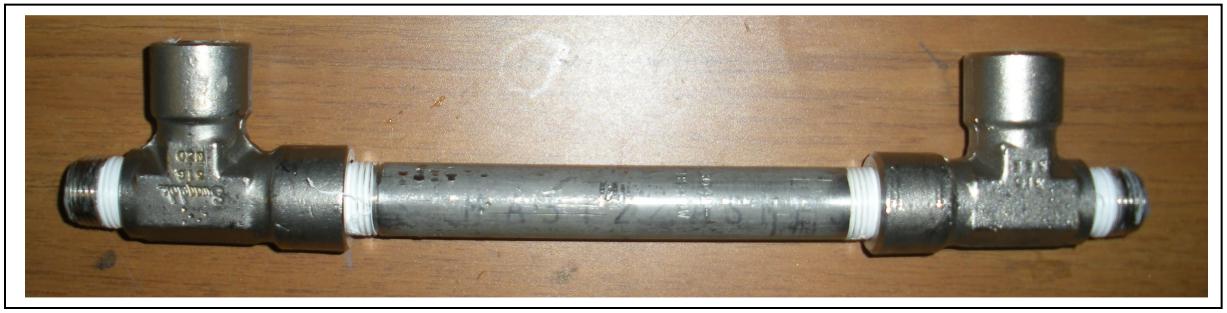

(d)

Figure 2.7 Photographs showing (a) stainless steel tube used as shell side of module, (b) fittings used for fabrication of module, (c) photo of potted fibers, (d) stainless steel module.

2.3.4 Characterization of Membranes by Gas Permeation Test

Gas permeation test was performed to measure the mean pore size and effective surface porosity over the effective pore length of the porous membrane. A gas permeation method was suggested to determine the volumetric porosity of porous membranes [52]. Later, a modified gas permeation method was introduced to measure the mean pore size and the effective surface porosity over the effective pore length of an asymmetric membrane [53, 54]. The total molar gas permeation flux (J_i) through a porous membrane is described by equation (2.15) where the first term represents the contribution from Knudsen flow and the second term is due to Poiseuille flow:

$$J_i = \frac{2}{3}\left(\frac{8RT}{\pi M}\right)^{0.5} \frac{1}{RT}\frac{r\varepsilon}{L_p} + \frac{\bar{p}}{8\mu_i RT}\frac{r^2\varepsilon}{L_p} \tag{2.15}$$

Here ε is surface porosity, r is mean pore radius of the membrane, μ_i is gas viscosity, R is gas constant, $\bar{p}$ is the mean pressure (average of feed and permeate side pressure), M is molecular weight of gas, L_p is effective pore length and T is temperature (K).

The gas permeation flux, J_i, is calculated as follows

$$J_i = \frac{N_{t,i}}{A_t \Delta p} \tag{2.16}$$

Here $N_{t,i}$ is total molar gas permeation rate (mol/sec), Δp is the transmembrane pressure difference across the membrane area A_t. The experimental setup to determine nitrogen flux through the PTFE flat sheet membrane is shown in Figure 2.8. The total gas permeation rate through the membrane at different pressures was measured using a soap bubble flow meter for low flow rates of nitrogen and by another flow meter (Hewlett Packard) for high flow rates. From a plot of the nitrogen flux J_i against the mean gas pressure $\bar{p}$, the mean pore size (r) and the effective surface porosity over pore length, ε/L_p, can be obtained from the slope S_o and the intercept I_o as follows:

$$r = \frac{16}{3}\left(\frac{S_o}{I_o}\right)\left(\frac{8RT}{\pi M}\right)^{0.5}\mu_i \tag{2.17}$$

$$\frac{\varepsilon}{L_p} = \frac{8\mu_i RTS_o}{r^2} \tag{2.18}$$

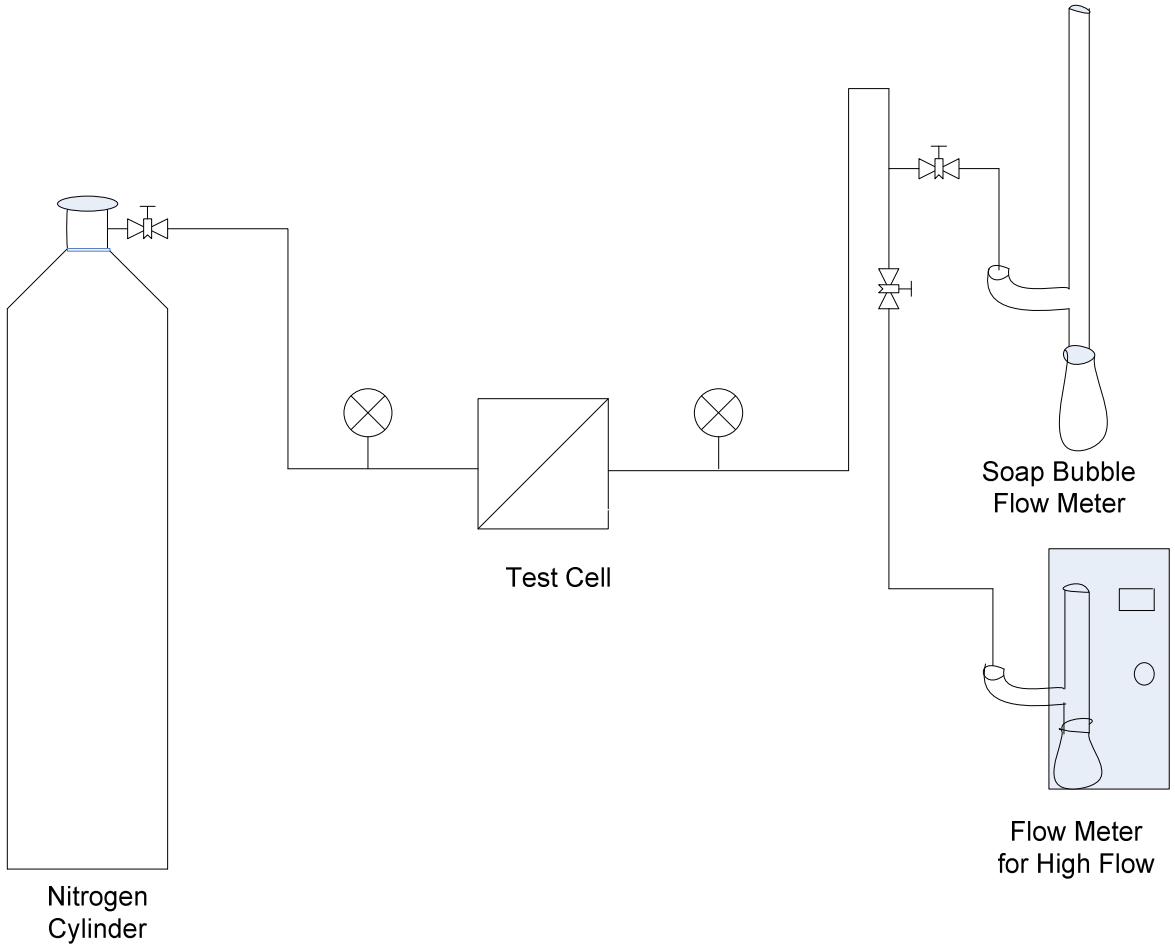

Figure 2.8 Schematic diagram for nitrogen gas permeation test through PTFE membrane.

2.3.5 Study of Membrane Surface by Scanning Electron Microscopy (SEM)

Scanning electron microscopy is a tool to study surface morphology of membranes. The Field Emission Scanning Electron Microscope (FESEM) (LEO 1520 VP FESEM) was used for this purpose. The principle of FESEM is that under vacuum, electrons generated by a source are accelerated in a field gradient. The beam passes through electromagnetic lenses, focusing onto the specimen. As a result of this bombardment different types of electrons are emitted from the specimen. A detector catches the secondary electrons and an image of the sample surface is constructed by comparing the intensity of these secondary electrons to the scanning primary electron beam. Finally the image is displayed on a monitor. FESEM offers ability to visually evaluate the porous nature of membrane's surface.

2.3.6. DCMD Experiments at Lower Brine Temperatures

The experimental apparatus employed to study the DCMD behavior for PTFE flat sheet membrane in lower temperature range is shown in Figure 2.9. Hot 1% NaCl brine solution was pumped over one side of the PTFE flat sheet membrane and cold distillate solution was passed on the other side of the membrane in a small stainless steel test cell (9 cm^2 area) by two peristaltic pumps (Masterflex, Cole-Parmer, Vernon Hills, IL). The brine feed solution was heated in a constant temperature bath (A81, HAAKE, Germany). The distilled water stream was heated up after passing through the membrane module; cooling of the distilled water stream was achieved by a chiller (12920-40, Cole-Parmer, Vernon Hills, IL). The brine reservoir was well covered to prevent evaporation of water to laboratory environment. A filter holder (47 mm, Sterlitech, Washington, contains slits

1 mm x 3 mm long) was placed before the membrane module to avoid any damage to the membrane from larger particles. The liquid level inside the brine beaker was kept constant using two level probes and a level controller which was connected to a peristaltic pump to supply water from the make-up water reservoir.

The inlet and outlet temperatures of the brine and the distillate stream passing through the membrane module were measured by thermocouples (EW-08516-74, Cole-Parmer, Vernon Hills, IL) connected to a data acquisition logger (OM-DAQPRO-5300, Omega Engineering, Stamford, CT). The pressures of brine in and distillate in stream were measured with a digital pressure gauge (DPG1000DAR-15G-1N, Omega Engineering, Stamford, CT) and an analog pressure gauge. The electrical conductivity on the distillate side was measured by a conductivity meter (Orion 115A^{+}, Thermo Electron Corporation, MA) to monitor for possible leaks of salt on the distillate side. Water vapor flux through the membrane module was calculated from the overflow of water from the distillate tank. Any experiment under given conditions was run for 6 hours.

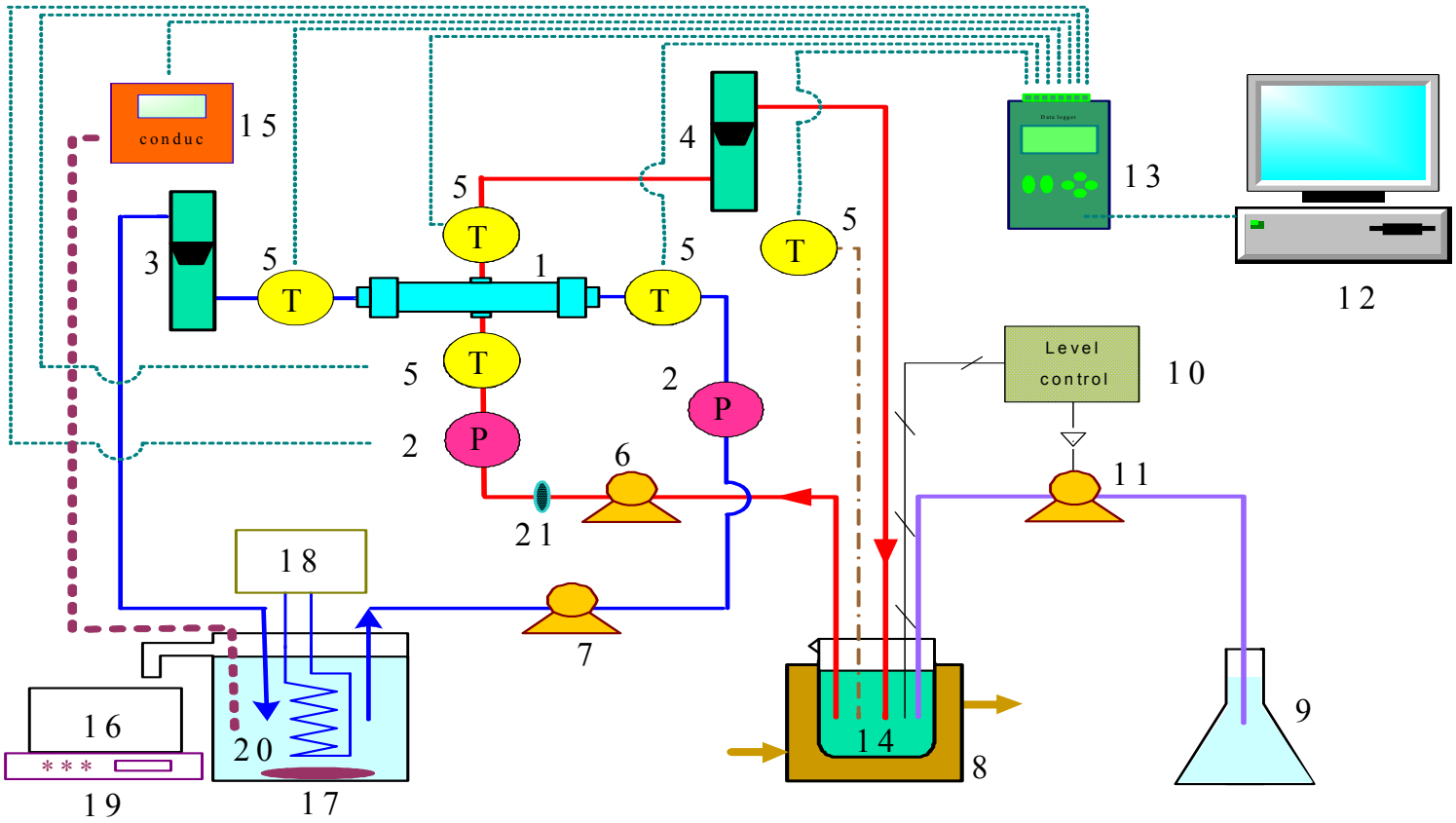

Figure 2.9 Low temperature DCMD setup:
1. Membrane module; 2. Pressure indicator; 3. Distillate flowmeter ; 4. Urine flowmeter; 5. Thermocouple; 6. Hot urine pump ; 7. Distillate pump; 8. Constant temperature bath; 9. Make-up water reservoir; 10. Level controller; 11. Make-up pump; 12. Computer; 13. Data logger; 14. Hot brine beaker ; 15. Conductivity transmitter; 16. Distillate overflow reservoir; 17. Magnetic stirrer; 18. Chiller; 19. Weight balance; 20. Cold distillate beaker; 21. Filter holder.

2.3.7 DCMD Experiments at Higher Brine Temperatures

The schematic diagram and a photograph of the higher temperature/higher pressure DCMD set up are shown in Figure 2.10 and Figure 2.11, respectively. Brine from the brine tank (Alloys Product Corp, Waukesha, WI) was pumped to the shell side of the heat exchanger (Titanium Fabrication Corp., Fairfield NJ,) by a pump ('QD' Cerampump, Fluid Metering, Syosset, NY) where it was heated by steam circulated on the tube side of the heat exchanger. Steam was delivered from a steam generator (MBA3A, Sussman Electric Steam Generator, Long Island, NY) at different pressures corresponding to the temperature of the feed solution. The heated brine was fed to one side of the membrane in the DCMD cell; on the other side of the membrane, cold distilled water was circulated by a pump ('QD' Cerampump, Fluid Metering., Syosset, NY). After the DCMD cell, hot brine was recycled to the brine tank; distilled water was circulated to the shell side of another heat exchanger (Titanium Fabrication Corp., Fairfield NJ), where it was cooled down by cold water from a chiller (CH3000 Series Chiller, REMCOR, Anoka, MN) circulated on the tube side of the heat exchanger.

The cooled distilled water from the heat exchanger was recycled to the distillate tank which was fitted with a liquid level controller (Low-Amp Liquid-Level Switch, McMaster-Carr, Robbinsville, NJ) to avoid overflow of water from the tank due to continuous condensation of water vapor in the distilled water stream across the membrane from the hot brine feed solution. This liquid level controller activated a pump ('QD' Cerampump, Fluid Metering Inc., Syosset, NY) to take out extra water from the distillate tank into the makeup water storage tank which was also fitted with another liquid level controller activating the water refill pump to feed water into the brine tank for

maintaining constant salt concentration in the brine tank. Inlet and outlet temperatures of brine and distilled water streams through the test cell were monitored by thermocouples (EW-08516-74, Cole-Parmer, Vernon Hills, IL) connected to a data acquisition logger (SPER SCIENTIFIC, Thermometer 4 channel, Cole-Parmer Instrument Co.). The flow rates of distillate in and distillate out streams were monitored by two different flow meters (JV-KG series positive displacement flow meter, A W Lake Company, Franksville, WI). PFA tubing and different types of PFA fittings (Cole-Parmer) were used to make connections in the set up. Any experiment under given conditions was run for around 3-4 hours.

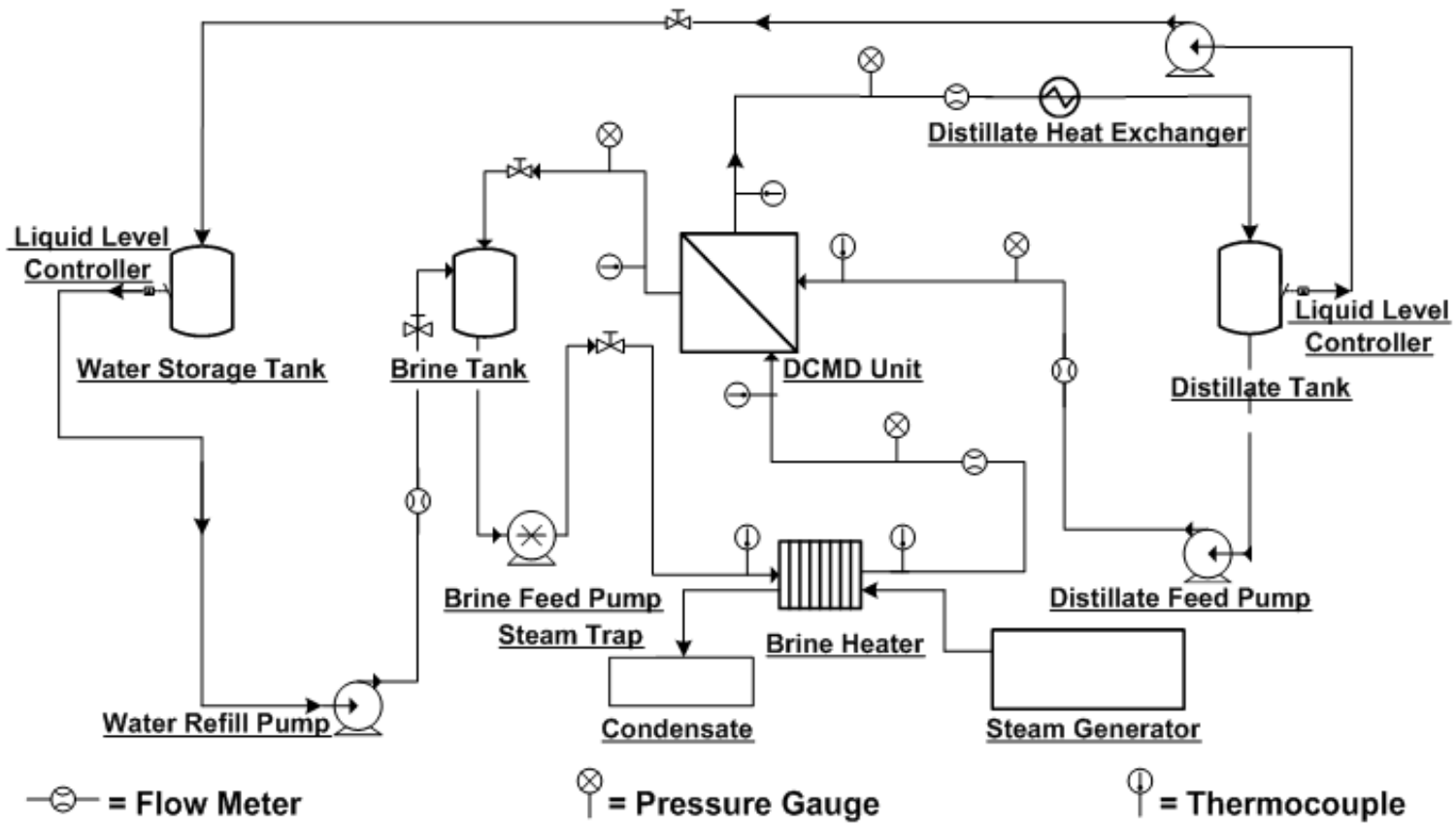

Figure 2.10 High temperature and high pressure DCMD set up.

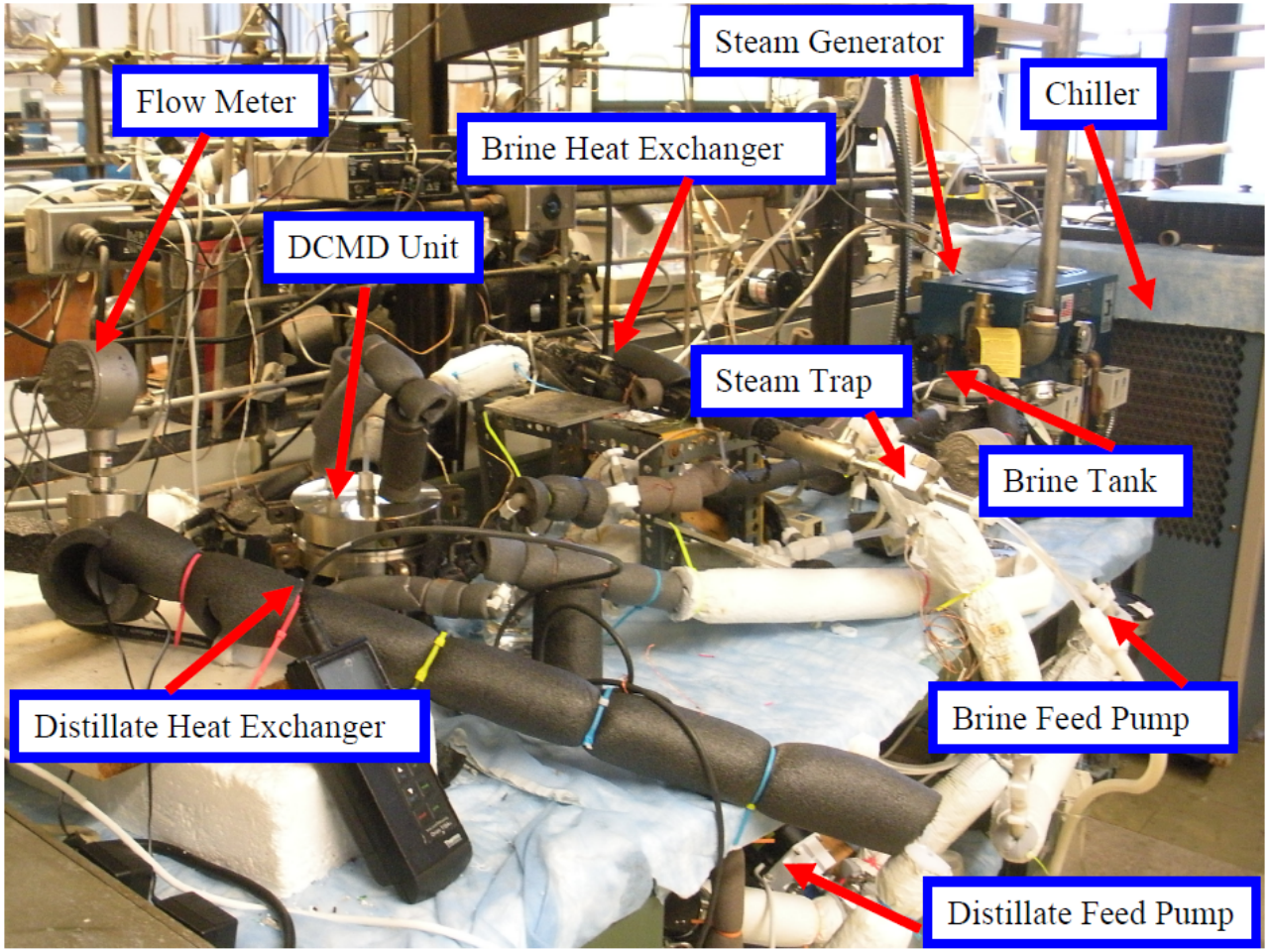

Figure 2.11 Photograph showing high temperature and high pressure DCMD set up.

2.3.8 Permeate Analysis by HPLC for Measurement of Phenol and Cresol

Concentrations of phenol and cresol in the distillate tank were determined by HPLC (Water Alliance HPLC, Waters 2690 Separation Module) having a C185U Econosphere column of length 15 mm and a UV detector at λ_{max} = 218 nm. The mobile phase used was 90/10 (v/v) methanol/water and 0.1% H_3PO_4 (v/v/) at a flow rate of 1 ml/min. The conditions for HPLC analysis are given in Table 2.2.

Table 2.2 HPLC Analysis Conditions

HPLC	Water Alliance HPLC
Column	C185U Econosphere column
Mobile phase	90/10 (v/v) methanol/water + 0.1 % H_3PO_4 (v/v)
Flow Rate	1 ml/min
UV detector	218 nm

2.3.9 Atomic Absorption Spectrometer for Measurement of Sodium Chloride on Permeate Side

Permeate side samples were analyzed by Atomic Absorption (AA) (AAnalyst 400, Atomic Absorption Spectrometer, Perkin Elmer, Norwalk, CT-06859) for sodium chloride; in addition the conductivity on distillate side was measured by a conductivity meter (Orion 115A^+, Thermo Electron Corporation, MA).

2.3.10 Gas Chromatography-Electron Impact-Mass Spectrometry (GC-EI-MS) for Measurement of Naphthenic Acid on the Permeate Side

Due to limitations of GC-EI-MS, naphthenic acids were extracted from water samples obtained from the distillate tank. According to the method suggested by Merlin et al. [55], concentrated HCl was first added to the water sample to maintain the pH at 2 and later 150g NaCl was dissolved into the sample. This sample was extracted three times with 60 ml of chloroform. The chloroform phase was subjected to extraction three times with 10 ml of an alkaline aqueous solution of 4 % (w/v) Na_2CO_3. The alkaline solution was acidified with concentrated HCl to pH 2 and free carboxylic acids from alkaline solution were extracted three times with 10 ml of dichloromethane (DCM). The extracted naphthenic acid with DCM was dried under nitrogen and the remaining sample was transferred to fresh DCM. The extracted naphthenic acids were derivatized by adding 100 µl of the MTBSTFA in 100 µl of a naphthenic acid standard (5 mg/ml) in dichloromethane [56]. The samples were next heated at 60^{o}C for 20 minute to get the t-BDMS derivative. Gas chromatography-electron impact mass spectrometry (GC-EI-MS) (HP 6890 Series GC system with Agilent 5973 Network Mass Selective Detector) was used next for analysis of the derivatized samples prepared by the above method.

2.3.11 Data Analysis

Steady state was assumed when the brine flow rate, the cold distilled water flow rate and the temperatures of the brine in and brine out as well as the temperatures of the distillate in and distillate out attained constant values.

At lower temperature experiments, after steady state was reached, the increase in the water level in the distillate tank over a certain time was used for calculation of water vapor flux (N_v) from the following relation:

$$N_v\left(\frac{kg}{m^2 \cdot h}\right) = \frac{volume\ of\ water\ transferred\ (L)\ x\ density\ of\ water\ (kg/L)}{membrane\ area\ (m^2)\ x\ time\ (h)} \quad (2.19)$$

Similarly for higher temperature experiments, after steady state was reached, change in flow rate of distillate out stream and distillate in stream was used for calculation of water vapor flux (N_v) from the following relation:

$$\text{Water vapor flux } (N_v) = \frac{(\text{Distillate flow rate})_{out} - (\text{Distillate flow rate})_{in}}{\text{Membrane area}} \quad (2.20)$$

Here, for flat sheet membrane, area was calculated on the basis of inside diameter of the gasket used over the membrane surface and for hollow fiber membrane module, area was calculated based on I.D. of the fiber. Each experiment was repeated three times for lower as well as for higher temperatures.

CHAPTER 3

RESULTS AND DISCUSSION FOR DCMD EXPERIMENTS

In Chapter 3, results and discussion for DCMD experiments performed at lower as well as higher temperatures are presented. Experiments were performed with ceramic disk/tubule and polymeric flat sheet/hollow fiber membranes for hot brine solutions.

3.1 DCMD Experiments at Lower Temperatures

Ceramic membranes and polymeric flat sheet/hollow fiber membranes were explored for 1% NaCl solution at lower temperatures in the set up designed for lower temperature DCMD experiments shown in Figure 2.9.

3.1.1. Experiments with Ceramic Disc Membrane

Since one has to use hydrophobic membranes only, a surface modification process for the ceramic membrane was developed. Anodisc membrane was modified with silicone oil at 160^{o}C for two hours. It was expected that alumina-based ceramic membranes having hydroxyl group on their surface might be grafted to a siloxane derivative as follows [57]:

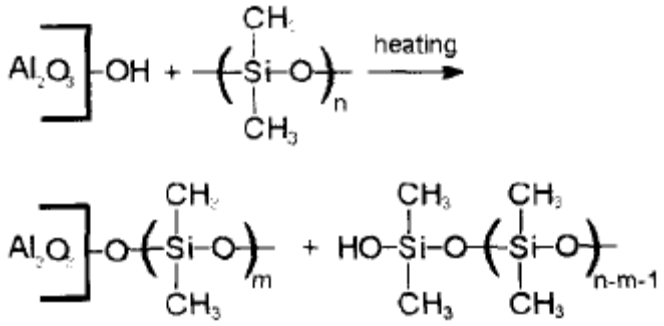

In the modification process, chances of blocking of pores are high, which is undesirable. To get rid of the blockage problem, N_2 gas was passed through the membrane. If one passes N_2 gas after heating of membrane for two hours, it is very difficult to remove the silicone oil from the pores. Hence before heating the silicone modified membrane, N_2 gas was passed at 1.6 atm pressure (gauge) through the membrane; this process removed bulk of the silicone oil from the pores of the membrane; the pore surface had silicone oil left for polymerization. After bulk polymerization was completed, toluene was passed through the membrane pores. The idea behind this is to remove any unbound silicone oil from the membrane surface and also from the pores of the membrane (Figure 3.1). It is also clear from the SEM images (Figure 3.2) that after keeping the Anodisc membrane in silicone oil for 12 hours and passing the nitrogen gas before heating the membrane at 160^{o}C for two hours, silicone oil is blown off from the pores, leaving only a thin layer of the silicone oil as shown in Figure 3.1.

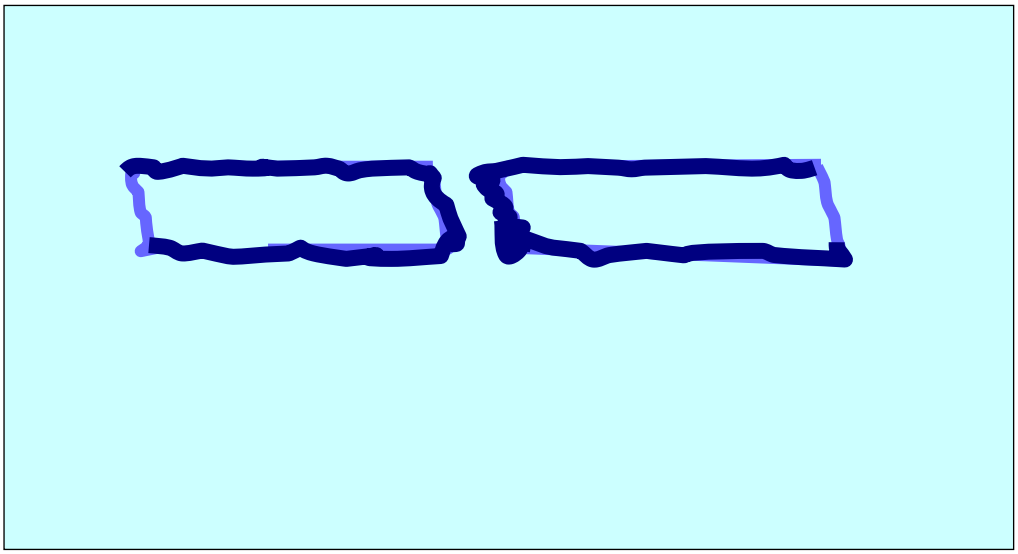

Figure 3.1 Schematic showing the hydrophobic coating on membrane surface including the walls of the membrane's pores.

In SEM micrographs, the surface of unmodified Anodisc membrane has a large number of pores (Figure 3.2(a)), which are blocked after the conventional modification process (see Figure 3.2(b)). But before the heating of membrane at 160^{o}C, if silicone oil in the pore bulk is blown off by N_2, pores will be open again. Pores will be more clearly visible, if toluene is passed to remove the unbound silicone oil (Figure 3.2(c)). No data could be gathered using the modified membrane since the membrane was very fragile.

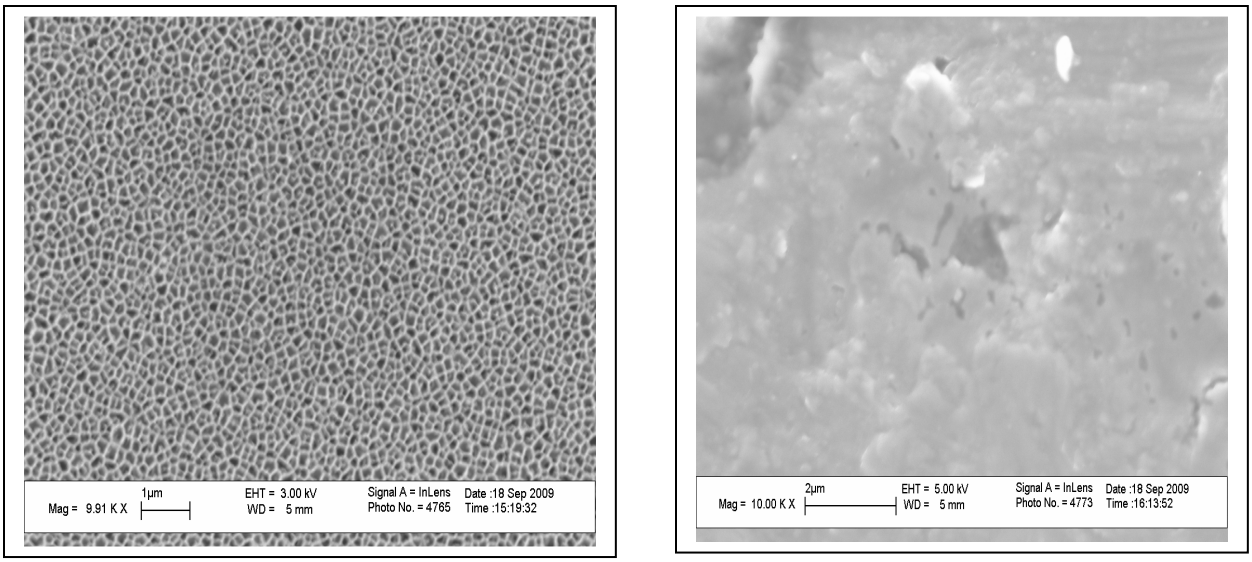

(a) (b)

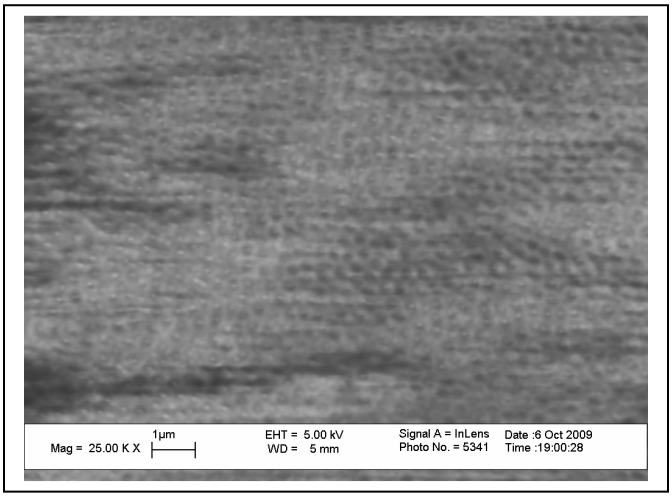

(c)

Figure 3.2 SEM micrographs showing the surfaces of Anodisc 47 modified with silicone oil (a) unmodified surface (b) N_2 gas is passed after heating the membrane at 160^oC (c) N_2 gas is passed before heating the membrane at 160^oC and after polymerization, toluene is passed through the membrane.

Another ceramic disc (alumina 86 %, SiO_2 12%) was procured from Refractron Technologies having a pore size 1.0 μm, porosity around 40-50 % and effective diameter 2.6 cm. Before doing any experiments, the ceramic disc was hydrophobized according to the procedure developed for anodisc. The performance of the hydrophobized ceramic disc was explored with 1 % NaCl solution at lower temperatures. The volume of water vapor flux was very low and difficult to measure because of the small effective area of ceramic disc and its lower porosity (Table 3.1). The important part of the experiments was that there was no salt detected on permeate side illustrating the effectiveness of modification procedure developed to hydrophobize the ceramic disc.

Table 3.1 Performance of Hydrophobized Ceramic Disc (from Refractron) with 1% NaCl Solution

Brine Inlet T_{bi} (^oC)	Brine Outlet T_{bo} (^oC)	Distillate Inlet T_{di} (^oC)	Distillate Outlet T_{do} (^oC)	Brine In Flow Rate F_{bi} (ml/min)	Distillate In Flow Rate F_{di} (ml/min)	Water Vapor Flux (kg/m^2-hr)
80.1	78.2	20.4	22.3	250	250	*
92.0	90.0	21.1	22.9	250	250	*

3.1.2 Experiments with Ceramic Membrane Module

Experiments were carried out with a ceramic membrane tubule having a hydrophobized surface. The physical properties of the ceramic membrane tubule are as follows; O.D.= 3.8 mm, I.D.= 1.5 mm, length = 45 cm and pore size = 50 Å (M & P Technologies, Pittsburgh, PA). The water vapor flux at a temperature of 70.7^{o}C for 1% NaCl feed solution was insignificant and immeasurable but conductivity on distillate side with time

was constant. At a temperature of 87°C, the water vapor flux was 1.14 kg/m^2-hr with constant conductivity on distillate side. But at higher temperatures, conductivity on the distillate side increased with time, indicating the problem was related to sealing of the ceramic tubule. The results are summarized in Table 3.2. The low flux is due to very high conductive heat transfer among others.

Table 3.2 Performance of Hydrophobized Ceramic Tubule with 1% NaCl Solution

Brine Inlet T_{bi} (°C)	Brine Outlet T_{bo} (°C)	Distillate Inlet T_{di} (°C)	Distillate Outlet T_{do} (°C)	Brine In Flow Rate F_{bi} (ml/min)	Distillate In Flow Rate F_{di} (ml/min)	Water Vapor Flux (kg/m^2-hr)
70.7	56.3	25.6	34.5	500	150	*
87.0	76.8	20.9	50.1	500	150	1.14
110.9	78.8	32.8	44.5	500	500	*
120.8	92.8	36.8	48.7	500	500	*

3.1.3. Experiments with PVDF Flat Sheet Membrane

Experiments were carried out with DI (deionized) water as feed solution for a flat PVDF membrane (procured from Millipore Corporation) having a pore size 0.1 μm and effective diameter 32 mm. The results indicate that water vapor flux increased from 15.55 kg/m^2-hr to 53.95 kg/m^2-hr as the temperature of the feed solution was increased from 80°C to 95°C. The feed and distilled water flow rates were held constant at 450 ml/min. In all experiments, the distilled water inlet temperature was maintained at 20°C. The results are summarized in Table 3.3 and Figure 3.3.

Table 3.3 Performance of PVDF Flat Sheet Membrane with DI Water

Brine Inlet T_{bi} (°C)	Brine Outlet T_{bo} (°C)	Distillate Inlet T_{di} (°C)	Distillate Outlet T_{do} (°C)	Water Vapor Flux (kg/m^2-hr)
80.1	78.6	19.9	21	15.55
85.1	83.1	20	21.4	17.77
90.1	88.3	20.1	21.9	26.87
95	92.5	20	21.9	53.95

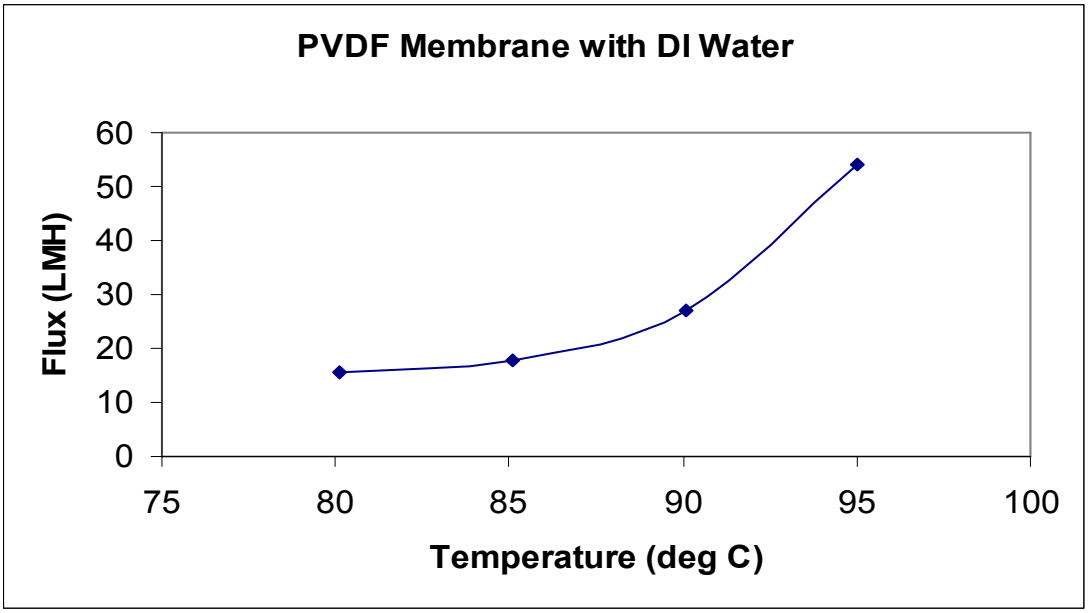

Figure 3.3 Change in water vapor flux with temperature for PVDF flat membrane.

Experiments were performed with the same PVDF membrane using 1% NaCl solution as feed. The water vapor flux increased from 13.17 to 50.68 kg/m^2-hr, as feed solution temperature was increased from 80^{o}C to 95^{o}C. No salt leakage was observed in the distillate. The results are summarized in Table 3.4 and Figure 3.4. It is clear from Figure 3.5 that there are no significant changes in the water vapor fluxes for 1 % NaCl feed solution and pure deionized water at lower temperatures.

Table 3.4 Water vapor flux data for PVDF Flat Sheet Membranes with 1% NaCl Feed Solution

Brine Inlet T_{bi} (^{o}C)	Brine Outlet T_{bo} (^{o}C)	Distillate Inlet T_{di} (^{o}C)	Distillate Outlet T_{do} (^{o}C)	Water Vapor Flux (kg/m^2-hr)
80.1	78.9	19.8	21	13.17
85.1	83.5	19.9	21.3	16.58
90.3	88.3	20.3	21.8	23.57
95	92.6	19.8	22.2	50.68

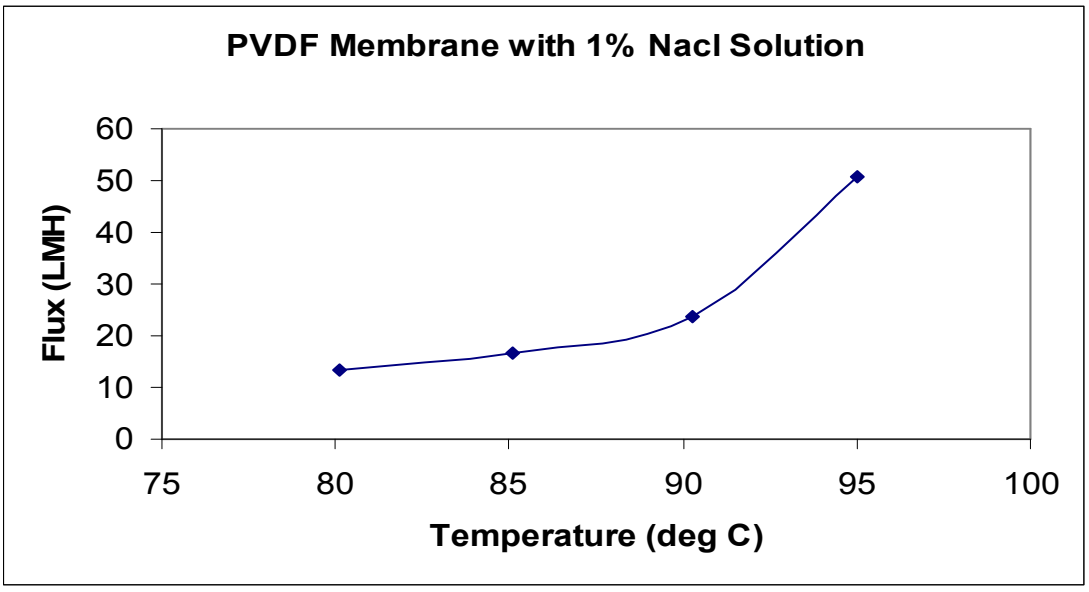

Figure 3.4 Change in water vapor flux with temperature for PVDF flat membrane.

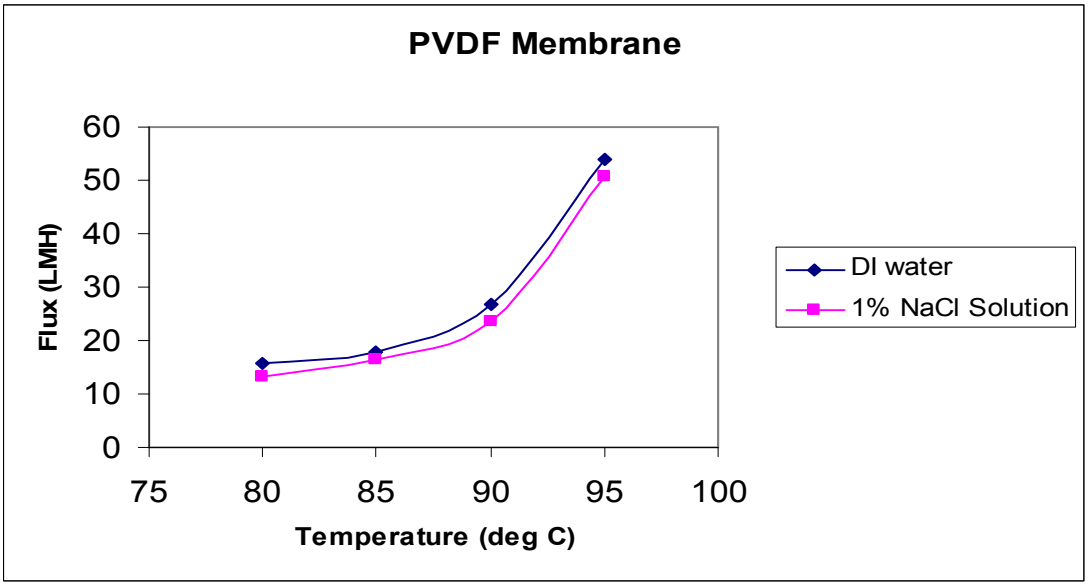

Figure 3.5 Comparison of water vapor flux behavior for DI water and 1% NaCl solution.

3.1.4. Experiments with PTFE Flat Sheet Membrane

PTFE flat sheet membranes used for experiments were characterized by scanning electron microscopy. It is clear from Figures 3.6(a) and 3.6(b) that both sides of the membrane have a similar morphology illustrating the symmetric nature of the membrane. Nitrogen gas permeation flux through the flat sheet membrane was measured at different pressures and plotted against the mean pressure, $\bar{p}$. From the intercept and slope of the line in Figure 3.7, the effective porosity (ε/L_p) for the flat sheet membrane was found to be 1.77 x 10^4 m^{-1}. The value of tortuosity factor was calculated to be 1.58 taking into account the value for porosity of PTFE membrane (ε=0.65) from the manufacturer (Table 2.1).

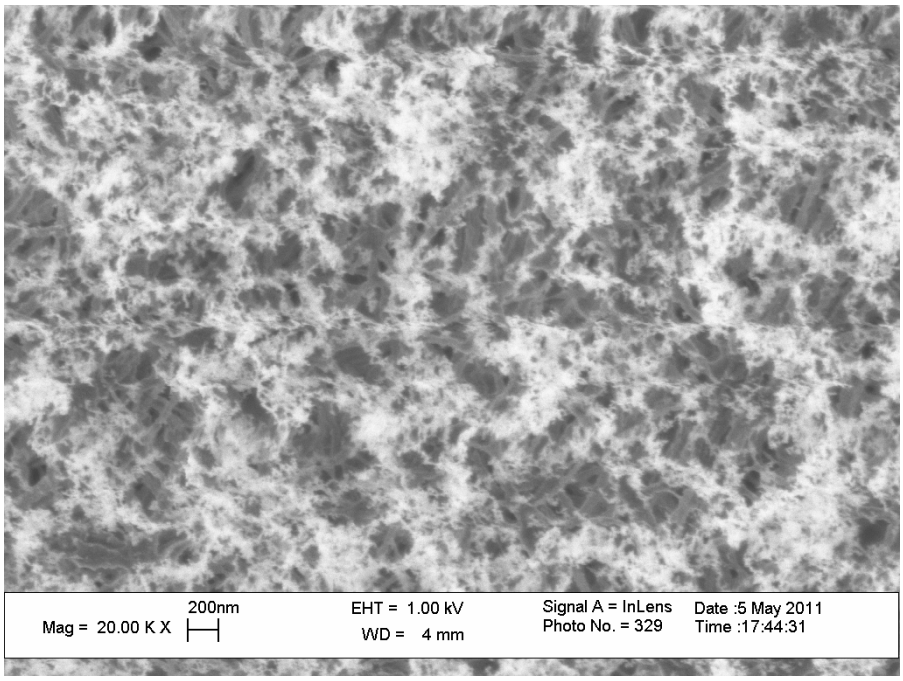

(a)

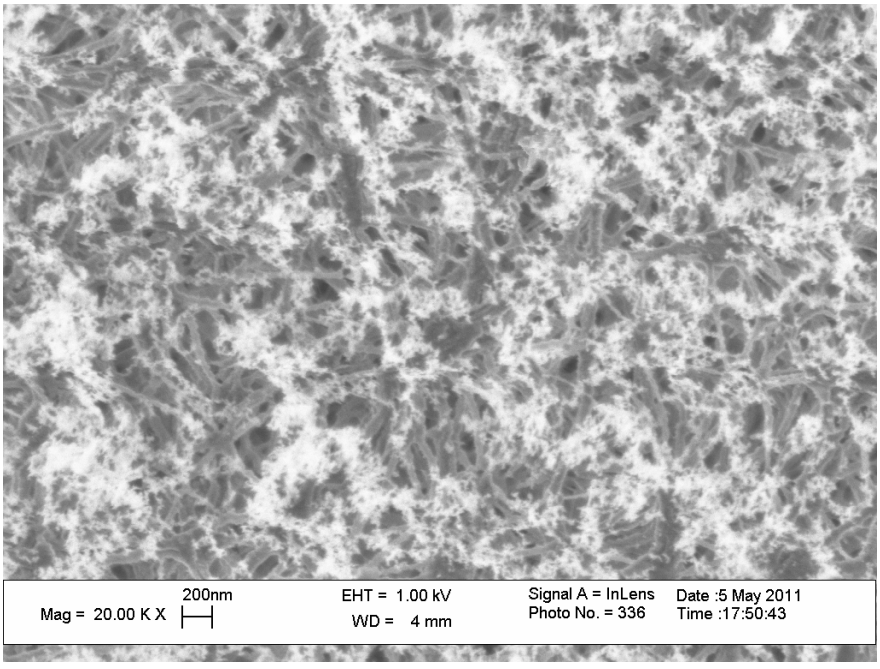

(b)

Figure 3.6 Scanning electron micrographs for PTFE flat sheet membrane: (a) top surface and (b) bottom surface.

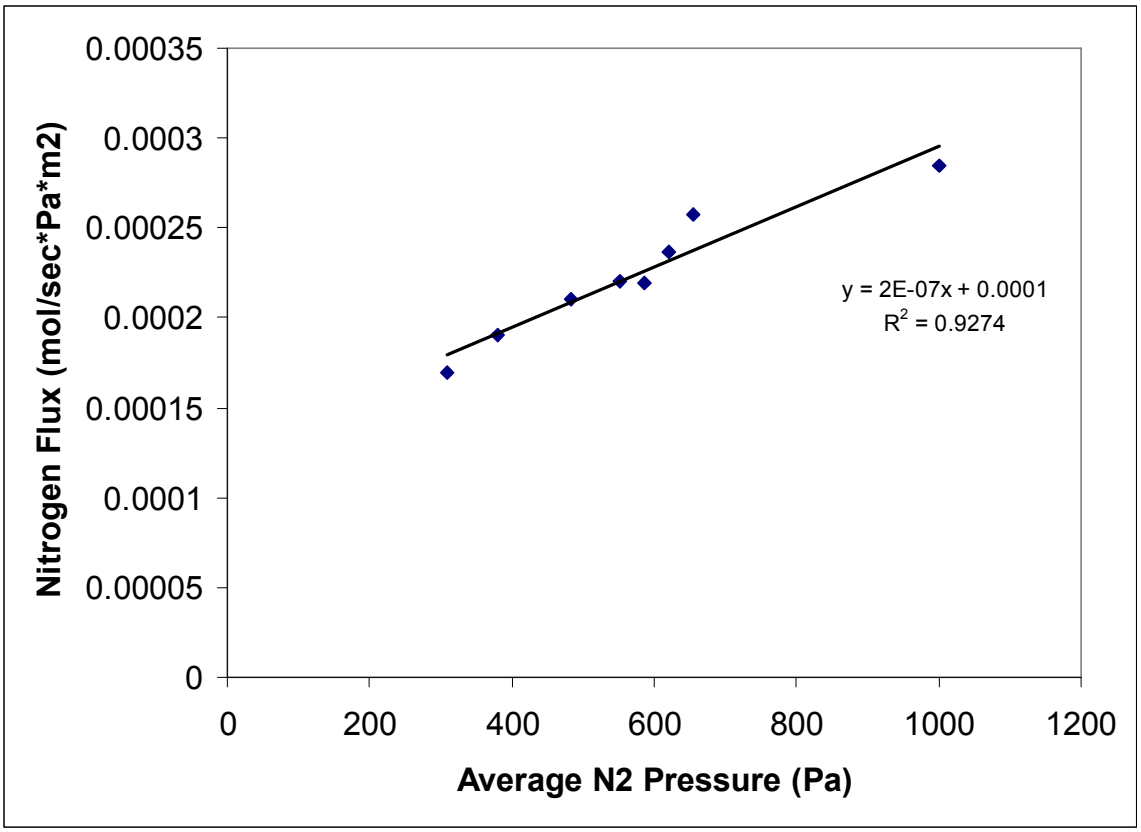

Figure 3.7 Nitrogen flux through porous PTFE flat sheet membrane at different average nitrogen pressure across the membrane.

First, experiments were performed with PTFE membranes in lower temperature range using 1% NaCl feed solution. The PTFE flat sheet membrane has a pore size of 0.03 μm and an effective diameter of 32 mm. It was observed that water vapor flux increased from 14.45 kg/m^2-hr to 66.46 kg/m^2-hr as temperature was increased for the feed solution from 80^{o}C to 95^{o}C. In all experiments, the distilled water inlet temperature was maintained around 20^{o}C. The feed and distilled water flow rates were held constant at 450 ml/min. The results are summarized in Table 3.5 and Figure 3.8. No salt leakage into the distillate was observed.

Table 3.5 Performance of PTFE Flat Sheet Membranes with 1% NaCl Feed Solution

Brine Inlet T_{bi} (^oC)	Brine Outlet T_{bo} (^oC)	Distillate Inlet T_{di} (^oC)	Distillate Outlet T_{do} (^oC)	Water Vapor Flux (kg/m^2-hr)
80	78.6	19.9	21.6	14.45
85.1	82.2	20	22.9	20.39
90	86.7	19.8	24.1	37.32
95	90.9	20	24.4	66.46

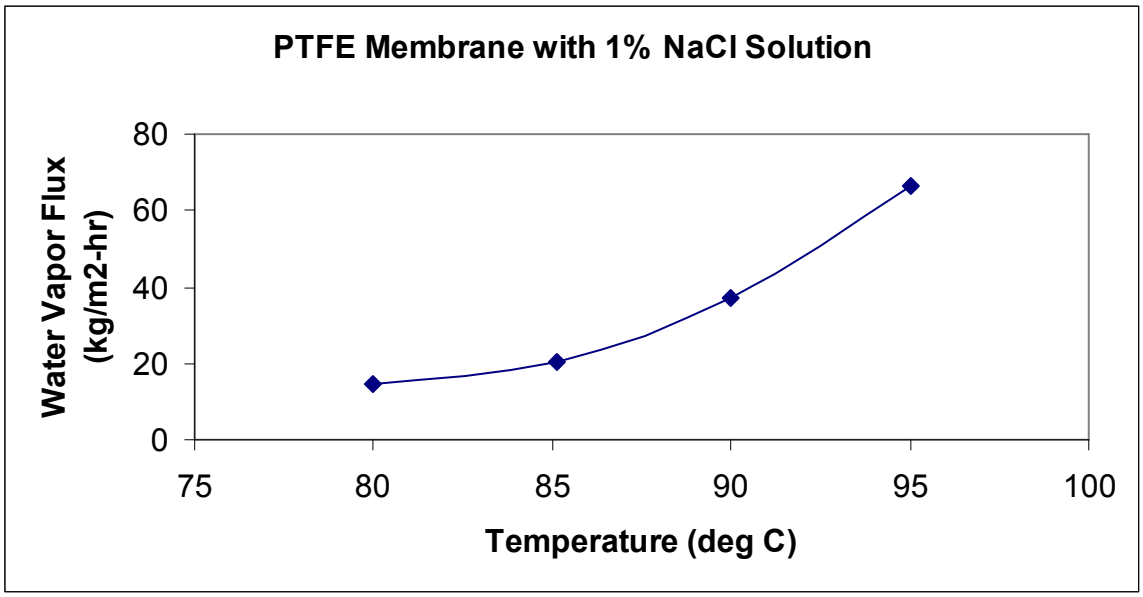

Figure 3.8 Change in water vapor flux with temperature using PTFE membrane.

3.1.5. Experiments with PMP Hollow Fiber Membrane

A module was fabricated using PMP (Poly (4- methyl -1- pentene)) hollow fibers. The physical properties of the fiber are as follows; O.D.=260 μm, I.D.=180 μm, fiber wall porosity =0.3 and wall thickness = 40 μm. The PMP fiber however has a dense skin which is not porous in the conventional sense. But, a combination of the bulky side group and specificity of the polymer packing results in the low-density polymer having large micropores in the range 4.3-5 Å. This may allow transport to take place in a way similar to that in molecular sieves (zeolites). A hot 1% NaCl solution was passed on the shell side and cold distilled water was passed through the lumen side. The experiments were carried out at two feed solution temperatures; 80^{o}C and 90^{o}C; in all experiments the distilled water temperature was maintained at 20^{o}C. The feed and distilled water flow rates were held constant at 400 ml/min and 25 ml/min, respectively. After running the experiments for more than six hours, no water vapor flux was observed for this module. The results are summarized in Table 3.6.

It is interesting to note that PMP fibers are not yielding any measurable flux in DCMD. However, earlier a low water vapor flux was achieved in vacuum membrane distillation (VMD) mode using PMP fibers. In DCMD, the sensible heat of the hot brine is utilized to evaporate water which is recovered in the cold distillate stream. But, in DCMD, a significant part of the sensible heat lost by the hot feed brine is transferred by conduction through the solid polymeric wall and the vapor-filled pore space to the cold distillate stream. This conductive heat flux is not utilized to evaporate water in DCMD. The presence of a reasonably high vacuum on the other side of the membrane in VMD drastically reduces the extent of conductive heat loss from the hot brine. In the case of

PMP fiber, which has a thin 40 μm wall thickness and porosity around 30%, this phenomenon of high heat conduction is the main cause for not having any measurable water vapor flux in DCMD.

Table 3.6 Performance of PMP Hollow Fiber Membrane with 1% NaCl Solution

Brine Inlet T_{bi}(°C)	Brine Outlet T_{bo}(°C)	Distillate Inlet T_{di}(°C)	Distillate Outlet T_{do}(°C)	Brine Inlet Pressure P_{bi} (psi)	Brine Outlet Pressure P_{di} (psi)	Water Vapor Flux (kg/m^2-hr)
80.2	77.5	19.4	68.8	5	20	0
90	87.1	20.5	70.4	5	20	0

3.1.6 Experiments with PVDF Hollow Fiber H Membrane Module

The cross section and the outer surface of PVDF fiber H were analyzed by SEM. For preparing the SEM sample, the fiber was dipped into liquid nitrogen to avoid any damage during its cutting. The SEM micrograph in Figure 3.9(a) revealed the following information about PVDF fiber; O.D. = 1600 μm, I.D. = 900 μm and wall thickness = 350 μm. The porous nature of PVDF fiber can be visualized from SEM micrograph of fiber's surface in Figure 3.9(b).

The porosity of the membrane was measured by using pore wetting liquid such as isopropyl alcohol (IPA), which penetrates the membrane pores. Here porosity is defined as the ratio between the volume of the pores and the total volume of the membrane. This technique yielded a porosity of the PVDF fiber of 0.52. The membrane porosity and mean pore radius were also calculated by gas permeation test; the values are 0.47 and 0.623 μm, respectively.

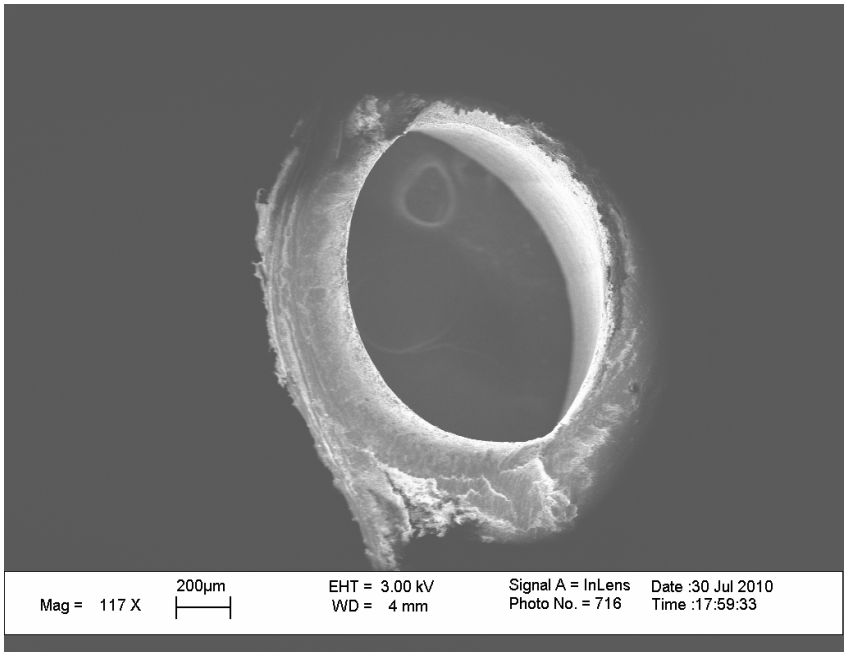

(a)

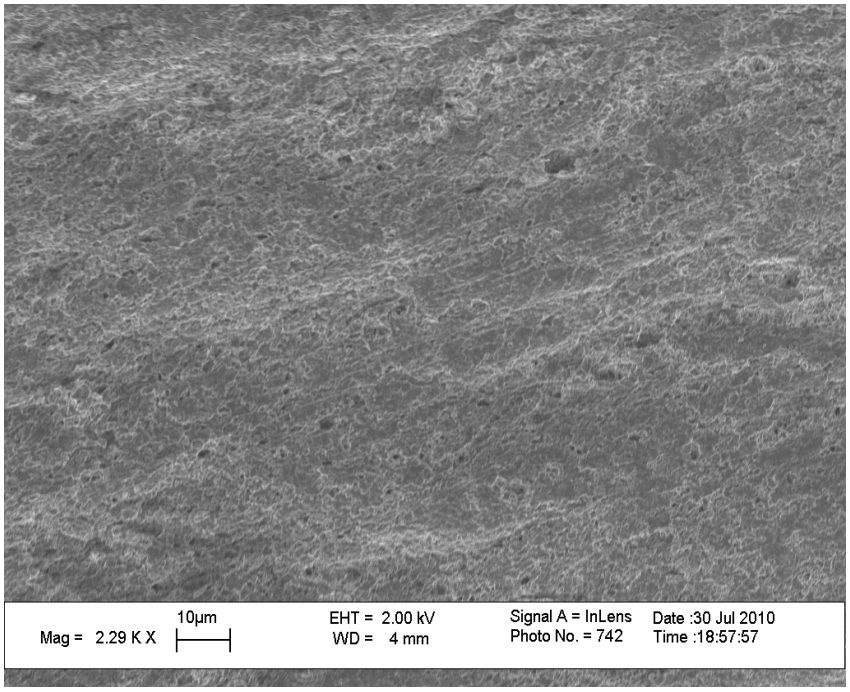

(b)

Figure 3.9 SEM micrographs of PVDF hollow fiber H showing (a) cross section view of the fiber, (b) outer surface of the fiber.

Experiments were carried out with 1% NaCl as feed solution for a PVDF hollow fiber membrane (procured from Hyflux Inc., Singapore)) having a pore size of 0.623 μm and porosity close to 0.50. The modules were fabricated at NJIT with an effective length 0f 20 cm, number of fibers, 5 and an effective area of 28.62 cm^2 (based on I.D.). The results in Figure 3.10 indicate that water vapor flux increased from 14.21 kg/m^2-hr to 27.03 kg/m^2-hr as the temperature of the feed solution was increased from 85°C to 95°C. The feed and distilled water flow rates were held constant at 450 ml/min and 125 ml/min respectively. In all experiments, the distilled water inlet temperature was maintained at 20°C. The results are summarized in Table 3.7. Brine flowed on the shell side for any experiments with hollow fiber module.

Table 3.7 Performance of PVDF Hollow Fiber Membrane H with 1% NaCl Solution

Brine Inlet T_{bi} (°C)	Brine Outlet T_{bo} (°C)	Distillate Inlet T_{di} (°C)	Distillate Outlet T_{do} (°C)	Brine In Flow Rate F_{bi} (ml/min)	Distillate In Flow Rate F_{di} (ml/min)	Water Vapor Flux (kg/m^2-hr)
85.3	81.4	19.6	21.6	450	120	14.21
90.2	86.7	20.1	22.9	450	120	20.11
95.7	93.1	20.1	23.2	450	120	27.03

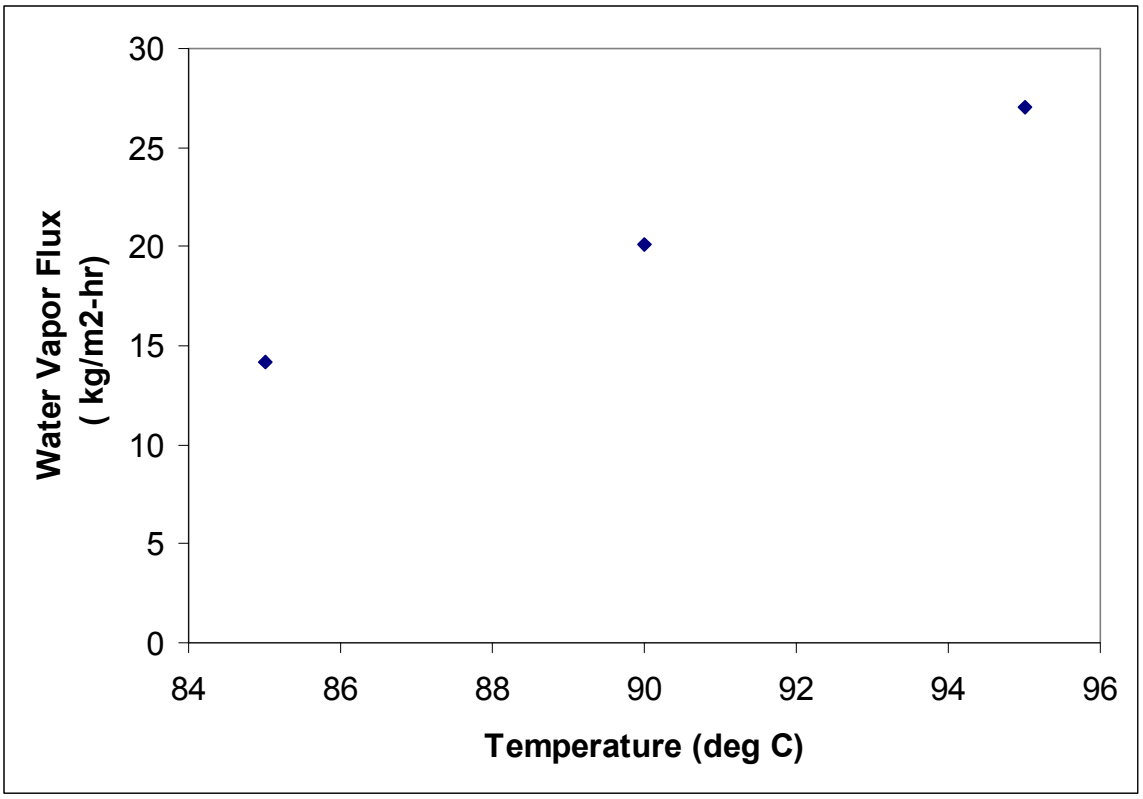

Figure 3.10 Change in water vapor flux with temperature using PVDF hollow fiber H membrane.

3.1.7. Characterization of PVDF Hollow Fiber E Membrane and Module

The cross section, inner surface and outer surface of PVDF fiber E (Arkema Inc., King of Prussia, PA) were analyzed by SEM. For preparing the SEM sample, the fiber was dipped into liquid nitrogen to avoid any damage during its cutting. The SEM micrograph in Figure 3.11(a) revealed the following information about PVDF fiber; O.D. = 925 μm, I.D. = 691.7 μm and wall thickness = 117 μm. The porous nature of PVDF fiber can be visualized from SEM micrograph of fiber's surfaces in Figure 3.12 and Figure 3.13. Nitrogen gas permeation results for hollow fiber E is shown in Figure 3.14.

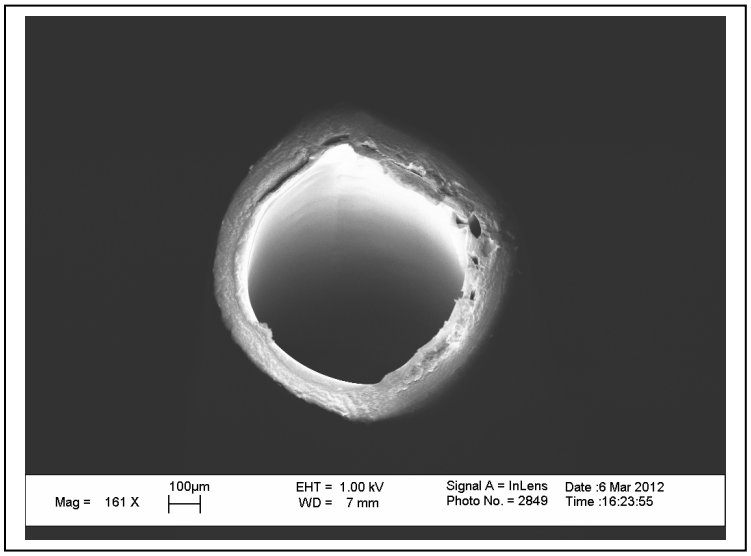

(a)

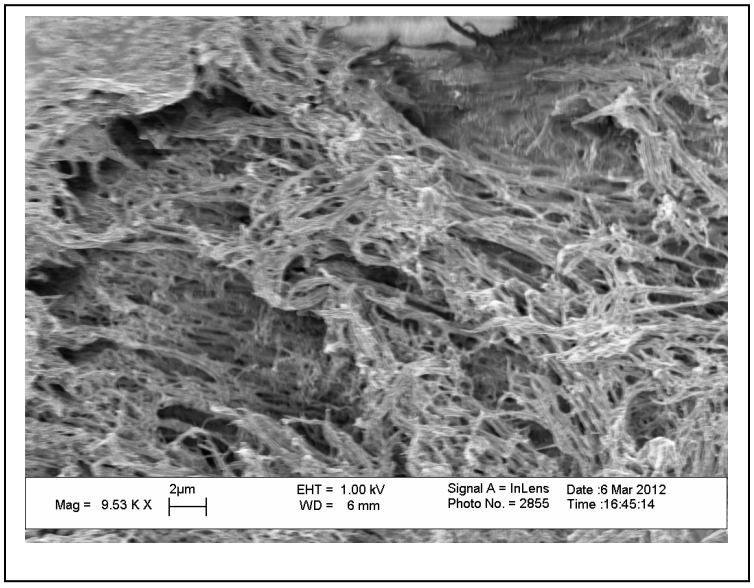

(b)

Figure 3.11 SEM micrographs showing the (a) cross section of PVDF hollow fiber E (b) structure of wall at lower 2.0 KX (c) structure of wall at 9.5 KX.

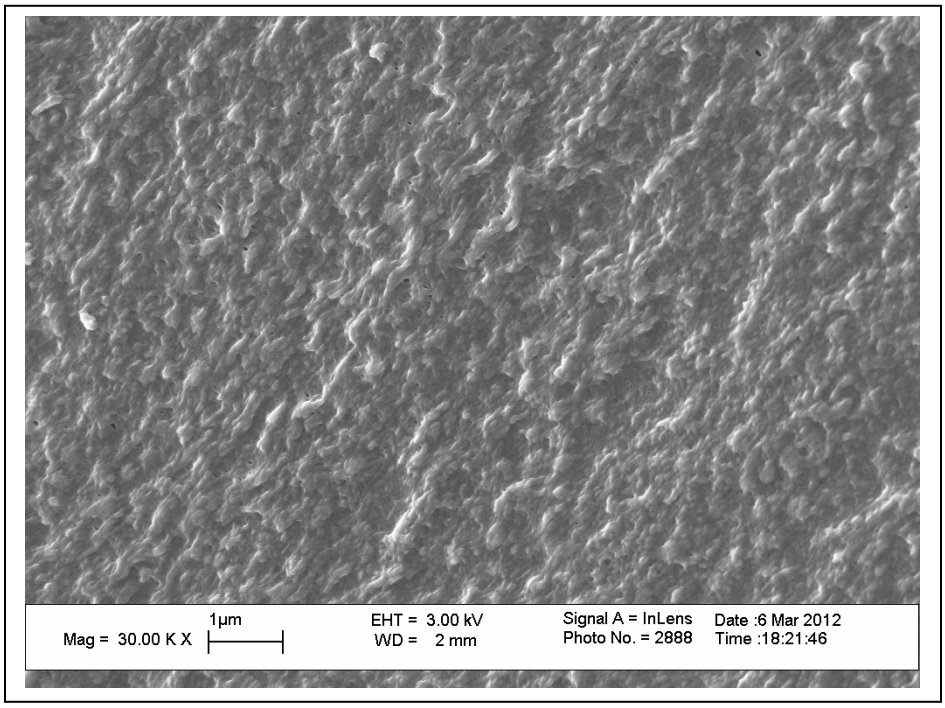

(a)

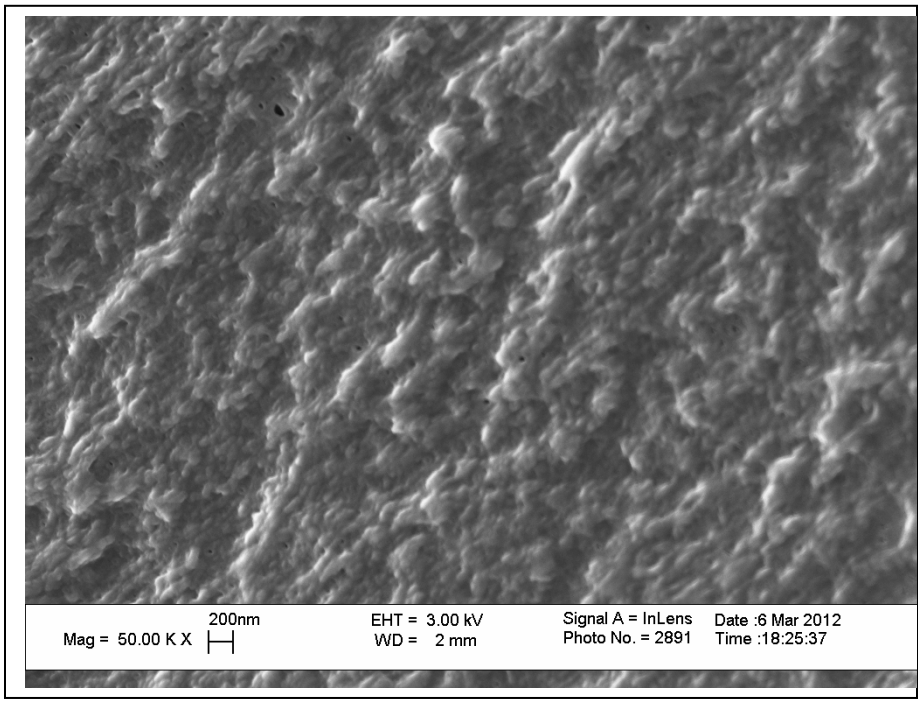

(b)

Figure 3.12 SEM micrographs showing the (a) inner surface of PVDF hollow fiber E at 30.0 KX (b) inner surface of PVDF hollow fiber E at 50.0 KX.

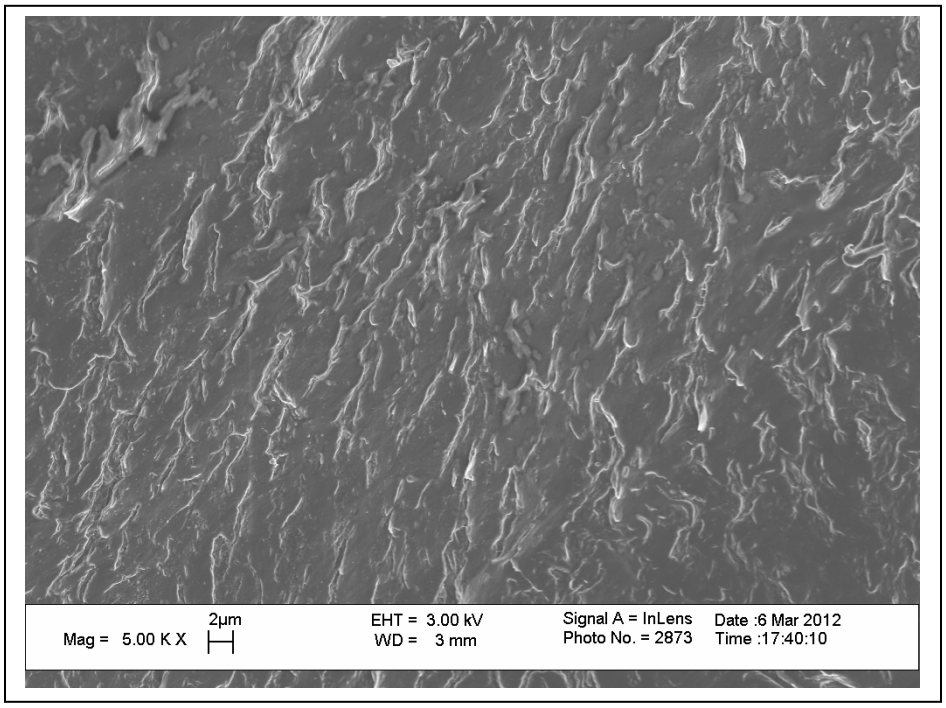

(a)

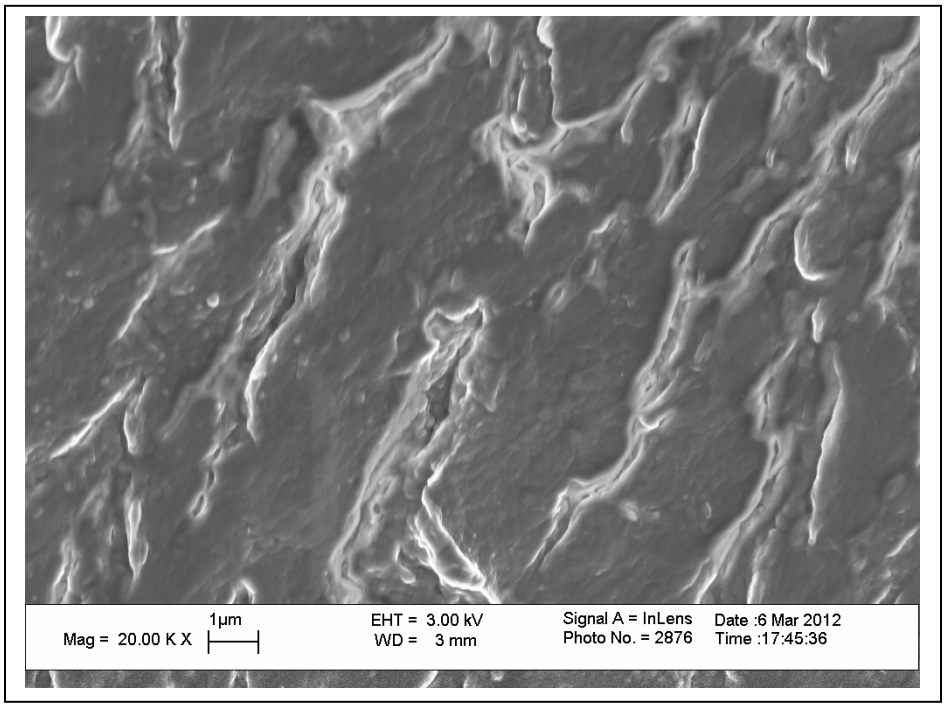

(b)

Figure 3.13 SEM micrographs showing the (a) outer surface of PVDF hollow fiber E at 5.0 KX (b) inner surface of PVDF hollow fiber E at 20.0 KX.

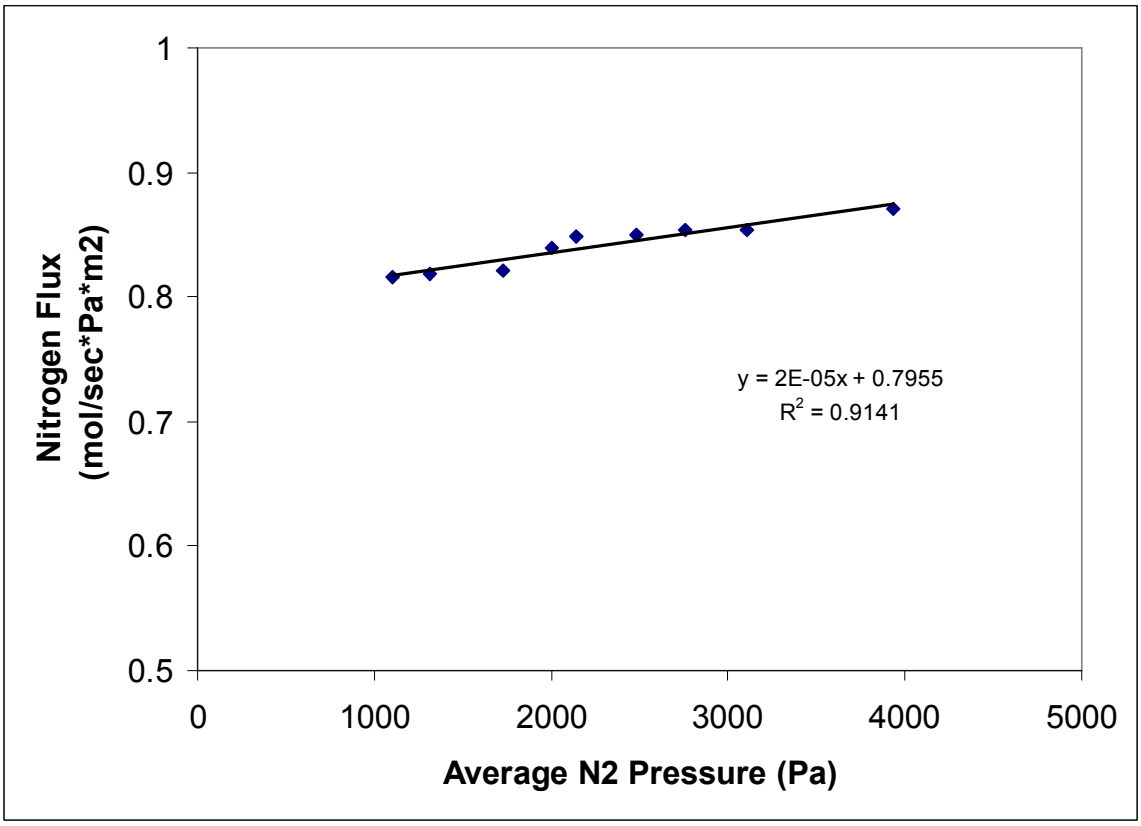

Figure 3.14 Nitrogen flux through porous PVDF hollow fiber E membrane at different average nitrogen pressure across the membrane.

3.1.8 Experiments with PVDF Hollow Fiber E Membranes

Experiments were carried out with 1% NaCl as feed solution for a module containing PVDF hollow fiber E membrane having a pore size of 0.2 μm and porosity close to 0.54. The modules were fabricated at NJIT with an effective length of 17.5 cm, number of fibers, 3 and an effective area of 11.41 cm^2 (based on I.D.). The results in Figure 3.15 indicates that the water vapor flux increased from 7.51 kg/m^2-hr to 17.1 kg/m^2-hr as the temperature of the feed solution was increased from 80^oC to 95^oC. The feed and distilled

water flow rates were held constant at 450 ml/min and 125 ml/min respectively. In all experiments, the distilled water (introduced into the tube side) inlet temperature was maintained at 20^{o}C. The results are summarized in Table 3.8. The water vapor fluxes of PVDF hollow fiber E for 1 % NaCl are lower than water vapor fluxes obtained with PVDF hollow fiber H. It is probably due to lower porosity of hollow fiber E compared to that of hollow fiber H; also the wall thickness of hollow fiber E is lower than hollow fiber H. Therefore heat loss by conduction through the wall of fibers will be more in hollow fiber E than hollow fiber H.

Table 3.8 DCMD Performance of PVDF Hollow Fiber E Membrane with 1% NaCl Solution

Brine Inlet T_{bi} (^{o}C)	Brine Outlet T_{bo} (^{o}C)	Distillate Inlet T_{di} (^{o}C)	Distillate Outlet T_{do} (^{o}C)	Brine In Flow Rate F_{bi} (ml/min)	Distillate In Flow Rate F_{di} (ml/min)	Water Vapor Flux (kg/m^2-hr)
80.4	81.4	19.6	21.6	450	120	7.51
85	86.7	20.1	22.9	450	120	9.5
90	93.1	20.1	23.2	450	120	14.72

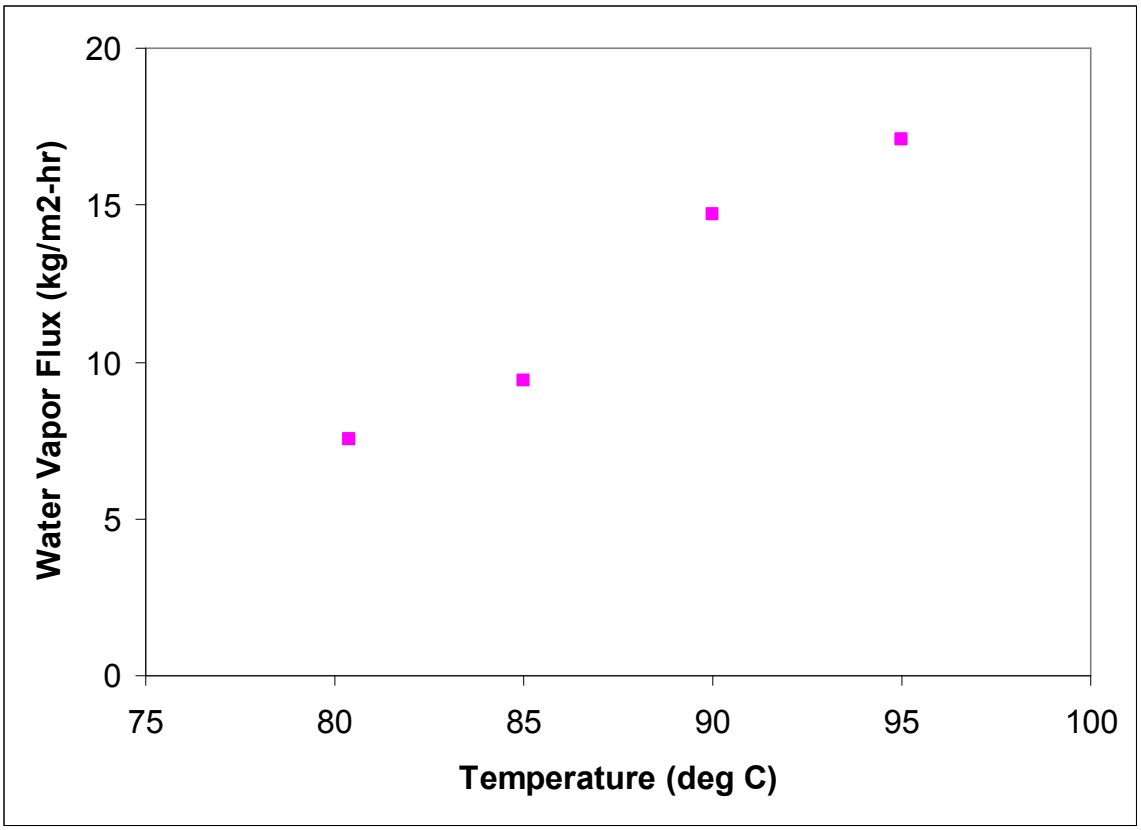

Figure 3.15 Change in water vapor flux with temperature for PVDF hollow fiber E membranes.

3.1.9 Experiments with PTFE Hollow Fiber M Membrane Module

The cross section, inner surface and outer surface of PTFE hollow fiber M (Markel Corporation, Plymouth Meeting, PA) were analyzed by SEM. For preparing the SEM sample, the fiber was dipped into liquid nitrogen to avoid any damage during its cutting. The SEM micrograph in Figure 3.16 revealed the tortuous path along the wall of fiber M. The porous nature of PTFE fiber can be visualized from SEM micrograph of fiber's surface in Figure 3.17 and Figure 3.18. It is clear from the SEM images that the inner surface has more number of pores than the outer surface of the fiber illustrating the asymmetric nature of the fiber M.

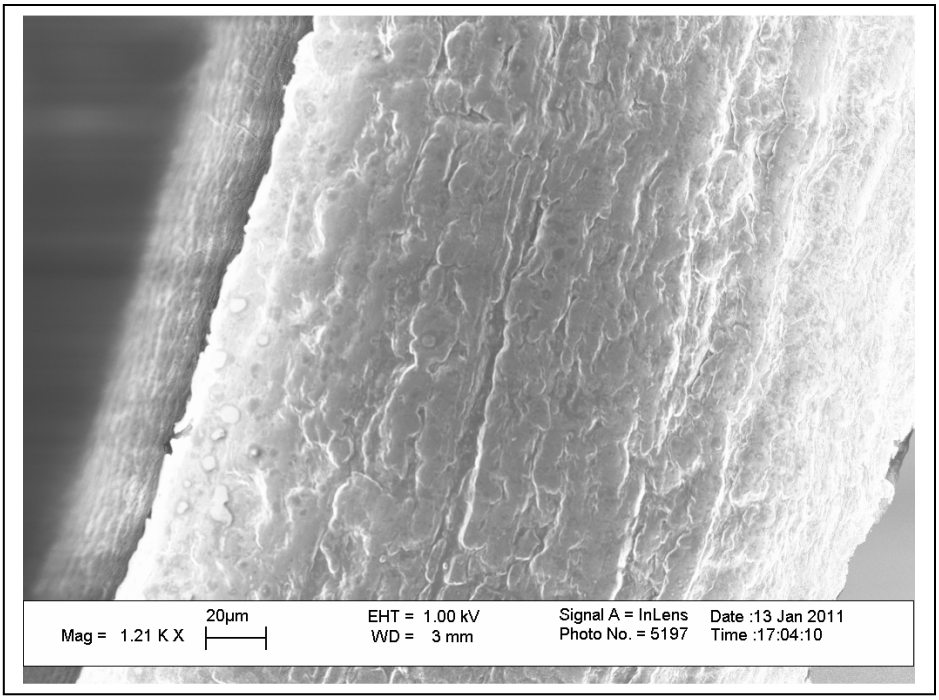

(a)

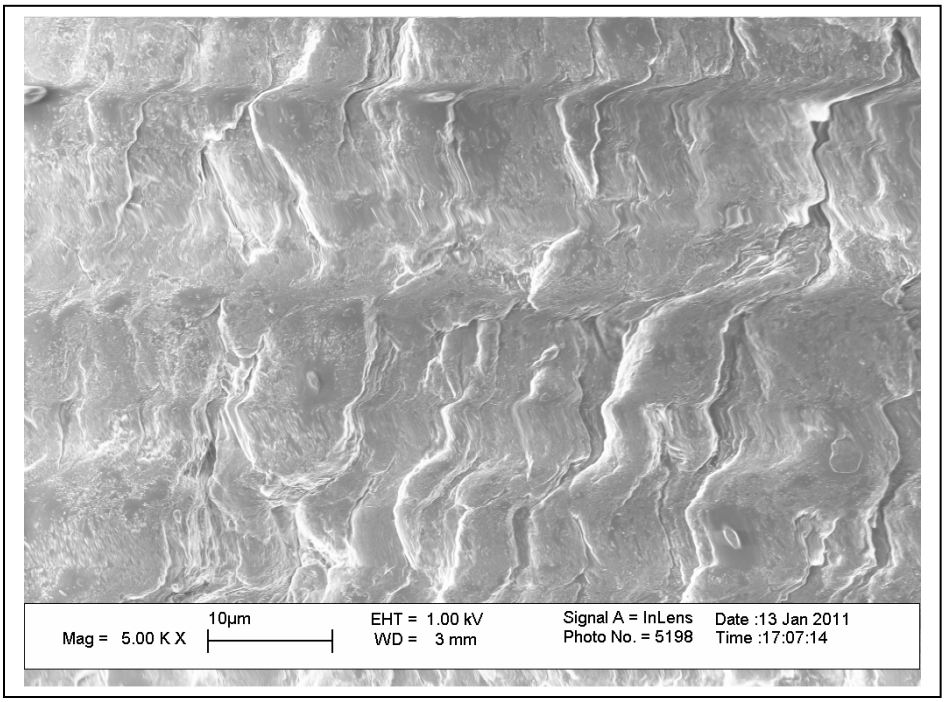

(b)

Figure 3.16 SEM micrographs showing the (a) structure of wall of PTFE hollow fiber M at lower 1.0 KX (b) structure of wall at 5.0 KX.

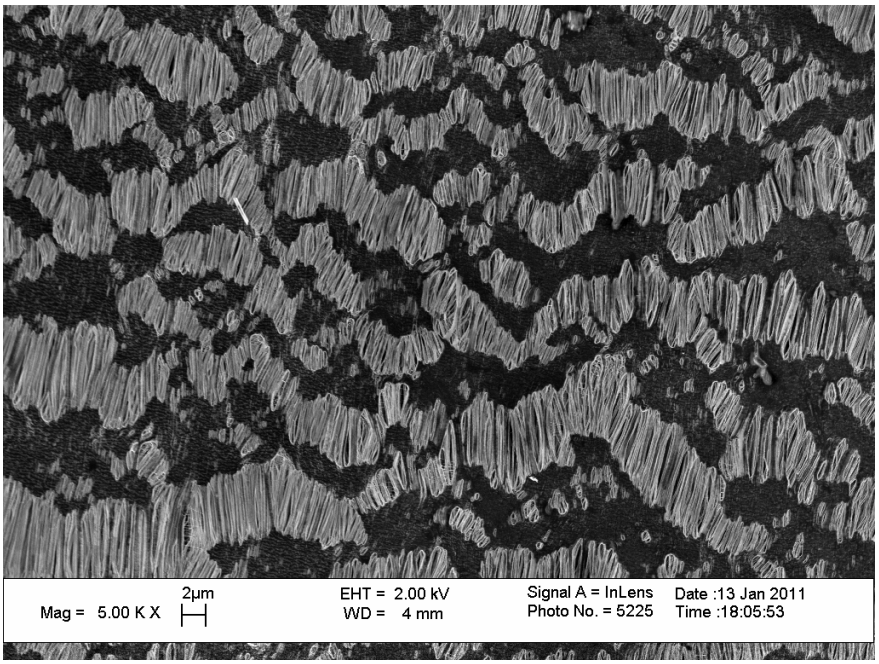

(a)

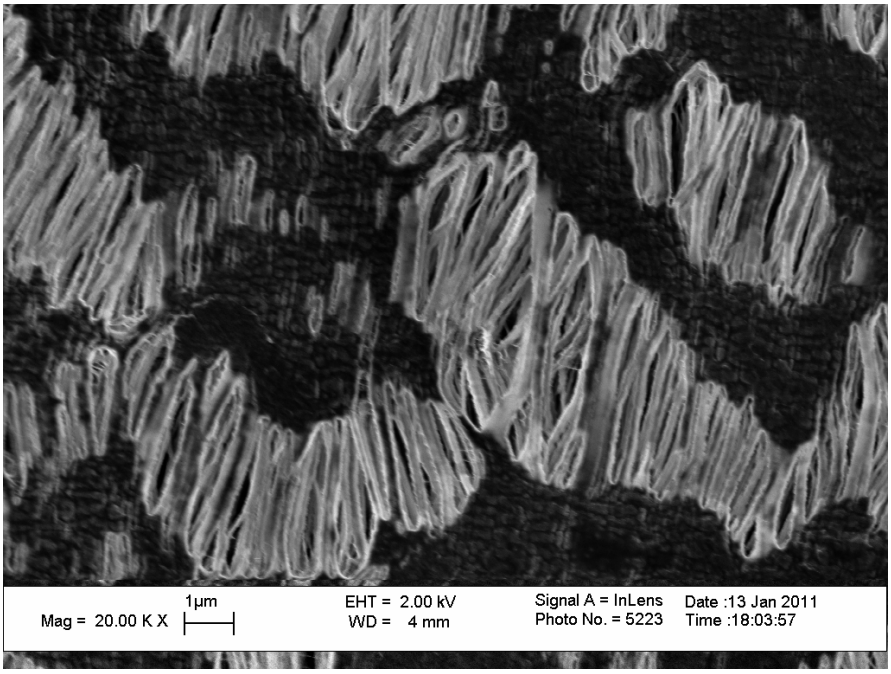

(b)

Figure 3.17 SEM micrographs showing the inner surface of PTFE hollow fiber M (a) at 5.0 KX (b) at 20.0 KX.

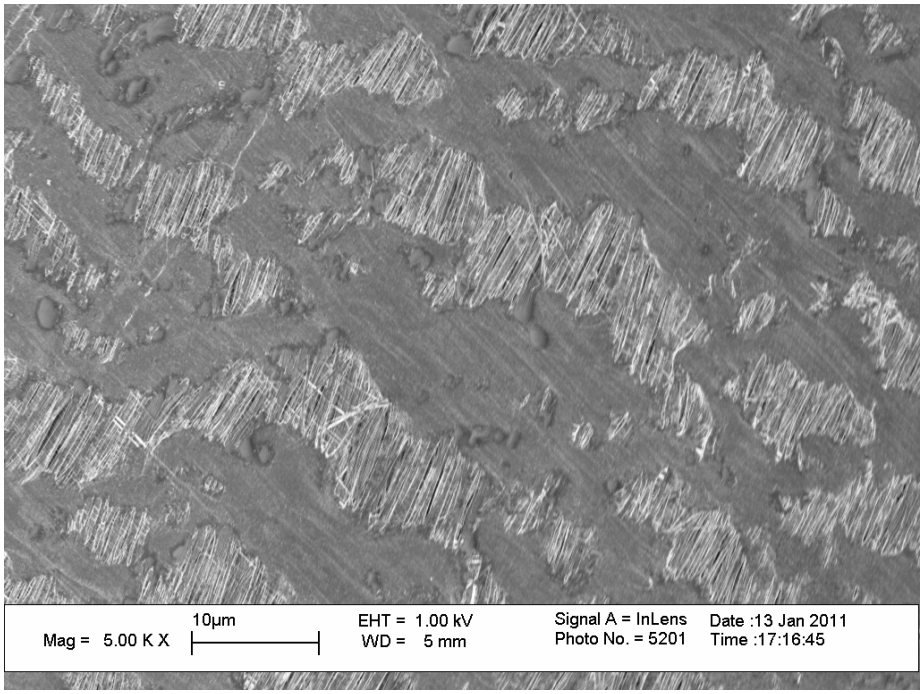

(a)

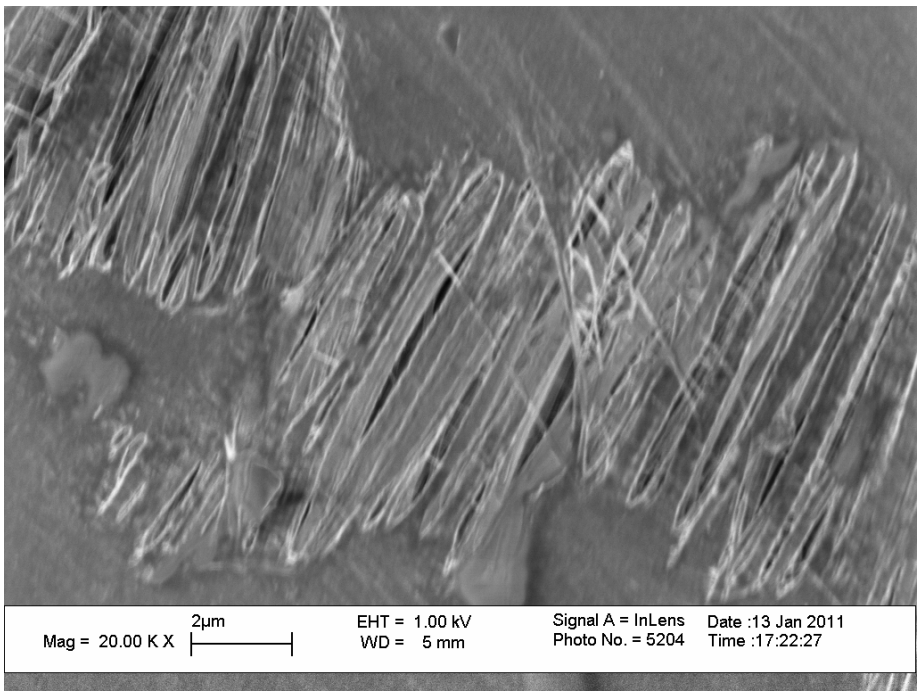

(b)

Figure 3.18 SEM micrographs showing the outer surface of PTFE hollow fiber M (a) at 5.0 KX (b) at 20.0 KX.

A module containing porous PTFE hollow fiber membranes (procured from Markel Corporation, Plymouth Meeting, PA) was fabricated at NJIT. The details of the hollow fibers are as follows; O.D.= 1.94 mm, I.D.= 1.53 mm, fiber wall porosity = 0.5 and average pore size = 0.24 μm. The effective length of the module = 20.5 cm, number of fibers in module = 5 and effective area of the module = 46.12 cm^2 (based on I.D.). The PTFE membrane module was tested with 1% NaCl feed solution at lower temperature. The water vapor flux increased from 10.7 kg/m^2-hr to 21.0 kg/m^2-hr as temperature was increased for the feed solution from 85°C to 95°C (Figure 3.19). In all experiments, the distilled water inlet temperature was maintained around 20°C. The feed and distilled water flow rates were held constant at 450 ml/min. The results are summarized in Table 3.9. The conductivity on the distillate side was constant; this result signifies no leakage of salt to the distillate side.

Table 3.9 Performance of PTFE Hollow Fiber M Membrane with 1% NaCl Solution at Lower Temperatures

Brine Inlet T_{bi} (°C)	Brine Outlet T_{bo} (°C)	Distillate Inlet T_{di} (°C)	Distillate Outlet T_{do} (°C)	Brine In Flow Rate F_{bi} (ml/min)	Distillate In Flow Rate F_{di} (ml/min)	Water Vapor Flux (kg/m^2-hr)
85.1	79.5	20.0	24.7	450	450	10.7
90.0	84.0	19.9	25.5	450	450	16.9
95.0	89.0	20.0	24.7	450	450	21.0

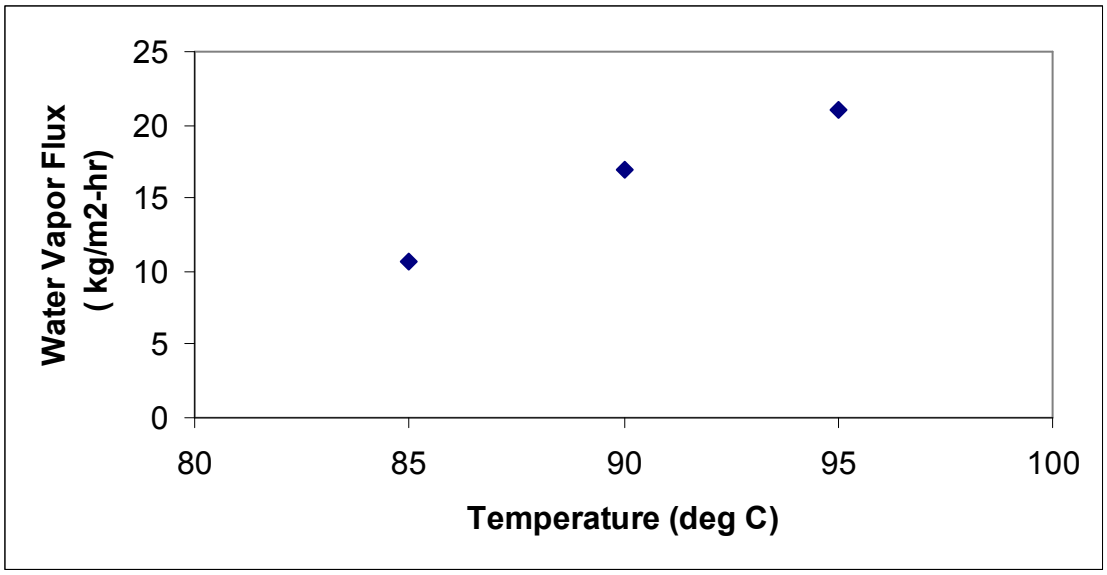

Figure 3.19 Change in water vapor flux with temperature for PTFE hollow fiber M membrane.

3.1.10 Experiments with PTFE Hollow Fiber N Membrane Module

The cross section, inner surface and outer surface of PTFE hollow fiber N were analyzed by SEM. For preparing the SEM sample, the fiber was dipped into liquid nitrogen to avoid any damage during its cutting. The SEM micrograph in Figure 3.20 revealed the tortuous path along the wall of fiber N. The porous nature of PTFE fiber can be visualized from SEM micrograph of fiber's surface in Figure 3.21 and Figure 3.22. It is clear from the SEM images that the inner surface has more number of pores than the outer surface of the fiber illustrating the asymmetric nature of the fiber N.

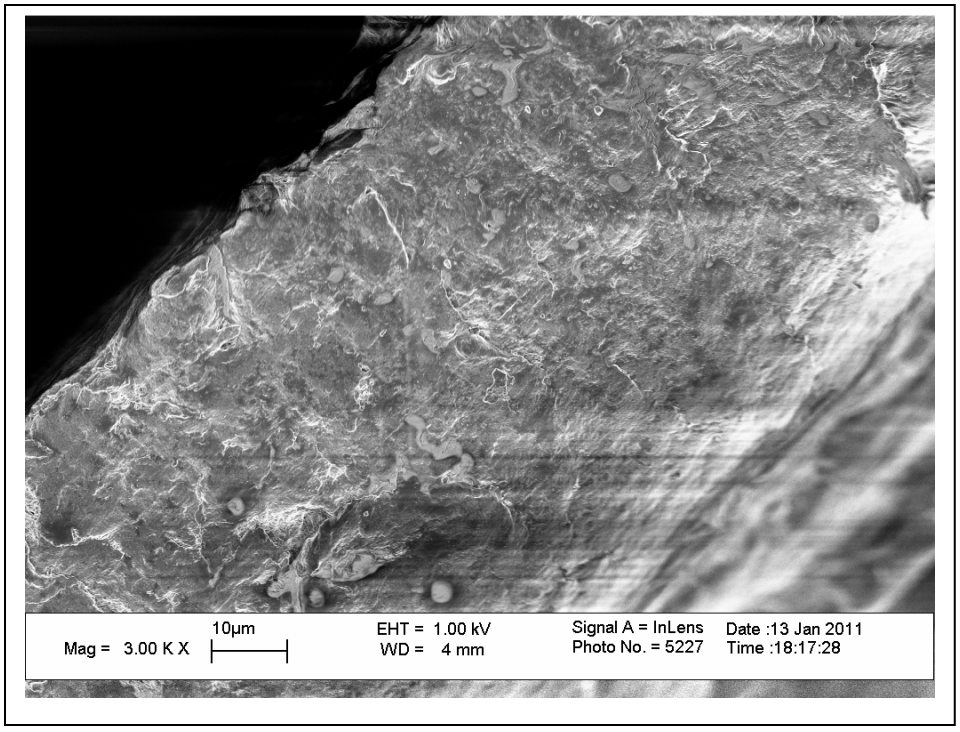

(a)

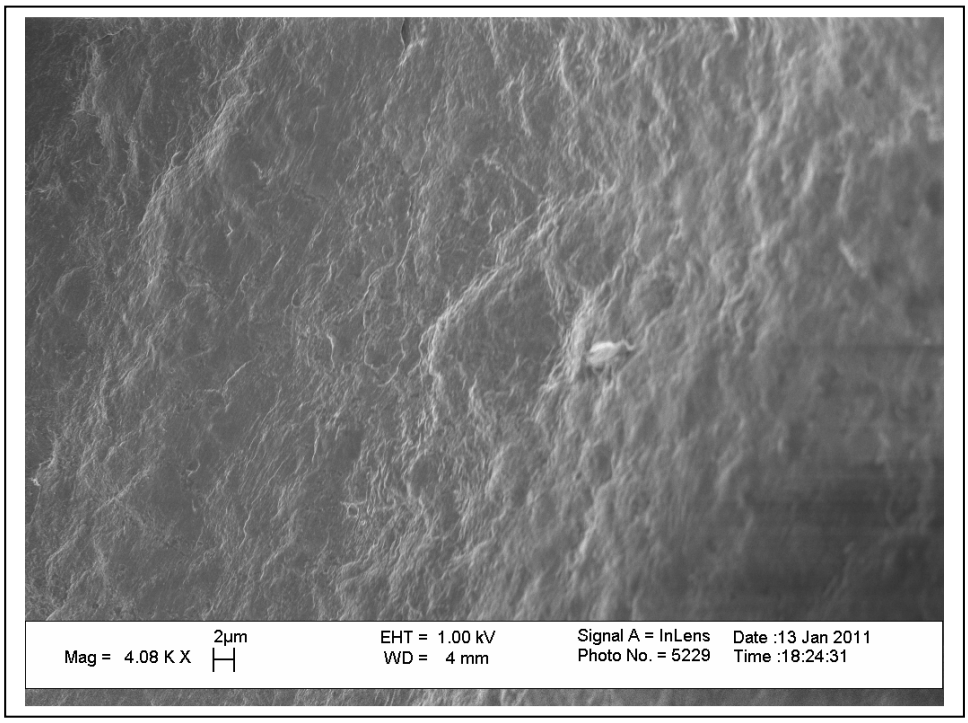

(b)

Figure 3.20 SEM micrographs showing the structure of wall of PTFE hollow fiber N (a) at lower 1.0 KX (b) structure of wall at 5.0 KX.

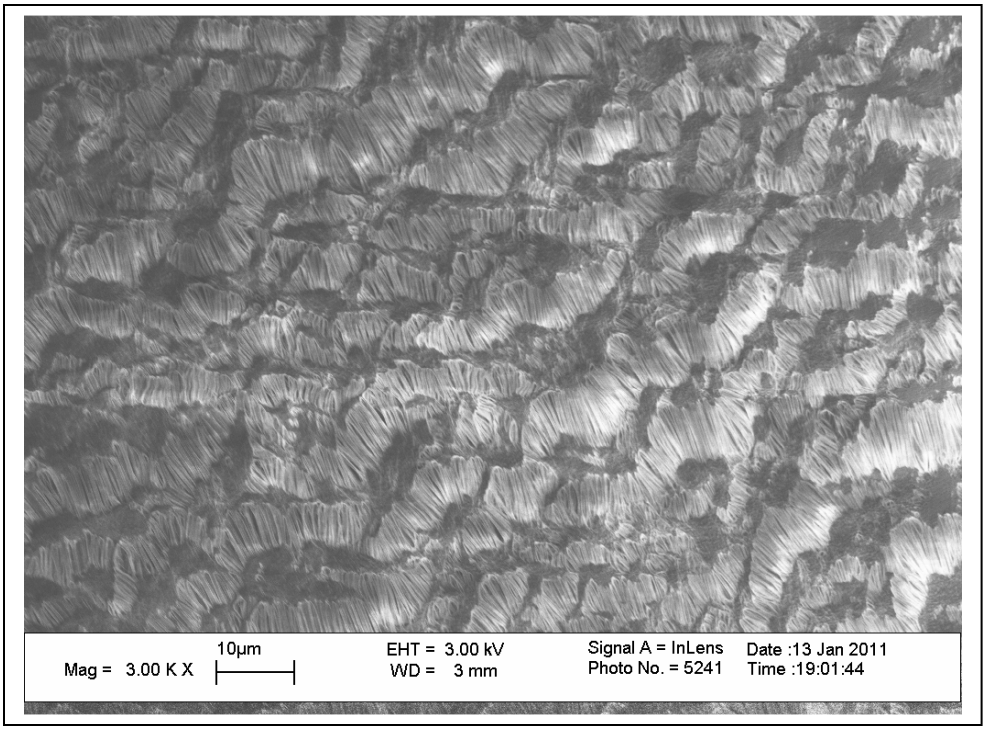

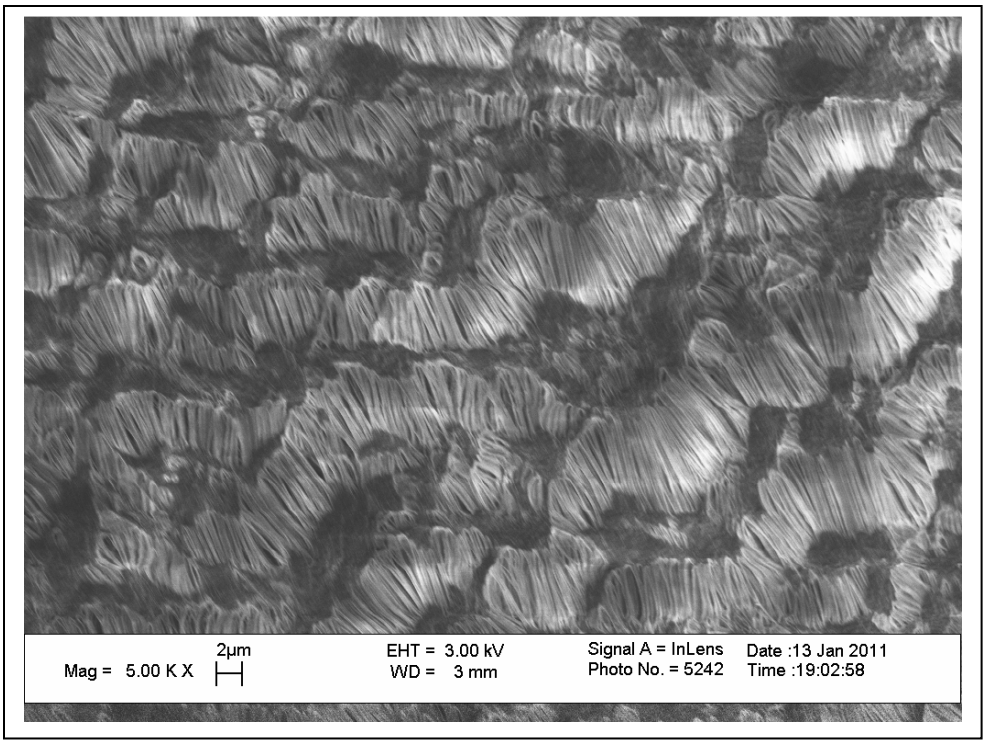

Figure 3.21 SEM micrographs showing the inner surface of PTFE hollow fiber N (a) at 3.0 KX (b) at 5.0 KX.

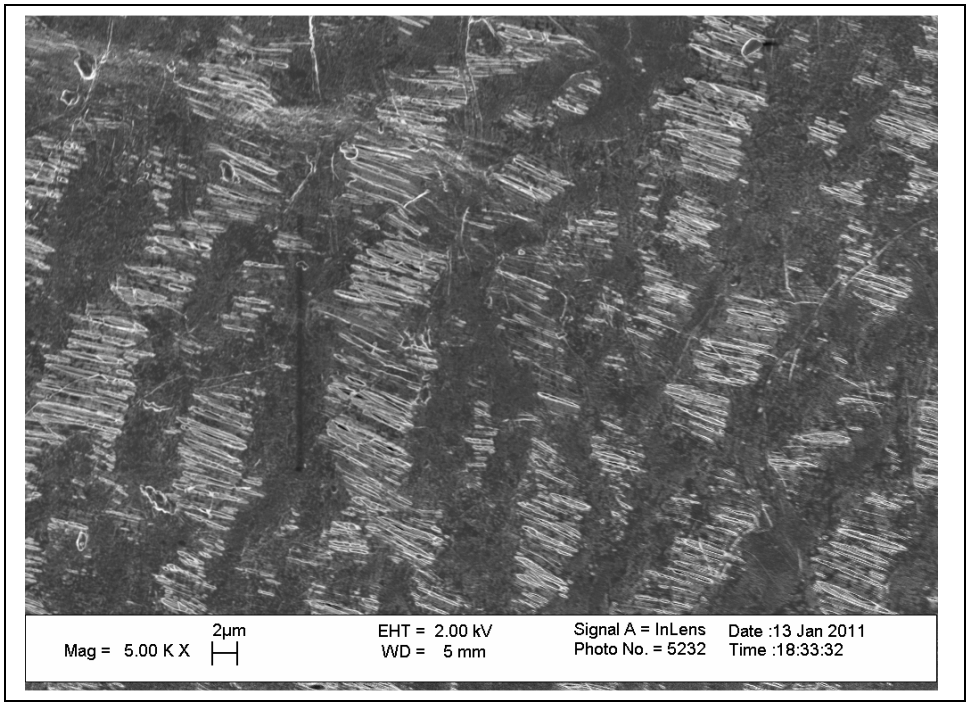

(a)

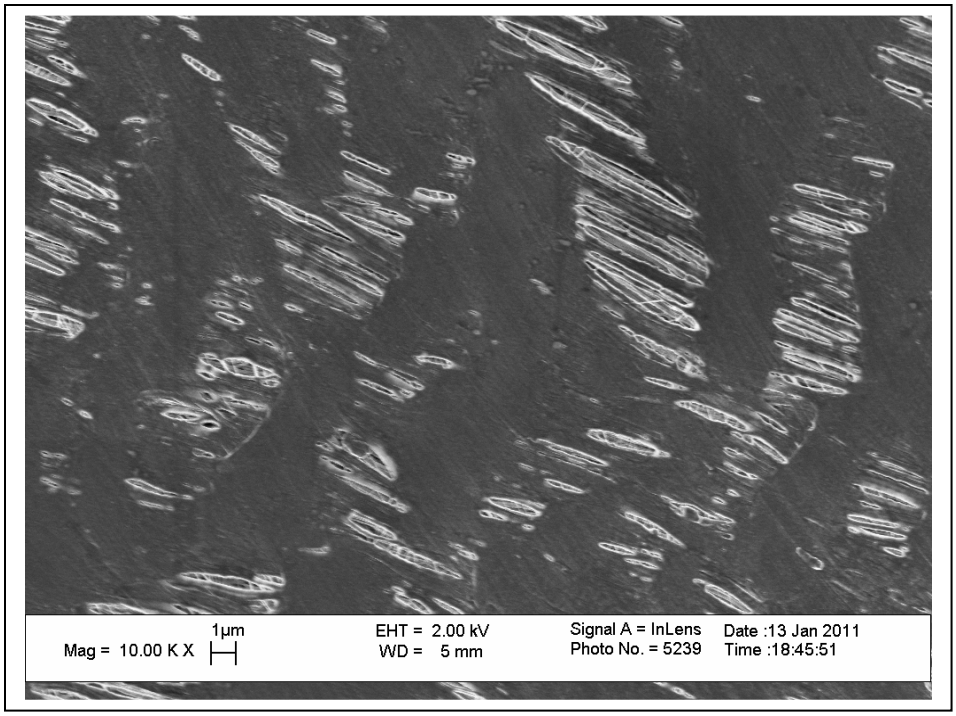

(b)

Figure 3.22 SEM micrographs showing the outer surface of PTFE hollow fiber N (a) at 5.0 KX (b) at 10.0 KX.

Another module was fabricated using porous PTFE hollow fiber N membranes (Markel Corporation, Plymouth Meeting, PA 19462) at NJIT. The details of the hollow fibers are as follows; O.D.= 1.92 mm, I.D.= 1.51 mm, fiber wall porosity = 0.47 and average pore size = 0.27 μm. The effective length of the module = 20.5 cm, number of fibers in module = 2 and effective area of the module = 19.45 cm^2 (based on I.D.). The PTFE membrane module was tested with 1% NaCl feed solution at lower brine temperatures. The water vapor flux increased from 6.8 kg/m^2-hr to 15.0 kg/m^2-hr as temperature was increased for the feed solution from 85°C to 95°C (Figure 3.23). In all experiments, the distilled water inlet temperature was maintained around 20°C. The feed and distilled water flow rates were held constant at 450 ml/min. The results are summarized in Table 3.10. The conductivity on the distillate side was constant indicating no salt leakage.

Table 3.10 Water Vapor Flux of PTFE Hollow Fiber N Membrane with 1% NaCl Solution at Lower Temperatures

Brine Inlet T_{bi} (°C)	Brine Outlet T_{bo} (°C)	Distillate Inlet T_{di} (°C)	Distillate Outlet T_{do} (°C)	Brine In Flow Rate F_{bi} (ml/min)	Distillate In Flow Rate F_{di} (ml/min)	Water Vapor Flux (kg/m^2-hr)
85.2	82.9	20.0	21.9	450	450	6.8
90.0	87	20.0	22.0	450	450	10.7
95.0	91.8	20.1	22.4	450	450	15.0

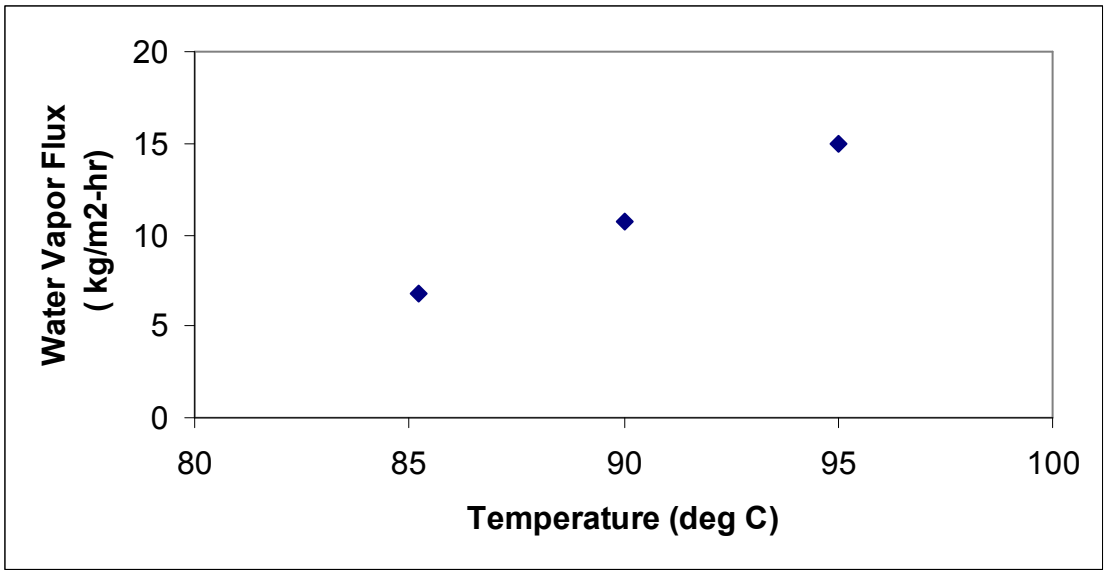

Figure 3.23 Change in water vapor flux with temperature for 1 % NaCl solution for PTFE hollow fiber N membranes.

3.1.11 Experiments with PTFE Hollow Fiber P Membrane Module

Another PTFE hollow fiber membrane module from AMT (Minnetonka, MN) which incorporated 29 PTFE hollow fibers type P of 0.53 mm x 1.08 mm. The effective length of the module = 43 cm, number of fibers in module = 29 and effective membrane area of the module = 207 cm^2 based on I.D. Experiments were performed with 1% NaCl feed solution and results are summarized in Table 3.11. The water vapor flux increased from 0.28 kg/m^2-hr to 0.86 kg/m^2-hr as temperature of 1% NaCl feed solution was increased from 85^oC to 95^oC. The flux values are low due among others to lower pore size and lower porosity. The feed and distillate water flow rates were held constant at 450 ml/min. No salt leakage was observed.

Table 3.11 Performance of PTFE Hollow Fiber P with 1% NaCl Solution at Lower Temperatures

Brine Inlet T_{bi} (^oC)	Brine Outlet T_{bo} (^oC)	Distillate Inlet T_{di} (^oC)	Distillate Outlet T_{do} (^oC)	Brine In Flow Rate F_{bi} (ml/min)	Distillate In Flow Rate F_{di} (ml/min)	Water Vapor Flux (kg/m^2-hr)
85.3	72.4	20.4	33.6	450	450	0.28
90.3	77.9	20.3	34.6	450	450	0.36
94.7	84.5	22.1	36.2	450	450	0.86

3.2. DCMD Experiments with 1 % NaCl Solution at Higher Temperatures

All high temperature experiments were performed in the set up designed for high temperature and high pressure DCMD.

3.2.1. Experiments with PTFE Flat Sheet Membrane

Experiments were carried out with the same PTFE flat sheet membrane at higher temperatures using 1% NaCl feed solution. The water vapor flux was found to be very high as the temperature was increased up to 110^{o}C. But, results were inconsistent and questionable. Reproducibility was poor. Our method for calculation of water vapor flux is based on the difference in flow rates of distillate out and distillate in. Since, the area of the membrane in test cell (Figure 3.24) is around 9 cm^2, the change in flow rate between distillate out and distillate in was quite small. The results are summarized in Table 3.12.

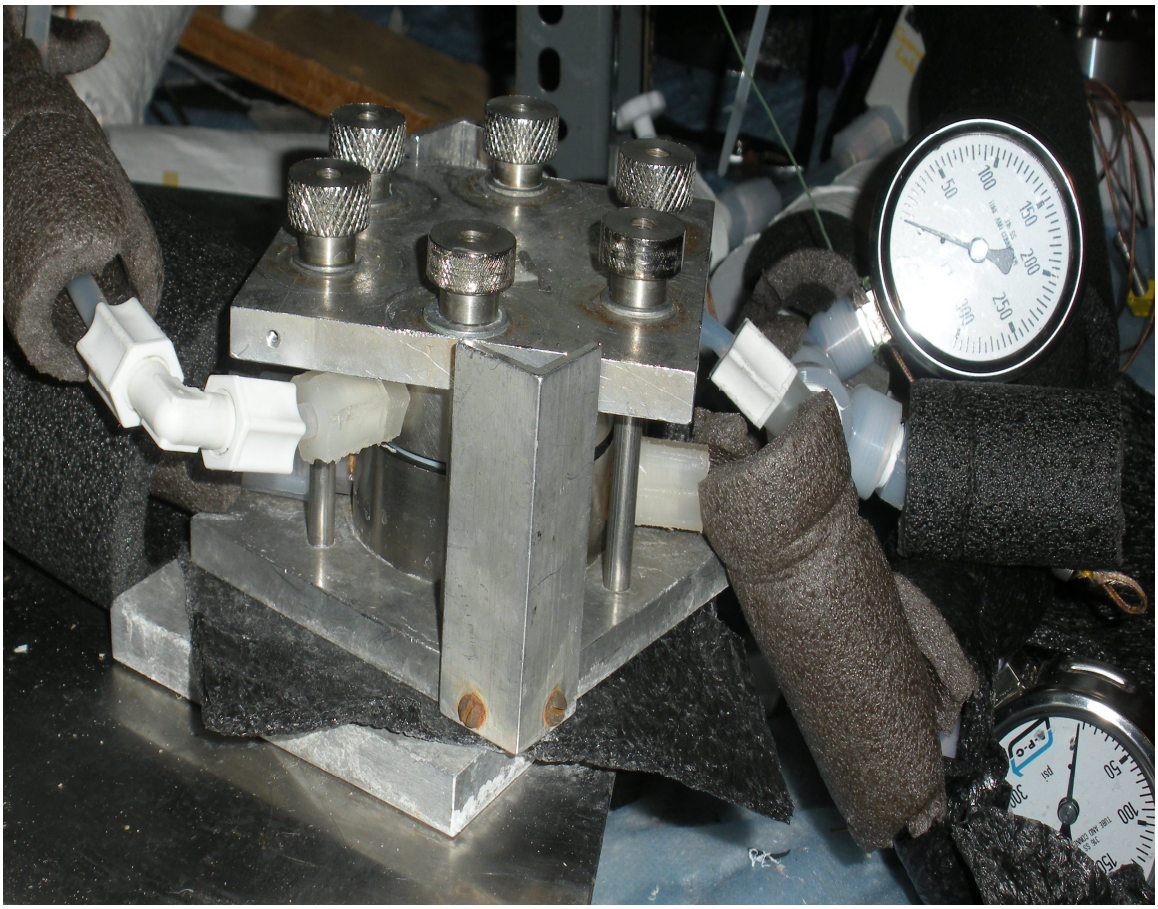

Figure 3.24 Photograph of a single cell having a membrane area of 9 cm^2.

Table 3.12 Performance of PTFE Flat Sheet Membranes with 1% NaCl Solution using One Small Cell at Higher Brine Temperatures

Brine Inlet T_{bi} (^oC)	Brine Outlet T_{bo} (^oC)	Distillate Inlet T_{di} (^oC)	Distillate Outlet T_{do} (^oC)	Distillate In Flow Rate F_{di} (ml/min)	Distillate Out Flow Rate F_{do} (ml/min)	Change in Distillate Flow Rate (ml/min)	Water Vapor Flux (kg/m^2-hr)
95.7	90.6	19.7	33.9	483.30	484.46	1.16	77.0
95.8	90.5	19.9	33.7	482.81	483.99	1.18	77.9
96.54	91.36	20.8	34.84	511.65	512.51	0.86	57.1
97.4	89.83	21.8	35.61	504.31	505.03	0.72	47.3
97.73	90.71	20.8	35.3	510.73	511.58	0.85	55.9
99.42	91.32	20.8	35.03	510.73	512.51	1.78	117.7
100.6	94.67	20.8	35	508.89	512.04	3.15	208.1
102.7	96.55	21.1	35.4	508.89	512.04	3.15	208.1
109.9	99.94	20.7	35.2	480.85	484.46	3.61	238.6
110.2	99.95	20.8	35.4	481.34	484.94	3.60	237.7

As can be observed from Table 3.12 (rows 3 and 10), a change in flow rate of 0.86 ml/min corresponds to 57.1 kg/m^2-hr water vapor flux and change in flow rate of 3.59 ml/min corresponds to 237 kg/m^2-hr water vapor flux. This very small change in distillate flow rate is observed due to the small area of the membrane. There was considerable variation from experiment to experiment. Due to this reason, the results were inconsistent and questionable. Therefore experiments were carried out using two cells in series to increase the membrane area as shown in Figure 3.25. The change in distillate flow rate was significantly higher. The results are summarized in Table 3.13.

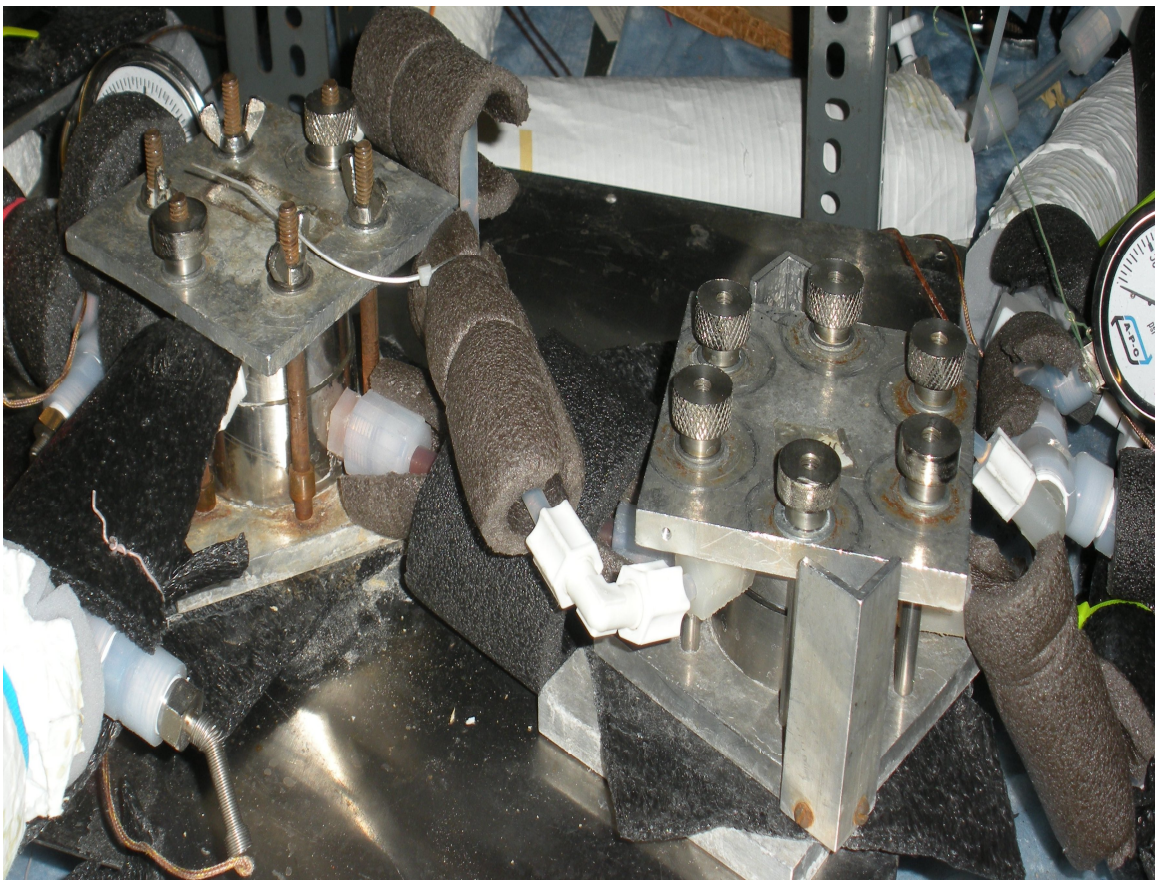

Figure 3.25 Photograph of two cells in series having area of 20.4 cm^2.

Table 3.13 Performance of PTFE Flat Sheet Membranes with 1% NaCl Solution using Two Small Cells in Series at Higher Brine Temperatures

Brine Inlet T_{bi} (^oC)	Brine Outlet T_{bo}(^oC)	Distillate Inlet T_{di} (^oC)	Distillate Outlet T_{do}(^oC)	Distillate In Flow Rate F_{di} (ml/min)	Distillate Out Flow Rate F_{do} (ml/min)	Change in Distillate Flow Rate (ml/min)	Water Vapor Flux (kg/m^2-hr)
106.8	97.6	23.1	37.5	566.37	571.78	5.41	159.2
107.3	98.1	23.2	37.5	566.85	572.22	5.37	158.0
108	98.2	23.3	37.6	567.81	573.56	5.75	168.9
110.5	99.1	22.7	39.3	544.19	550.00	5.81	170.9
111.2	99.3	23.4	40.1	542.75	551.78	9.03	265.6
111.5	99.5	23.7	40.6	544.19	553.11	8.92	262.3
112.5	99.6	24.1	41.0	544.19	553.56	9.37	275.4
113.9	99.7	24.1	41.3	545.16	555.34	10.18	299.3

It is clear from Table 3.13, that the difference between the flow rates of the outgoing distillate stream and incoming distillate stream is more than 5 ml/min, which provided more consistent and reliable data than the results using only one cell. The consistency and reproducibility in results will be more prominent with an increase in the membrane area, which was achieved by a cell having a very large membrane area.

3.2.2. Experiments with PVDF Flat Sheet Membrane

Experiments were also performed with PVDF flat sheet membrane with 1% NaCl solution at higher temperatures in the same arrangement where two cells were put in series to increase the effective total area of the membrane. This provided a more accurate measurement of the change in flow rate of distillate out stream and distillate in stream. The flat PVDF membranes were procured from Millipore Corporation having a pore size 0.1 μm and effective diameter 32 mm. The results are summarized in Table 3.14.

Table 3.14 Performance of PVDF Flat Sheet Membranes with 1% NaCl Solution using Two Small Cells in Series at Higher Brine Temperatures

Brine Inlet T_{bi} (^oC)	Brine Outlet T_{bo} (^oC)	Distillate Inlet T_{di} (^oC)	Distillate Outlet T_{do} (^oC)	Distillate In Flow Rate F_{di} (ml/min)	Distillate Out Flow Rate F_{do} (ml/min)	Change in Distillate Flow Rate (ml/min)	Water Vapor Flux (kg/m^2-hr)
112.7	110	23.8	37.3	616.0	621.1	5.1	150
112.4	109.6	23.8	37.4	616.5	622.2	5.7	166.8
115.3	107	22.8	36.4	614.1	620.1	6.0	176.5
121	112.3	23.1	39.5	534.6	542.9	8.3	245.2
122.5	113.5	24.1	40.5	535.5	544.7	9.2	269.2
123.4	114.3	25	41.4	535.0	544.2	9.2	270

3.2.3. Experiments with PTFE Flat Sheet Membranes in a Large Cell

To overcome previous problems encountered with the low area of the small test cell, experiments were performed in a large test cell shown in Figure 3.26. The cell has a 6 mm thick stainless steel disc to support the PTFE membrane. This large cell was originally used as a pervaporation cell (model PTC-6, Carbone Lorraine, Salem, VA) and obtained from GFT, Neunkirchen-Heinitz, Germany. The gasket diameter of the cell was 12.8 cm and the effective membrane area in the cell was 128.67 cm^2. Such a large cell was necessary to generate enough vapor flux to reproducibly measure a large enough change in the distillate flow rate.

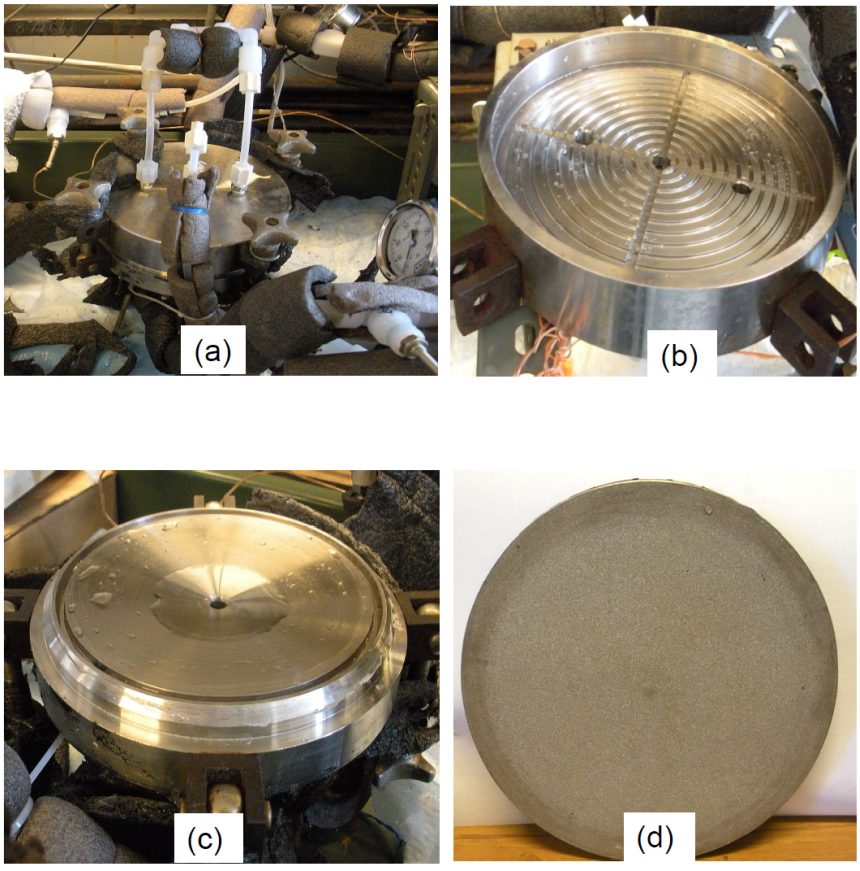

Figure 3.26 Photographs of (a) large cell used for experiments (b) top of the cell (c) bottom of cell (d) 6 mm thick stainless steel support for the membrane.

Experiments were carried out with PTFE flat sheet membrane (procured from W. L. Gore & Associates) using 1 % NaCl feed solution. All experiments were performed in the set up designed for high temperature and high pressure DCMD. On one side of the membrane, hot solution of 1% (by wt) NaCl was introduced as the brine feed; the other side of the membrane was exposed to deionized water at a low temperature as the distillate stream condensing the water vapor. Hot 1 % NaCl solution was pumped over one side of the membrane at 500 ml/min; the permeate side of the membrane was exposed to cold distilled water at a flow rate of around 500 ml/min at temperatures of 25^{o}C to 30^{o}C. As can be observed from Figure 3.27, the water vapor flux increased from 74.6 kg/m^2-hr to 195 kg/m^2-hr, as feed solution temperature was increased from 95^{o}C to 128^{o}C. As before, the method for calculation of water vapor flux is based on the difference in flow rates of the distillate out and the distillate in. Since the area of the membrane is around 128.6 cm^2, the change in flow rate between distillate out and distillate in was quite large. It is clear from Table 3.15, that the change in the distillate in and the distillate out flow rate is more than 25 ml/min at the higher temperatures; this provided much more consistent and reliable data than the results using only one small cell and two small cells in series, where the effective area of the membrane was 9 cm^2 and 20 cm^2 respectively. Even at the high temperature of 128^{o}C, no pore wetting phenomenon was observed; there was no increase in the conductivity of the distillate side water.

Table 3.15 Performance of PTFE Flat Sheet Membranes with 1% NaCl Solution using the Larger Cell at Higher Brine Temperatures

Brine Inlet T_{bi} (^oC)	Brine Outlet T_{bo} (^oC)	Distillate Inlet T_{di} (^oC)	Distillate Outlet T_{do} (^oC)	Distillate In Flow Rate F_{di} (ml/min)	Distillate Out Flow Rate F_{do} (ml/min)	Change in Distillate Flow Rate (ml/min)	Water Vapor Flux (kg/m^2-hr)
94.8	88.2	18.7	22.2	507	523	16	74.6
110.7	102.3	21.8	34.3	509	532	23	107.2
113.1	107.7	24.3	37.2	510	535	25	116.6
115.2	105.3	27.4	39.8	508	537	29	135. 2
118.8	114.6	29.3	42.7	507	538	31	144. 6
119.9	115.6	30	44.2	505	539	34	158. 5
123.9	118.39	29.4	42.1	536	575	39	181.9
124.3	119.6	29.5	42.3	536	575	39	181.9
124.8	119.6	29.6	43.1	516	554	38	177.2

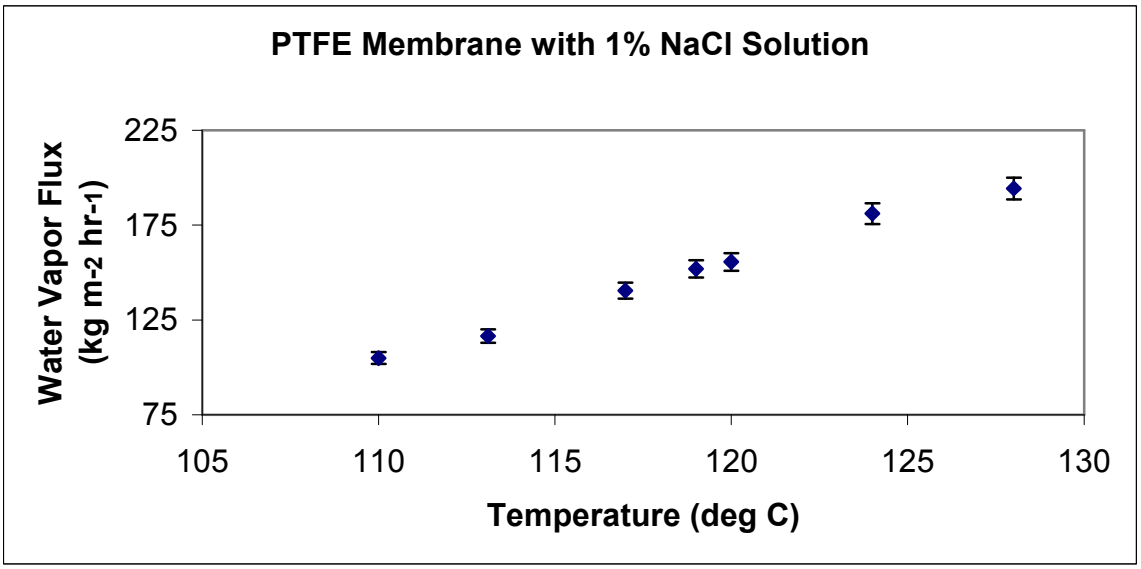

Figure 3.27 Variation of water vapor flux with temperature for 1% NaCl feed solution in higher temperature and higher pressure DCMD set up for PTFE flat sheet membrane.

Water vapor flux in the membrane distillation process is driven by water vapor pressure difference across the membrane; it can be described as follows:

$$J = C\,\Delta P = C\,(P_f - P_p) \qquad (3.1)$$

The proportionality constant C, a mass transfer coefficient, is determined by membrane properties like porosity, tortuosity, pore size, material and morphology of surface, etc. Although C, the membrane mass transfer coefficient, is dependent on temperature and pressure, in many cases it is approximately constant, which was also observed in the present system (Figure 3.28).

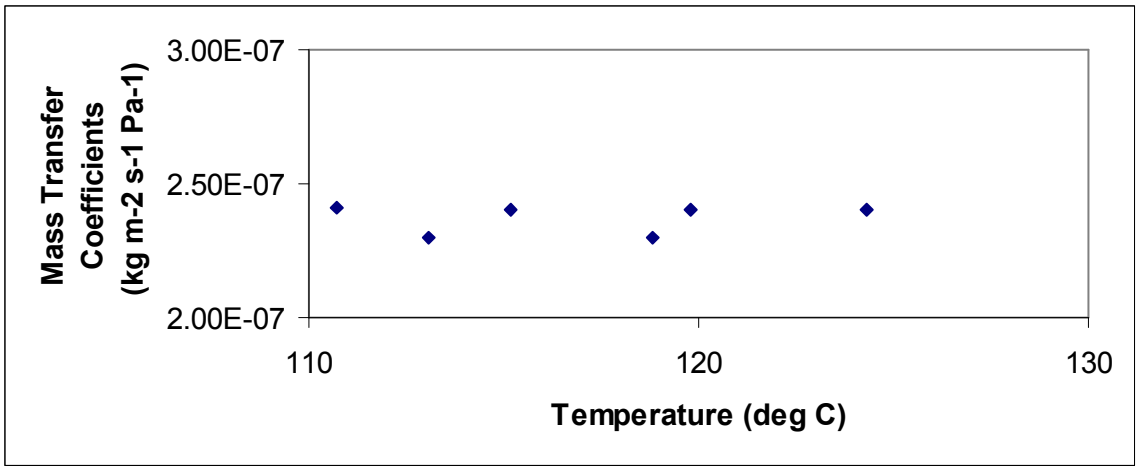

Figure 3.28 Variation of water vapor mass transfer coefficient with temperature of feed brine in DCMD experiment for PTFE flat sheet membrane.

The transmembrane water vapor pressure difference, ΔP, equal to the difference of feed side water vapor pressure P_f and the permeate side water vapor pressure P_p, is the driving force for water vapor transfer. The value of P_p was estimated at the average of inlet and outlet distilled water temperatures; the maximum temperature difference between the inlet and the outlet was 30°C. The enhancement in water vapor flux with temperature is a consequence of the exponential vapor pressure rise according to Antoine equation

$$P = \exp\left(23.238 - \frac{3841}{T_m - 45}\right) \tag{3.2}$$

Here P is the vapor pressure of water vapor in Pa and T_m is the temperature in K. Using values of water vapor pressure, theoretical values of water vapor pressure difference across the membrane were plotted against different values of brine temperature for fixed

temperature difference across the membrane in Figure 3.29. Experimentally, also the exponential growth in transmembrane vapor pressure difference and correspondingly the exponential growth in water vapor flux with temperature rise on feed side were observed; see Figure 3.30. Such trends have been reported in other desalination studies for lower temperature ranges [58, 59].

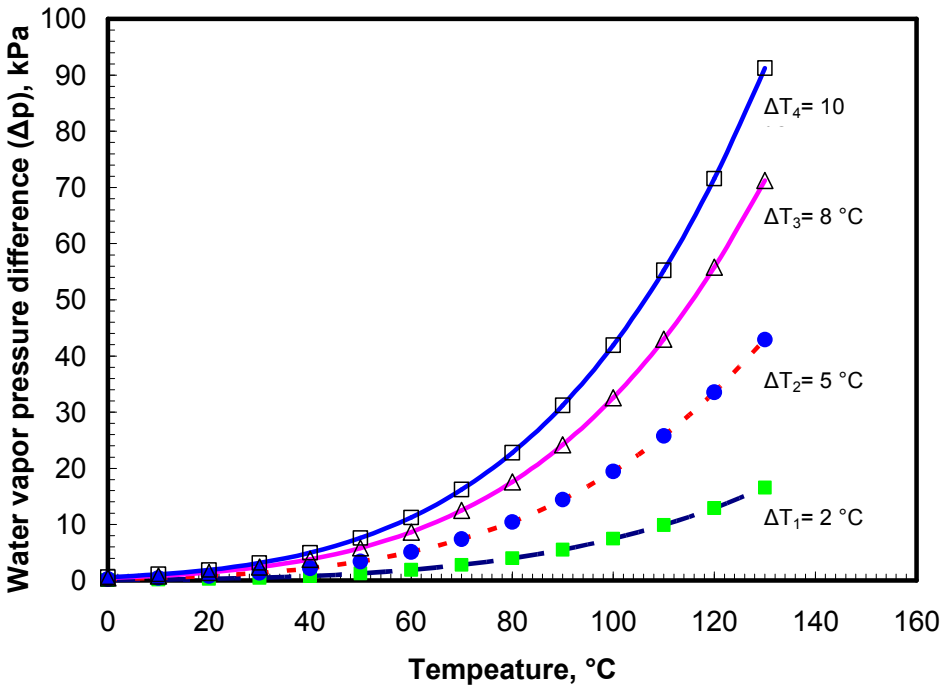

Figure 3.29 Water vapor pressure difference at different values of feed water temperature for fixed temperature difference across the membrane.

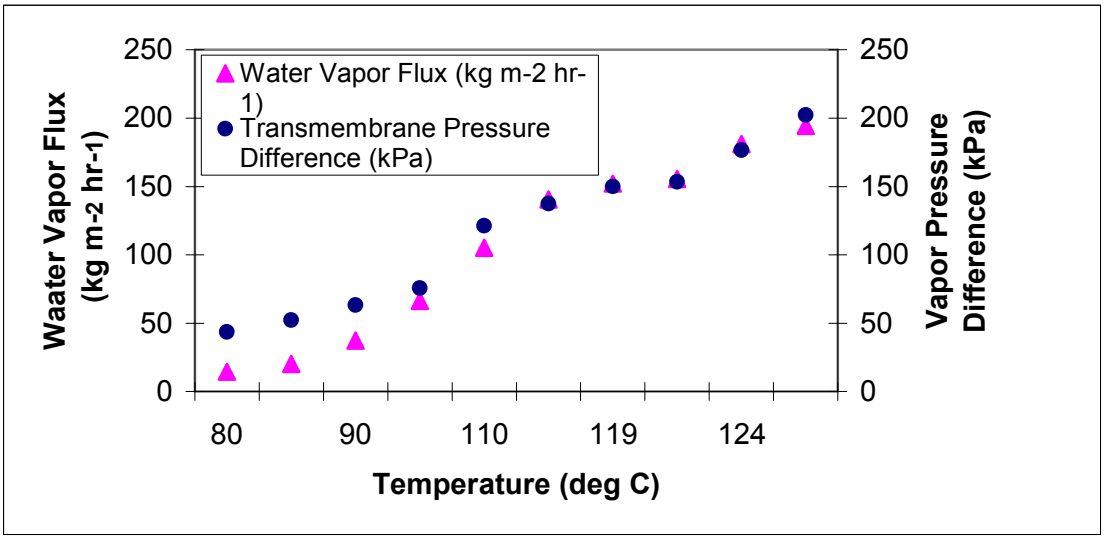

Figure 3.30 Water vapor flux and water vapor pressure difference across two sides of porous PTFE flat sheet membrane at different hot brine temperatures.

The effect of brine flow rate on water vapor flux for 1 % NaCl solution was studied at different temperatures of brine (Figure 3.31); it was observed that as the flow rate of brine was increased from 50 ml/min to 850 ml/min; there was no significant change in the value of water vapor flux. This behavior is potentially the result of the special design of the cell on the brine side. From Figure 3.32 and Figure 3.33, it is clear that the cell on the brine side is not completely flat in shape rather it has a depth of 1.6 cm in the center of the cell which gradually reduces towards the periphery of the cell; this stagnation flow creates enough turbulence on the brine side reducing the effect if any of temperature polarization.

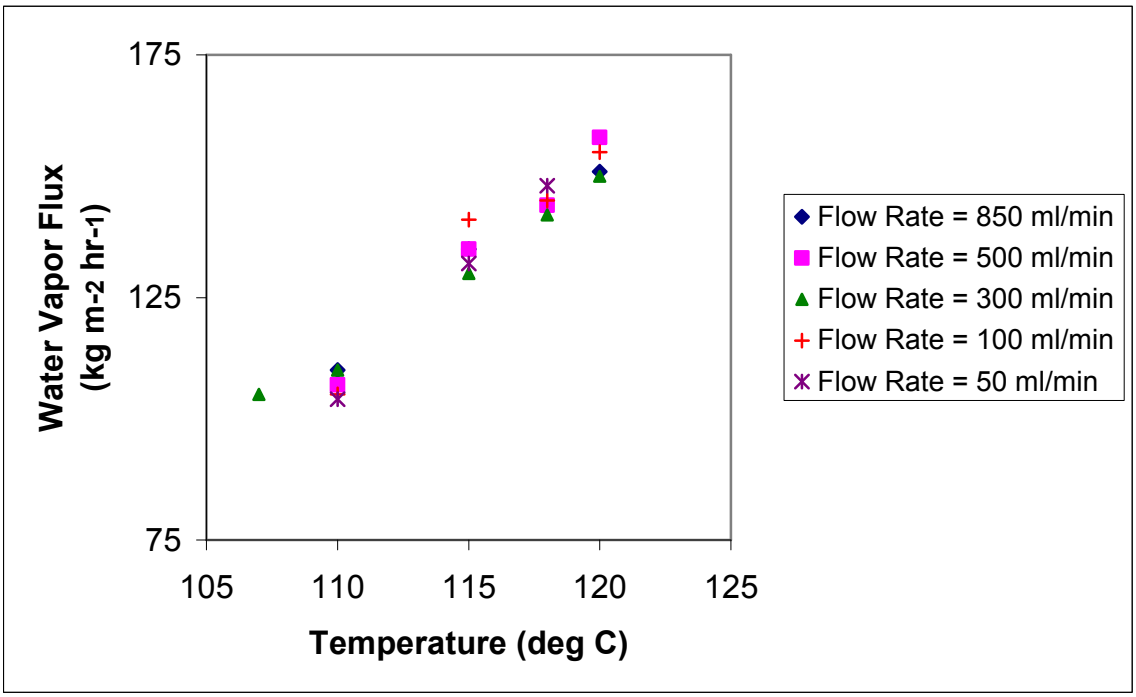

Figure 3.31 Variation of water vapor flux with different flow rates of 1% NaCl feed solution in higher temperature and higher pressure DCMD set up for PTFE flat sheet membrane.

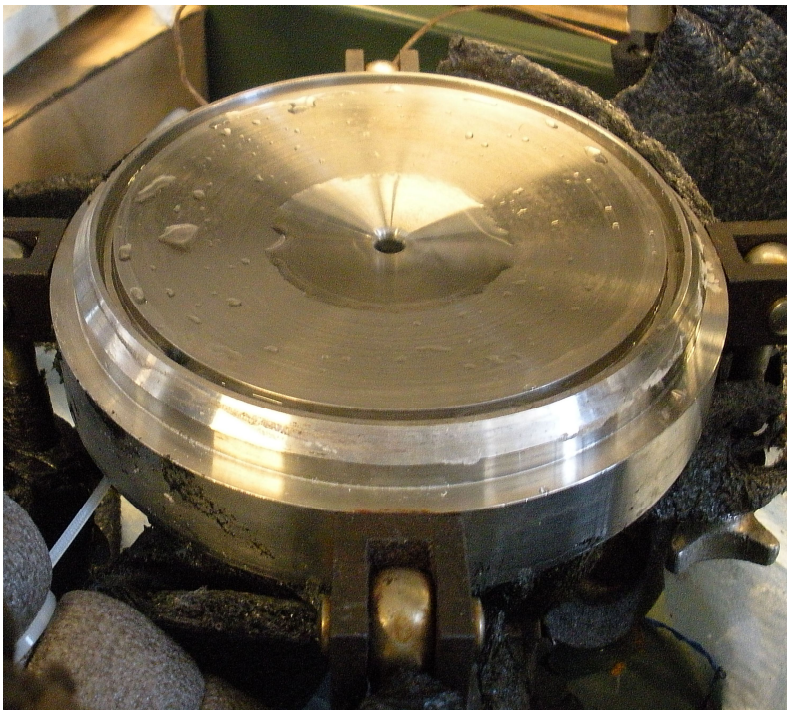

Figure 3.32 Photograph of the brine side of the big cell used for the experiments.

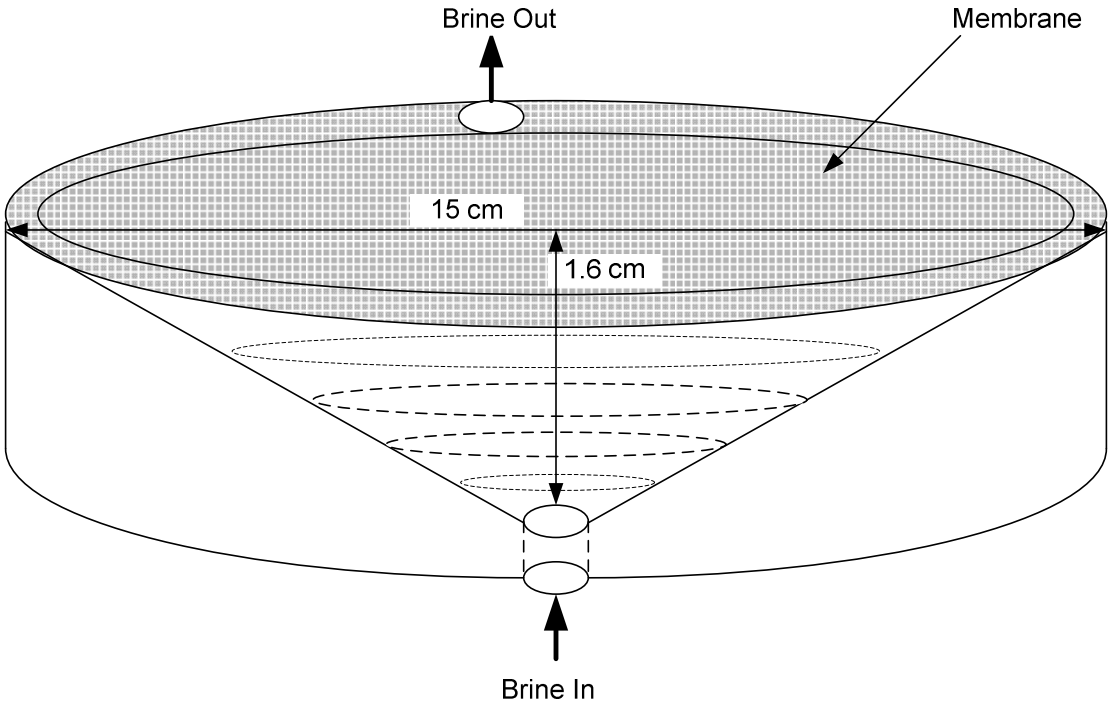

Figure 3.33 Schematic diagram of the brine side of the big cell used for the experiments.

The presence of sodium chloride in the feed will cause the reduction in vapor pressure on feed side; causing the reduction in driving force across the membrane. The vapor pressure, P_f^o, for pure water feed can be calculated from the interfacial temperature using Antoine equation. In the presence of a non-volatile solute, the vapor pressure on feed side can be calculated as follows:

$$P_f = \gamma\left(1 - x_m\right) P_f^o \tag{3.3}$$

Where, γ is the activity coefficient and x_m is the mole fraction of solute at the interface. The effect of salt concentration on water vapor flux with PTFE flat sheet membrane was studied at different temperatures for varying salt concentrations in the higher temperature

and higher pressure DCMD setup (Figure 3.34). It was observed that as the salt concentration of brine was increased from 0.1 % to 3.5 %; there was no significant change in the value of water vapor flux. But, for a salt concentration of 10% on brine side, there was slightly lower water vapor flux than the flux obtained for salt concentration up to 3.5 %.

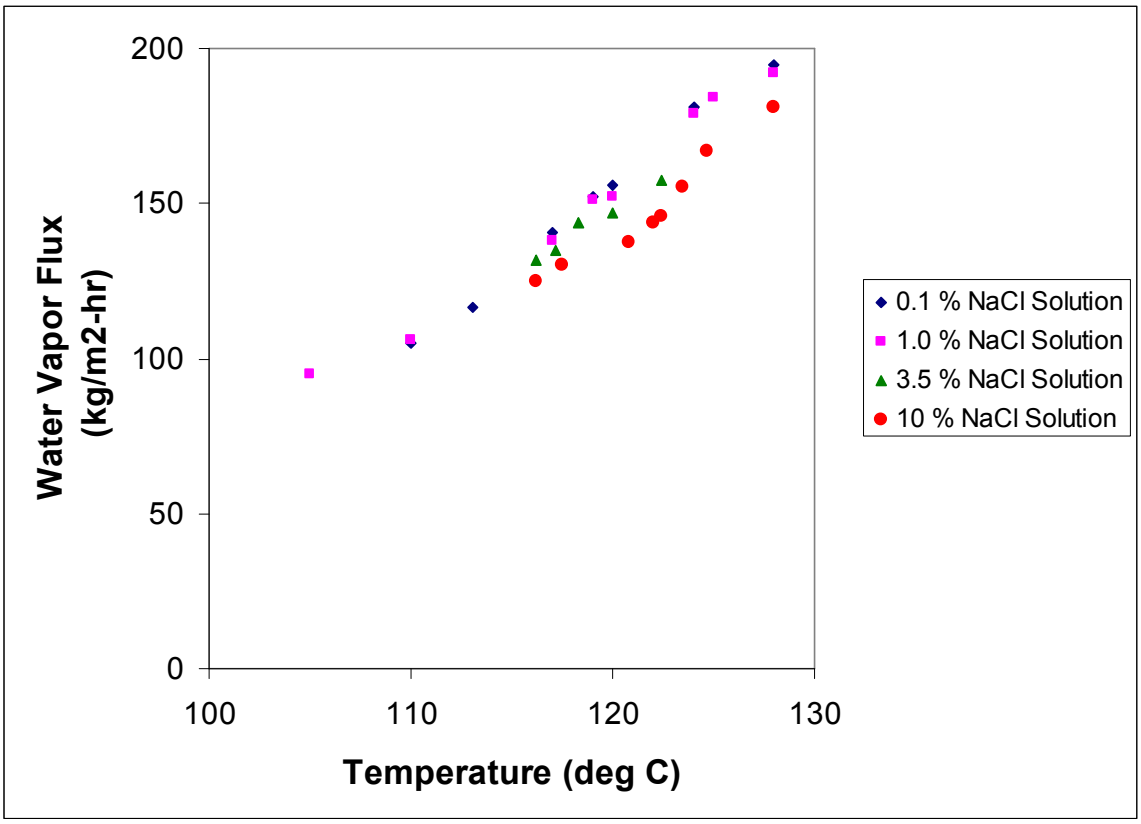

Figure 3.34 Variation of water vapor flux with different concentrations of NaCl in feed solution in higher temperature and higher pressure DCMD set up for PTFE flat sheet membrane.

Experiments were performed with PTFE flat sheet membrane for 1% NaCl solution at different temperatures of the incoming distillate stream. For a brine feed solution at 119^{o} C, as distillate in temperature was increased from 32^{o} C to 48^{o} C, water vapor flux decreased from 149 kg/m^{2}-hr to 131 kg/m^{2}-hr (Figure 3.35). Similarly, for a

brine feed solution at 126° C, as distillate in temperature was increased from 29° C to 45° C, water vapor flux decreased from 184 kg/m^2-hr to 170 kg/m^2-hr (Figure 3.36). Drop in water vapor fluxes are attributed to the corresponding drop in water vapor pressure across the membrane, causing a drop in the driving force across the membrane.

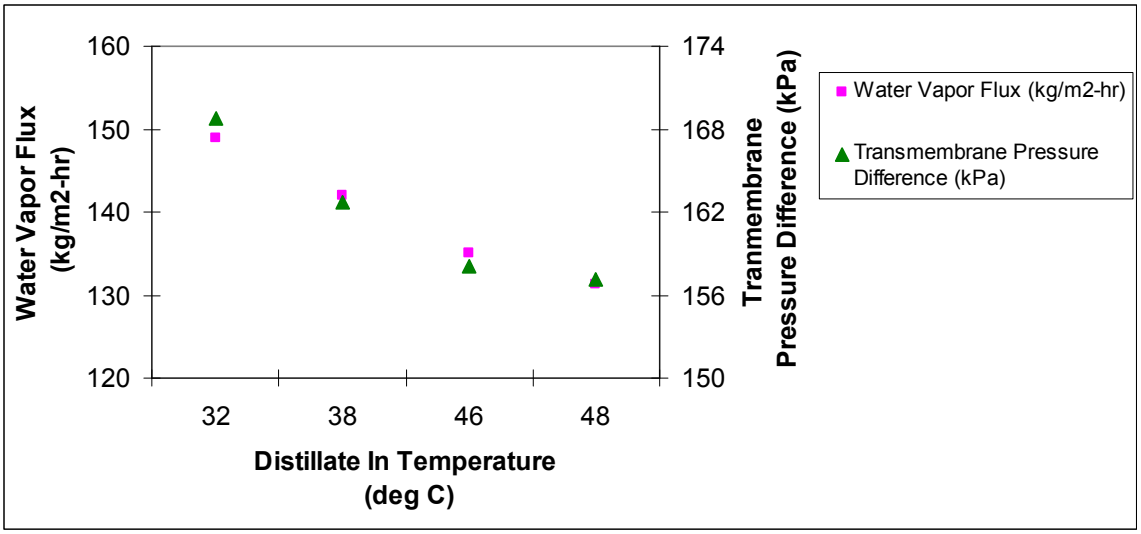

Figure 3.35 Effect of distillate in temperature on water vapor flux for 1% NaCl solution at temperature of 119°C for PTFE flat sheet membrane.

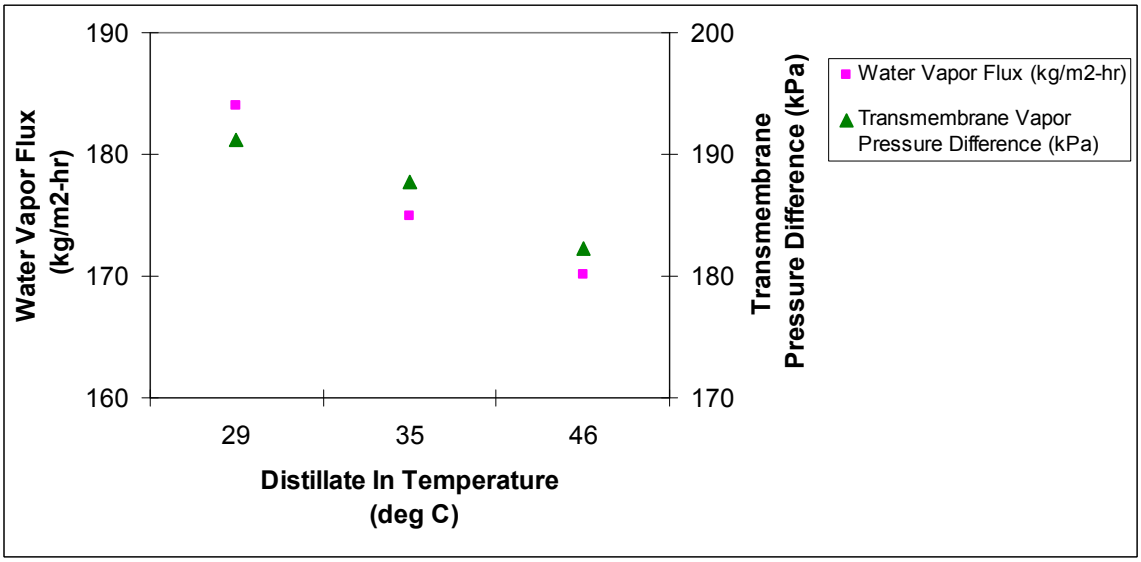

Figure 3.36 Effect of distillate in temperature on water vapor flux for 1% NaCl solution at temperature of 126°C for PTFE flat sheet membrane.

3.2.4. Experiments with PVDF Hollow Fiber H Membrane Module

Experiments were carried out with 1% NaCl as feed solution for a PVDF hollow fiber membrane (procured from Hyflux Inc., Singapore)) having a pore size of 0.623 μm and porosity close to 0.50. The modules were fabricated at NJIT with an effective length of 20 cm, number of fibers, 5 and an effective area of 28.62 cm^2 (based on I.D.). Experiments were performed with PVDF hollow fiber membrane module at a higher brine temperature in the setup designed for the high temperature and high pressure DCMD experiments. Above 100^oC, conductivity on the distillate side (tube side) increased. Even at room temperature, water flowed from the lumen side to the shell side for a high flow rate of distillate. This is probably due to pore wetting. It is clear from the SEM micrograph (see Figure 3.37) that the sizes of some pores are larger than 5 μm. This membrane develops pore wetting due to these defects at high pressure resulting from higher temperature.

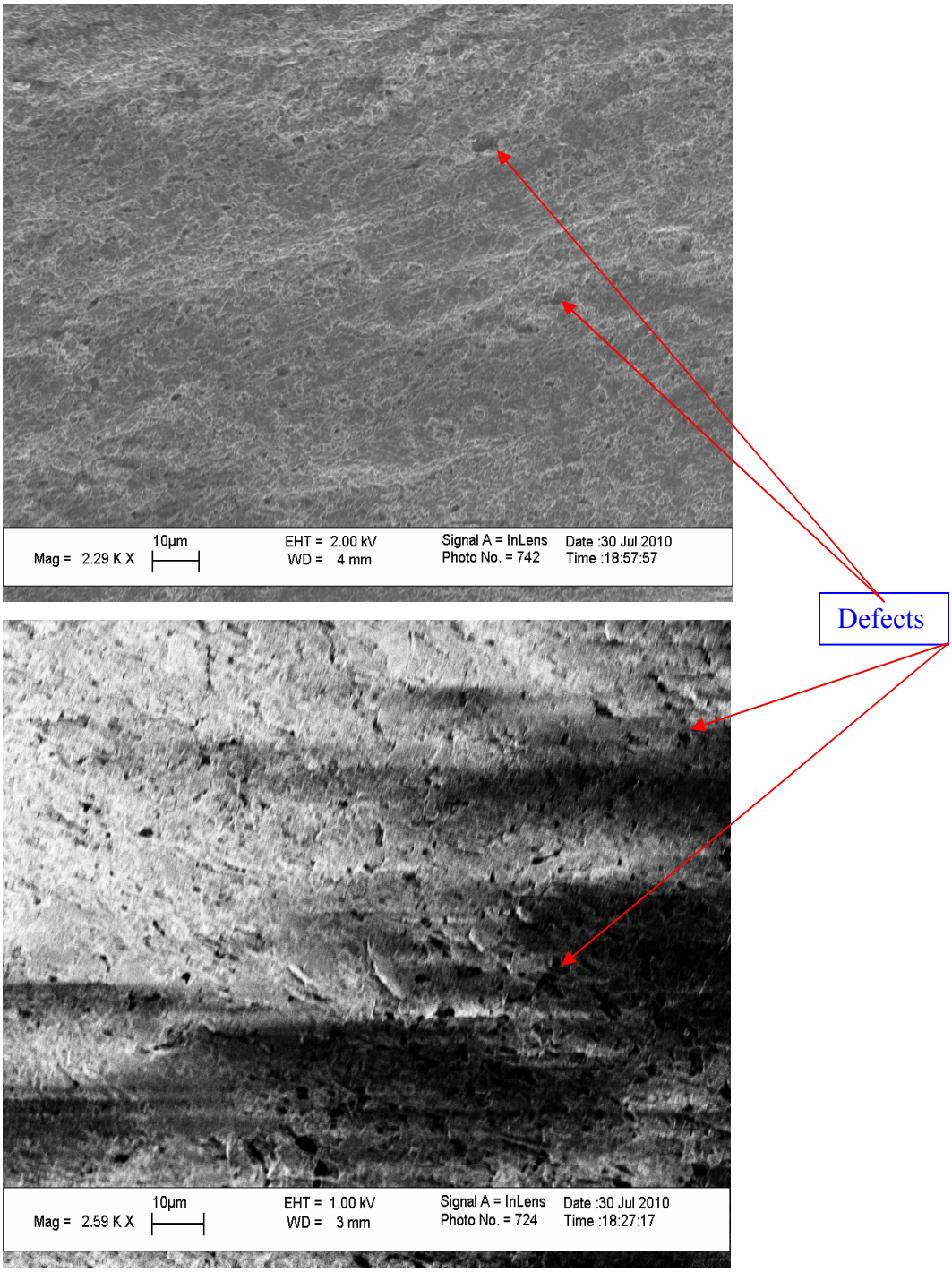

Figure 3.37 SEM micrographs showing the defects on surface of PVDF hollow fiber membrane causing the pore wetting.

3.2.5. Experiments with PVDF Hollow Fiber E Membrane Module

Experiments were carried out with 1% NaCl as feed solution for a PVDF hollow fiber E membrane having a pore size of 0.2 μm and porosity close to 0.54. The modules were fabricated at NJIT with an effective length of 19.2 cm, number of fibers, 9 and an effective area of 37.6 cm^2. The results in Figure 3.38, indicate that water vapor flux increased from 29 kg/m^2-hr to 88.5 kg/m^2-hr as the temperature of the feed brine solution was increased from 105°C to 124°C. The feed and distilled water flow rates were held constant at 500 ml/min and 250 ml/min, respectively. In all experiments, the distilled water inlet temperature was maintained at 20°C.

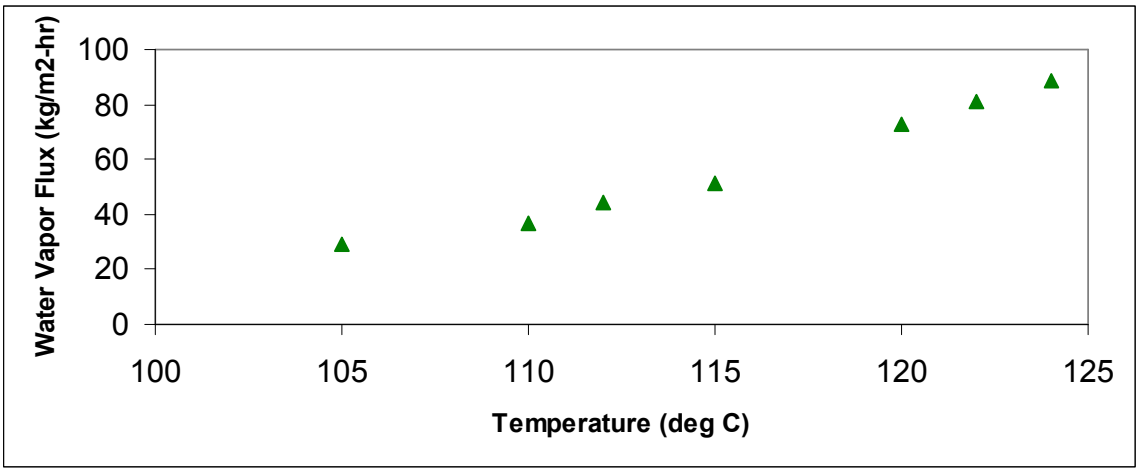

Figure 3.38 Variation of water vapor flux with temperature for 1% NaCl feed solution in higher temperature and higher pressure DCMD set up for PVDF hollow fiber E membrane.

3.2.6 Experiments with PTFE Hollow Fiber M Membrane Module at Higher Temperatures

A module was fabricated using porous PTFE hollow fiber membranes (procured from Markel Corporation, Plymouth Meeting, PA 19462) at NJIT. The details of the hollow fibers are as follows; O.D.= 1.94 mm, I.D.= 1.53 mm, fiber wall porosity = 0.5, average pore size = 0.24 μm; the effective length of the module = 20.5 cm, number of fibers in module = 5 and effective area of the module = 46.12 cm^2 based on I.D. Experiments were performed at both lower and higher temperatures. The module was employed at higher temperatures with hot 1% NaCl solution on shell side and cold distilled water on the lumen side. The results are summarized in Table 3.16 and Figure 3.39. It is clear from Figure 3.39 that the water vapor flux increased from 68 kg/m^2-hr to 115 kg/m^2-hr as the brine temperature was increased from 108^oC to 118^oC with constant conductivity on distillate side; above 118^oC the conductivity on the distillate side increased with time. The module was fabricated with a cyanoacrylate type adhesive, which softens at 118^oC. However, as the temperature was reduced, the distillate side conductivity increase stopped suggesting that the epoxy potting was affected by temperature in a reversible fashion.

Table 3.16 PTFE Hollow Fiber M with 1% NaCl Solution at Higher Temperature

Brine Inlet T_{bi} (^oC)	Brine Outlet T_{bo} (^oC)	Distillate Inlet T_{di} (^oC)	Distillate Outlet T_{do} (^oC)	Brine Inlet Pressure P_{bi} (psig)	Distillate In Flow Rate F_{di} (ml/min)	Distillate Out Flow Rate F_{do} (ml/min)	Change in Distillate Flow Rate (ml/min)	Water Vapor Flux (kg/m^2-hr)
108.3	105.1	25.0	29.0	10	469	473	4.0	68.0
110.6	107.5	25.4	34.2	10	542.7	548.4	5.7	75.7
112.4	108.5	25.3	30.3	12	465	472	7.0	98.4
117.8	114.3	23.4	32.6	14	539.7	548.4	8.7	115.5

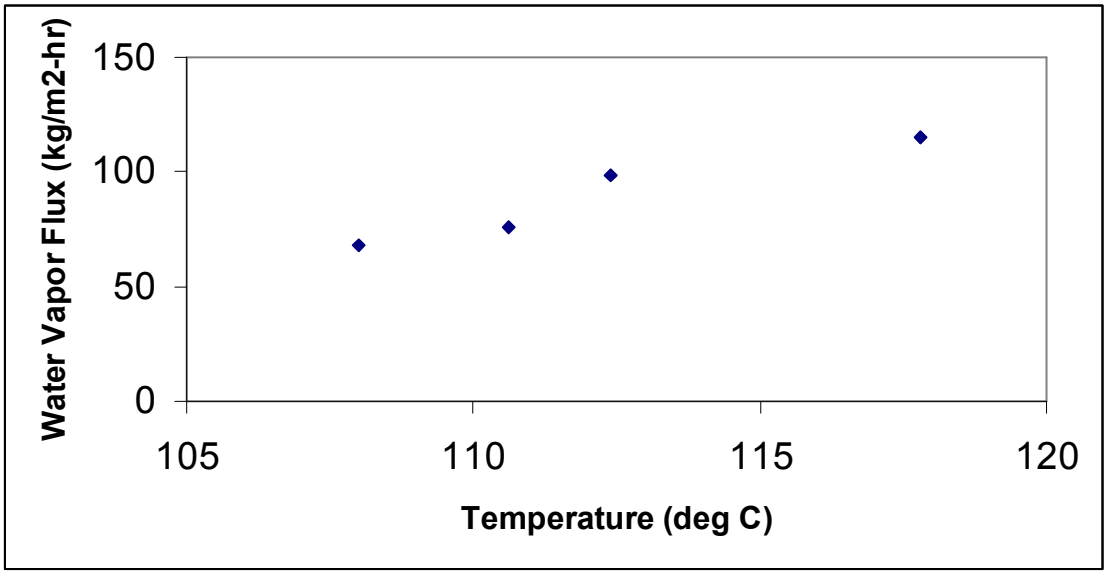

Figure 3.39 Variation of water vapor flux with temperature for 1% NaCl feed solution in higher temperature and higher pressure DCMD set up for PTFE hollow fiber M membrane.

The enhancement in water vapor flux with temperature is a consequence of the exponential vapor pressure rise according to Antoine equation (3.2). Experimentally also the exponential growth in transmembrane vapor pressure difference and correspondingly exponential growth in water vapor flux with temperature rise on feed side were observed for PTFE hollow fiber membrane modules in Figure 3.40 (and later in Figure 3.42).

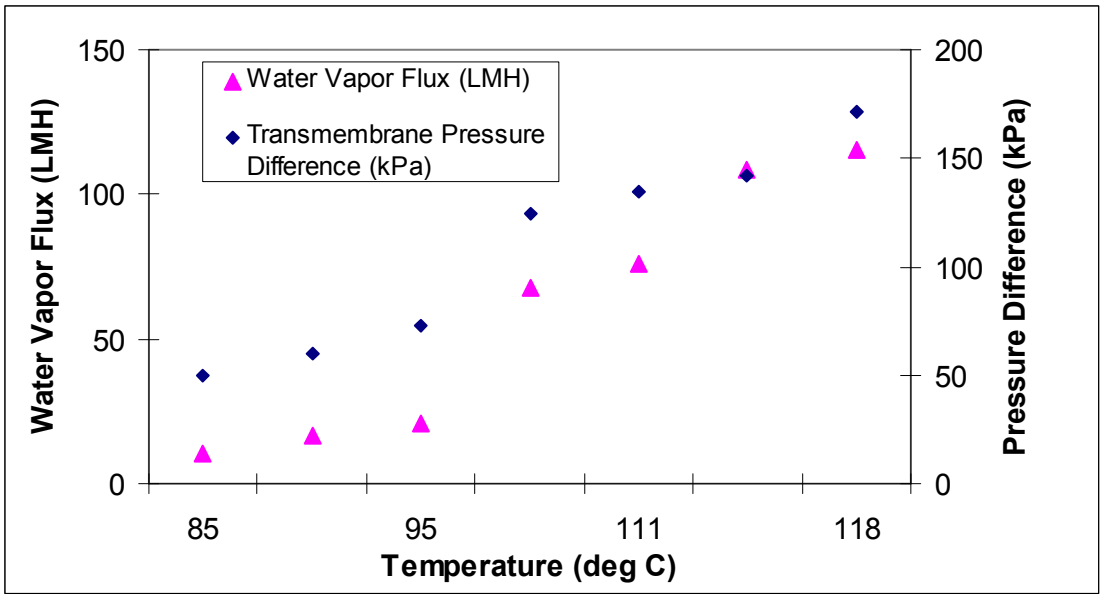

Figure 3.40 Water vapor flux and water vapor pressure difference across two sides of porous PTFE hollow fiber M membrane at different hot brine temperatures.

3.2.7 Experiments with PTFE Hollow Fiber N Membrane Module at Higher Temperatures

Another module was fabricated using porous PTFE hollow fiber N membranes (procured from Markel Corporation, Plymouth Meeting, PA 19462) at NJIT. The details of the hollow fibers are as follows: O.D.= 1.92 mm, I.D.= 1.51 mm, fiber wall porosity = 0.47 and average pore size = 0.27 μm; the effective length of the module = 20.5 cm, (19.8) number of fibers in module = 2 (5) and effective membrane area of the module = 19.45 (46.94) cm^2 based on I.D. Experiments were performed in higher temperature and higher pressure DCMD set up. Experiments were carried out with the same PTFE fiber membrane module at a high temperature of 1% NaCl feed solution. The results are summarized in Figure 3.41 and Table 3.17. The water vapor flux increased from 30.8 kg/m^2-hr to 97.6 kg/m^2-hr as temperature was increased from 108°C to 118°C with constant conductivity on distillate side, but above 118°C the conductivity on distillate

side increased with time because module was fabricated with cyanoacrylate type adhesive which softens at high temperature.

Table 3.17 Performance of PTFE Hollow Fiber N with 1% NaCl Solution at Higher Temperatures

Brine Inlet T_{bi} (^oC)	Brine Outlet T_{bo} (^oC)	Distillate Inlet T_{di} (^oC)	Distillate Outlet T_{do} (^oC)	Brine Inlet Pressure P_{bi} (psig)	Distillate In Flow Rate F_{di} (ml/min)	Distillate Out Flow Rate F_{do} (ml/min)	Change in Distillate Flow Rate (ml/min)	Water Vapor Flux (kg/m^2-hr)
107.8	104.6	22.2	29.0	10	565	566	1.0	30.8
113.1	108.2	23.4	30.1	12	563.6	565.9	2.3	68.5
118.2	115.1	26.8	36.7	14	563.6	566.8	3.2	97.6

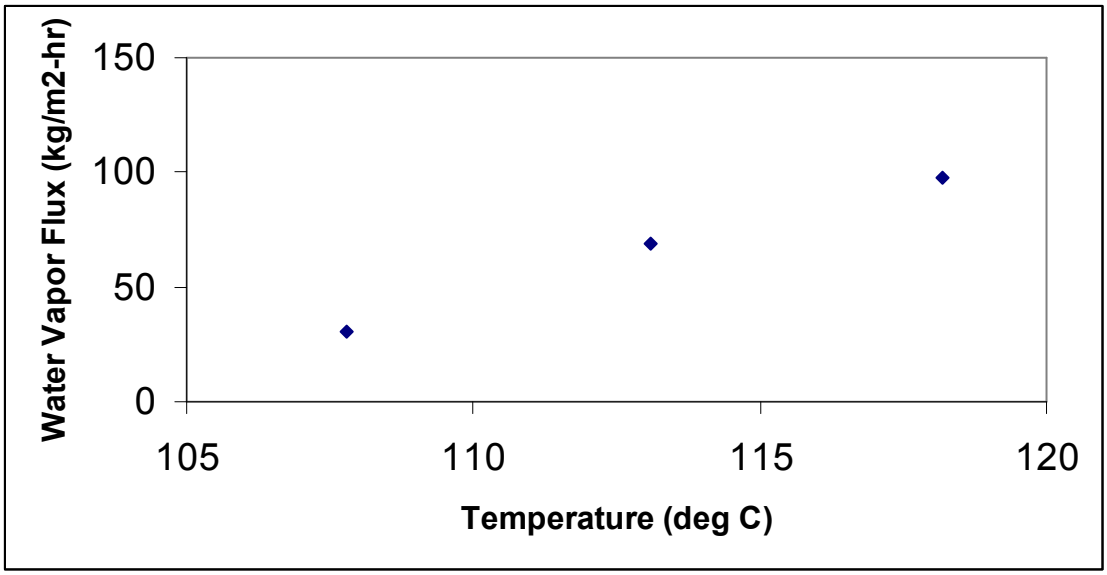

Figure 3.41 Variation of water vapor flux with temperature for 1% NaCl feed solution in higher temperature and higher pressure DCMD set up for PTFE hollow fiber N membrane.

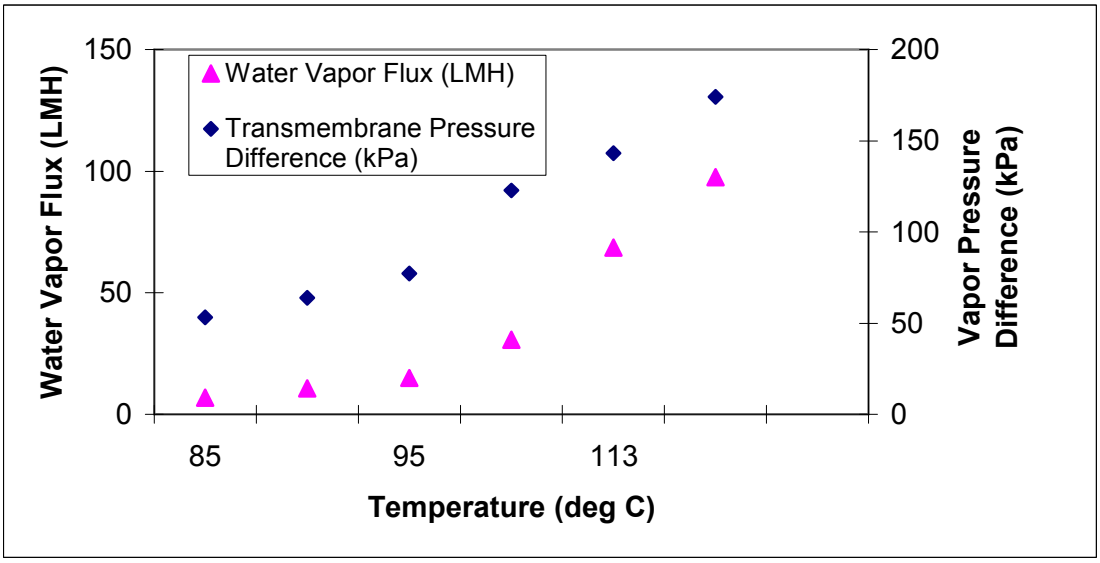

Figure 3.42 Water vapor flux and water vapor pressure difference across two sides of porous PTFE hollow fiber N membrane at different hot brine temperatures.

3.2.8 Experiments with PTFE Hollow Fiber P Membrane Module

Another PTFE module was procured from AMT (Minnetonka, MN) which incorporated 29 PTFE hollow fibers type P of 0.53 mm x 1.08 mm. The effective length of the module = 43 cm, number of fibers in module = 29 and effective membrane area of the module = 207 cm^2 based on I.D. The above module was also tested for 1% NaCl feed solution at higher temperatures. The water vapor flux increased from 2.4 kg/m^2-hr to 31.6 kg/m^2-hr as temperature of feed solution was increased from 105°C to 119°C with constant conductivity on distillate side (Figure 3.43). The module was not supposed to be tested above 120°C. The results are summarized in Table 3.18.

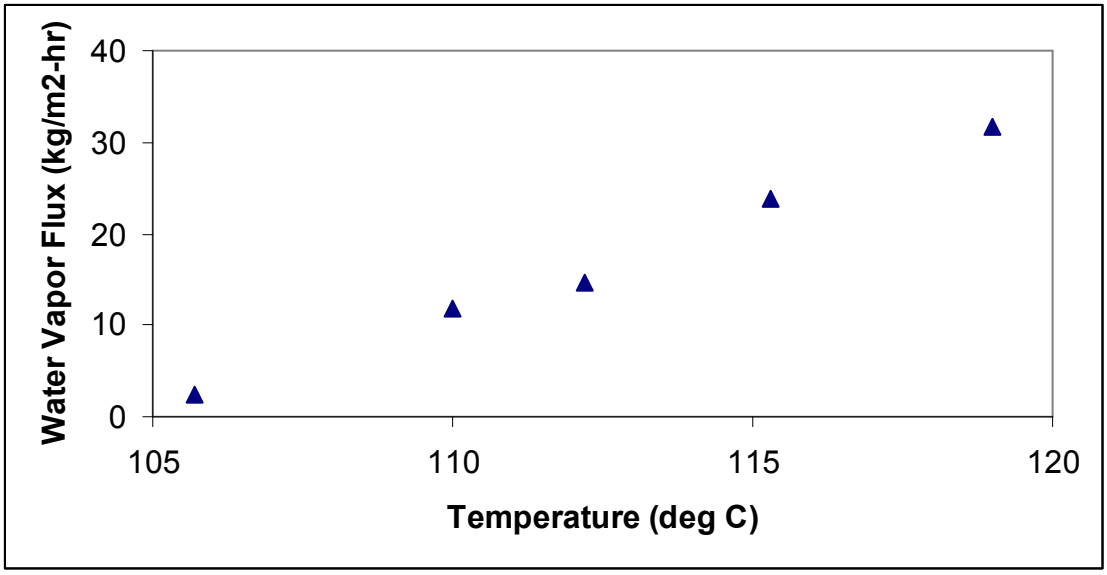

Figure 3.43 Variation of water vapor flux with temperature for 1% NaCl feed solution in higher temperature and higher pressure DCMD set up for PTFE hollow fiber P membrane module.

Table 3.18 Performance of PTFE Hollow Fiber P Membrane with 1% NaCl Solution at Higher Temperatures

Brine Inlet T_{bi} (^oC)	Brine Oulet T_{bo} (^oC)	Distillate Inlet T_{di} (^oC)	Distillate Outlet T_{do} (^oC)	Brine Inlet P_{bi} (psig)	Distillate In Flow Rate F_{di} (ml/min)	Distillate Out Flow Rate F_{do} (ml/min)	Change in Distillate Flow Rate (ml/min)	Water Vapor Flux (kg/m^2-hr)
105.7	91.2	25.4	36.7	4	376.6	377.7	1.1	2.4
110.0	94.0	24.5	37.1	8	373.6	377.6	4.0	11.7
112.2	95.0	24.6	37.7	10	376.8	381.8	5.0	14.6
115.3	97.7	25.6	38.4	12	373.6	381.8	8.2	23.8
119.0	101.0	26.0	40.0	15	369.9	380.7	10.8	31.6

3.2.9 Experiments with PTFE Large Hollow Fiber Membrane Module

A module having a large number of PTFE series O hollow fibers (Figure 3.44) was obtained from Markel Corporation, Plymouth, PA. The details of the hollow fibers and the module are as follows: O.D.= 1.90 mm, I.D.= 1.55 mm, fiber wall porosity = 0.42, average pore size = 0.24 μm, effective length of the module = 20.96 cm, number of fibers in module = 345 and effective area of the module = 3400 cm^2 based on I.D. Experiments were performed both at lower and higher temperatures. The water vapor flux increased from 0.43 kg/m^2-hr to 11.76 kg/m^2-hr as the temperature of feed solution was increased from 56^o C to 110^o C (Figure 3.45). The feed flow rates were very low for these preliminary experiments. It is expected that with higher flow rates, the flux will go up considerably. At a brine temperature of 70^o C, there was 13% increase in water vapor flux as the flow rate of brine was increased from 1000 ml/min to 2000 ml/min (Figure 3.46). The effect of brine flow rate on water vapor flux was also studied at higher temperatures. It was observed (Figure 3.47) that as brine flow rate was increased from 500 ml/min to 1100 ml/min for different temperatures, there was a significant increase in the value of water vapor flux. Due to limitations of the experimental setup, the large module performance could be explored only up to 110^o C at a brine flow rate of 1100 ml/min. It is expected that with higher flow rates, the flux will go up considerably.

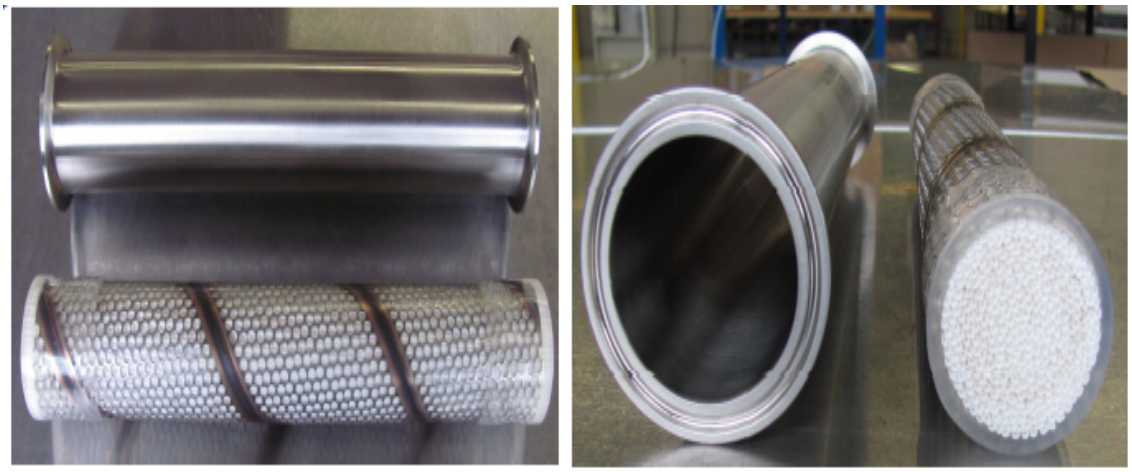

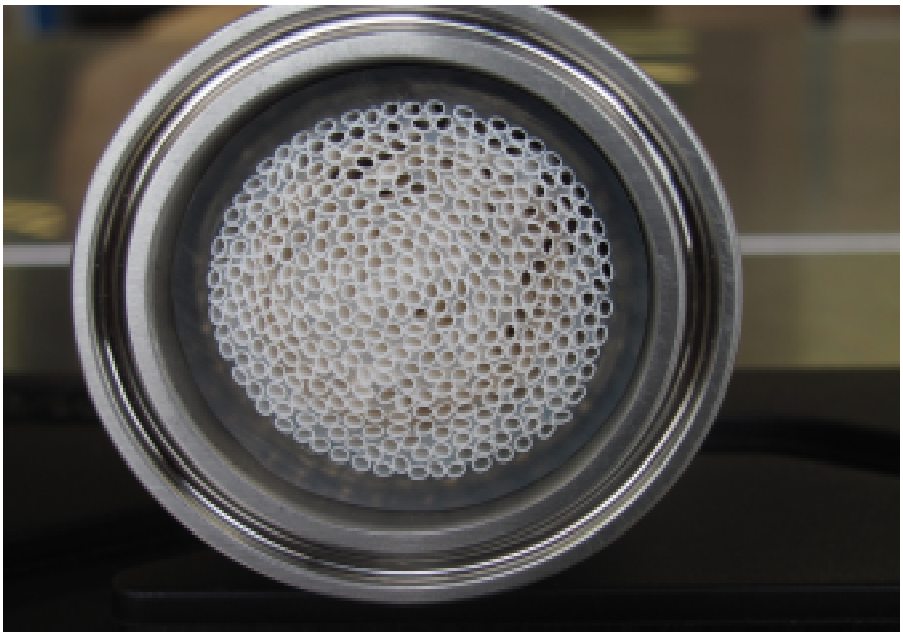

Figure 3.44 Photographs showing the large PTFE hollow fiber module.

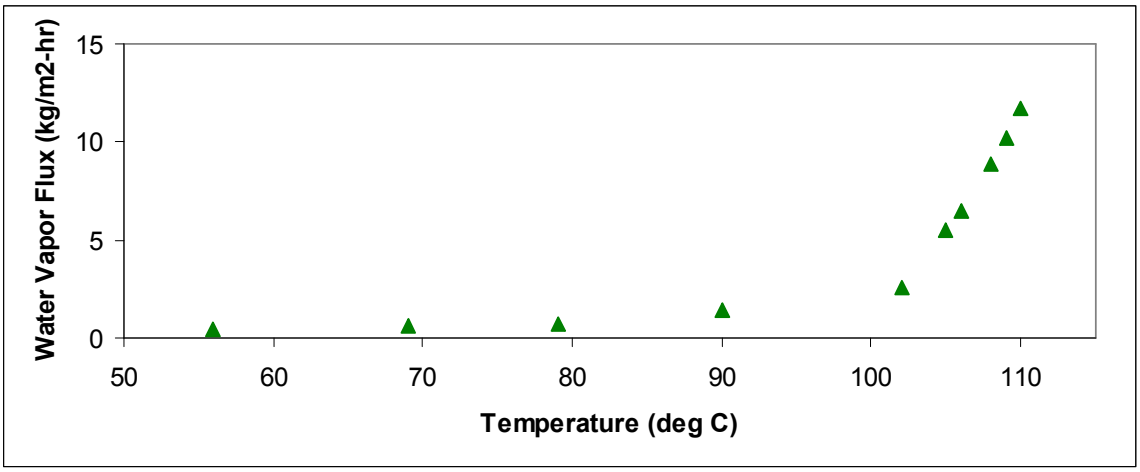

Figure 3.45 Variation of water vapor flux with temperature for 1% NaCl feed solution for hollow fiber-based PTFE large module.

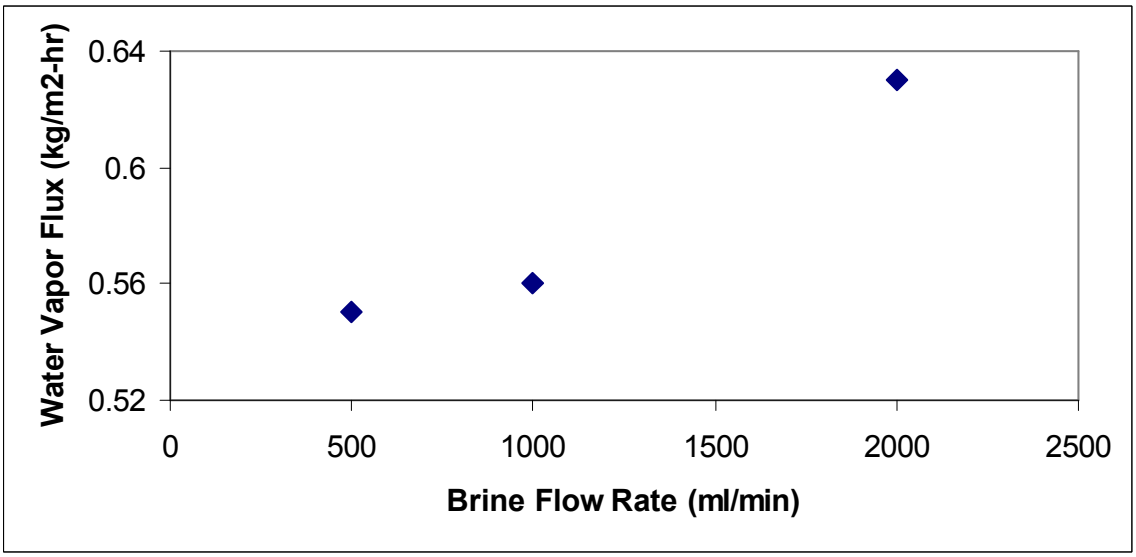

Figure 3.46 Effect of brine flow rate on water vapor flux for 1% NaCl solution at 70^{o}C with PTFE hollow fiber-based large module.

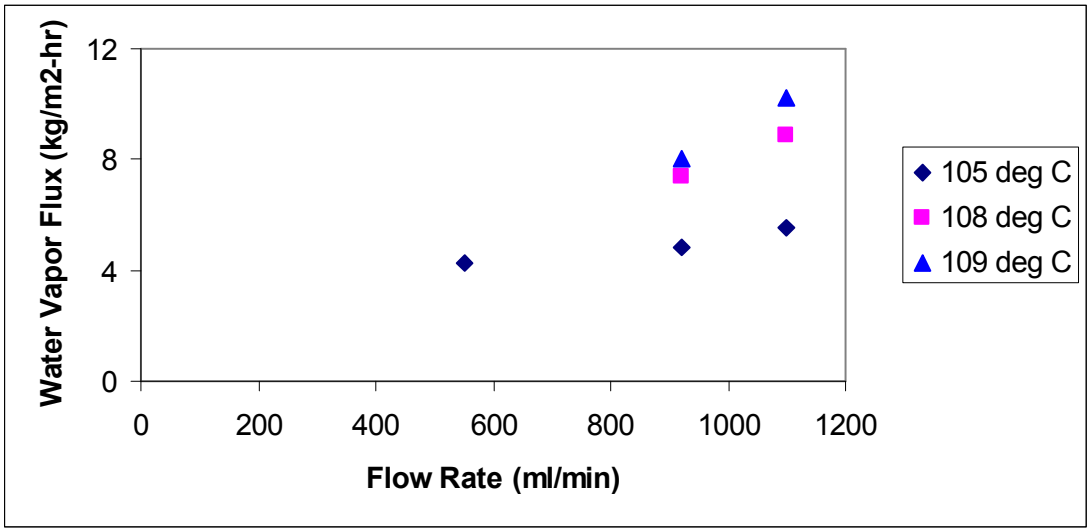

Figure 3.47 Variation of water vapor flux with different flow rates of 1% NaCl feed solution in higher temperature and higher pressure DCMD set up for PTFE hollow fiber-based large module.

3.3 DCMD Experiments with Produced Water

DCMD experiments at higher temperatures were performed with simulated SAGD produced water. The composition of simulated produced water is given in Table 3.19.

3.3.1 Experiments with Produced Water for PTFE Flat Sheet Membrane

The DCMD performance of this PTFE membrane was also explored with produced water feed at high temperatures. The produced water composition employed is characteristic of the SAGD process [60]. Water vapor fluxes measured were similar to those from a 1% NaCl feed solution for flat sheet membranes; it was unaffected by the presence of organic compounds in the feed brine. The boiling points of phenol and cresol are 182^{o}C and 191^{o}C respectively; it is expected that traces of phenol and cresol will be present on the distillate side (Figure 3.48). Water vapor was collected in the distillate tank and

concentrations of phenol and cresol would continuously increase with time. After 30 minutes, samples were taken from the distillate tank for analysis by HPLC to measure the concentrations of phenol and cresol. With mobile phase 90/10 (v/v) methanol/water and 0.1 % H_3PO_4 (v/v) at the flow rate of 1 ml/min, two distinct peaks (Figure 3.48) were obtained at retention times of 2.8 min and 4.1 min for phenol and cresol respectively.

Table 3.19 Simulated Composition of Produced Water

Phenol (ppm)	45
Cresol (ppm)	45
Naphthenic acid (ppm)	10
Sodium chloride (ppm)	3000
Sodium carbonate (ppm)	50

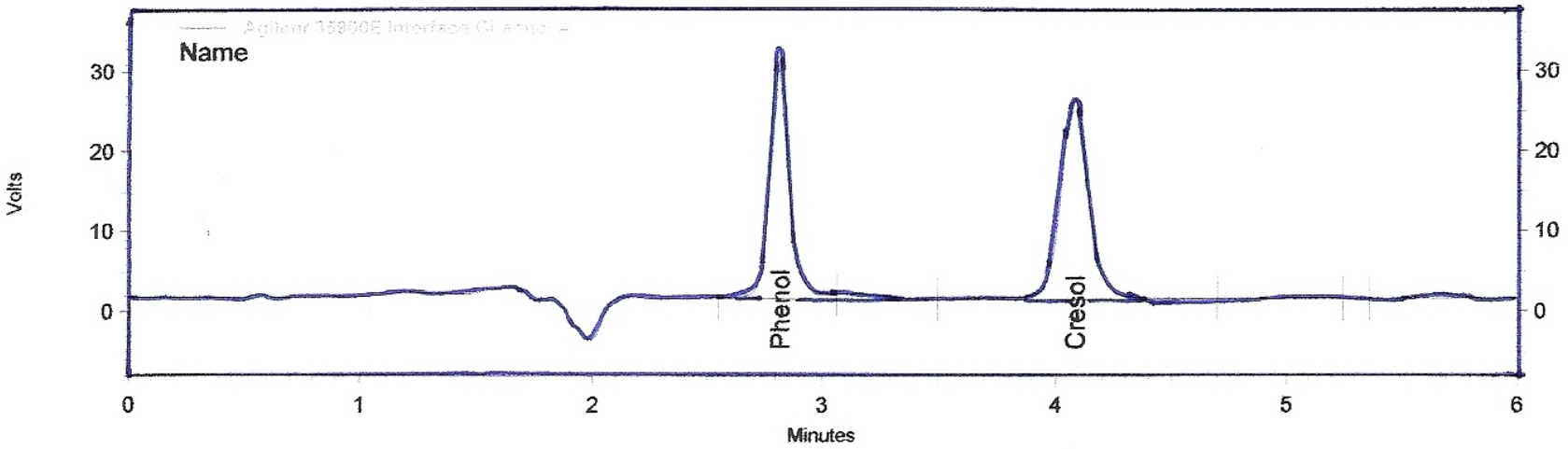

Figure 3.48 Chromatogram of phenol and cresol obtained from HPLC with mobile phase 90/10 (v/v) methanol/water and 0.1 % H_3PO_4 (v/v) at the flow rate of 1 ml/min by UV detector at λ_{max} = 218 nm.

The water vapor fluxes and concentration of phenol and cresol at high temperatures with produced water are reported in Figures 3.49 and 3.50; it is clear that concentrations of phenol and cresol are below 5 ppm even when the brine temperature is 125^{o}C. It is generally safe to use this water for steam generation for such concentrations of phenol and cresol. No trace of sodium chloride was found in the distillate stream during the experiments with produced water; this was verified by conductivity measurement as well as by AA analysis.

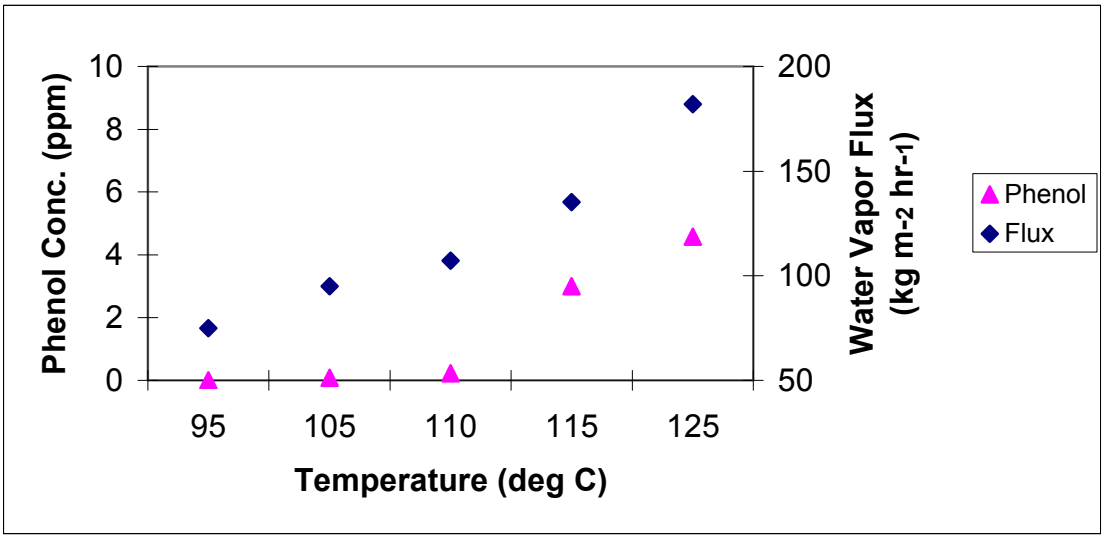

Figure 3.49 Concentration of phenol in the permeate side along with water vapor flux at different temperatures of simulated produced water in higher temperature and higher pressure DCMD set up for PTFE flat sheet membrane.

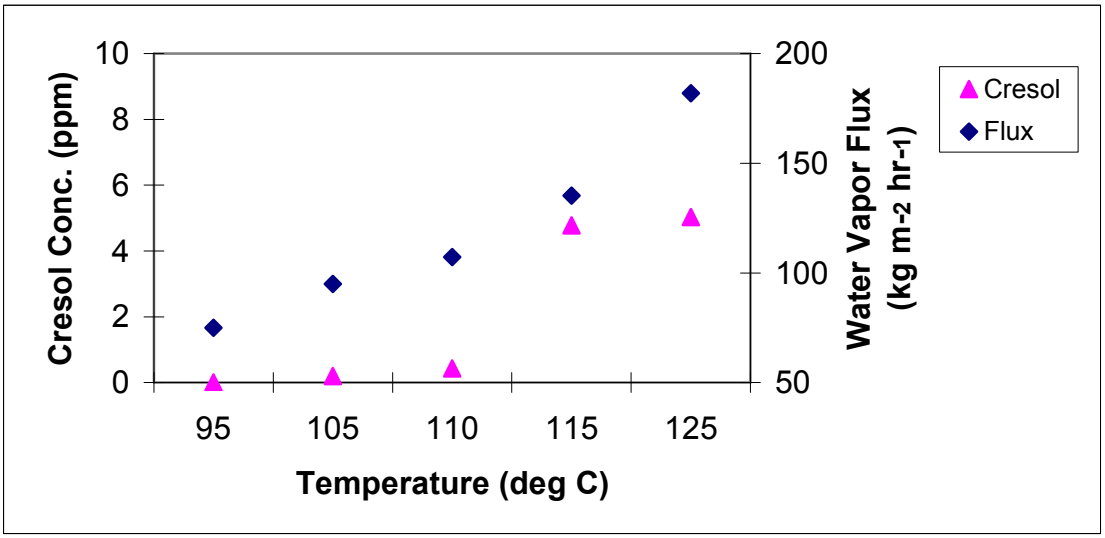

Figure 3.50 Concentration of cresol on permeate side along with water vapor flux at different temperatures of simulated produced water in higher temperature and higher pressure DCMD set up for PTFE flat sheet membrane.

Experiments were carried out using flat sheet PTFE membranes with simulated SAGD produced water containing sodium carbonate in the feed at different temperatures. The composition of produced water was as follows: phenol = 45 ppm, cresol = 45 ppm, naphthenic acid = 10 ppm, sodium carbonate = 50 ppm and NaCl = 3000 ppm. The water vapor fluxes with produced water containing sodium carbonate were somewhat lower than the water vapor fluxes for a 1% NaCl feed solution and also with produced water without sodium carbonate (Figure 3.51). It is probably due to the presence of carbon dioxide, generated from sodium carbonate in water.

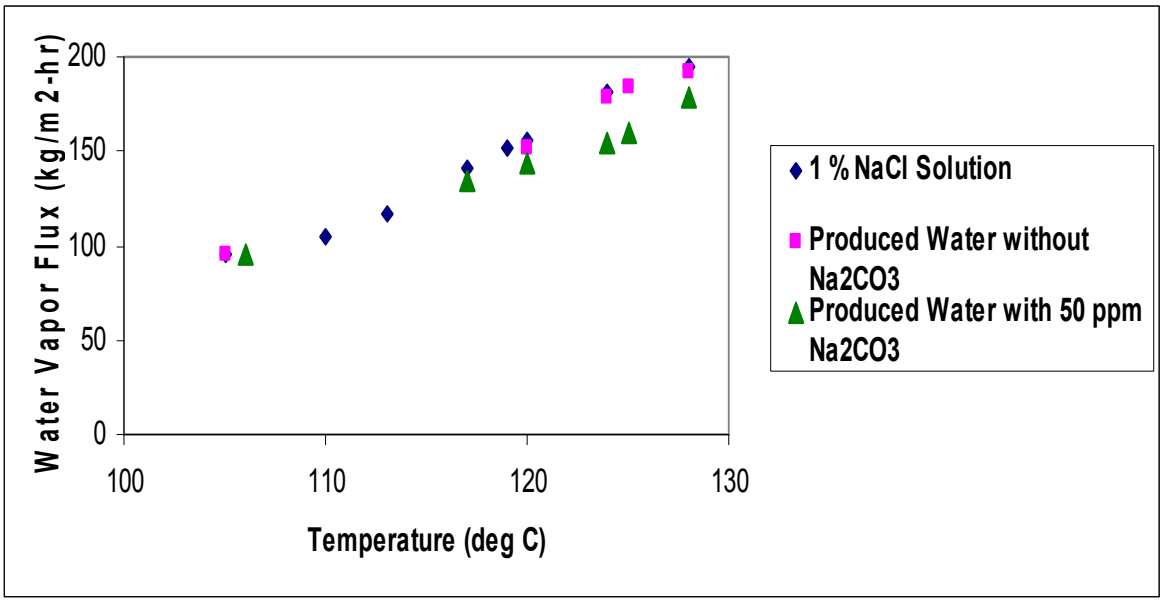

Figure 3.51 Effect of sodium carbonate in produce water on water vapor flux for PTFE flat sheet membrane.

Gas chromatography-electron impact mass spectrometry (GC-EI-MS) (HP 6890 Series GC system with Agilent 5973 Network Mass Selective Detector) was used next for analysis of the derivatized samples. The analysis of naphthenic acid is extremely difficult due to its compositional heterogeneity; as a result chromatogram of underivatized naphthenic acid resulted in a large hump in Figure 3.52(a), with very few resolvable peaks. But derivatized naphthenic acid components reduce extent of molecular fragmentation and resulted in strong base peaks in spectra of derivatized naphthenic acids as shown in Figure 3.52(b). The spectra of derivatized naphthenic acid extracted from the distillate tank at different temperatures have shown no traces of naphthenic acid; but at 125^{o}C few ppm (< 2ppm) of naphthenic acids were detected.

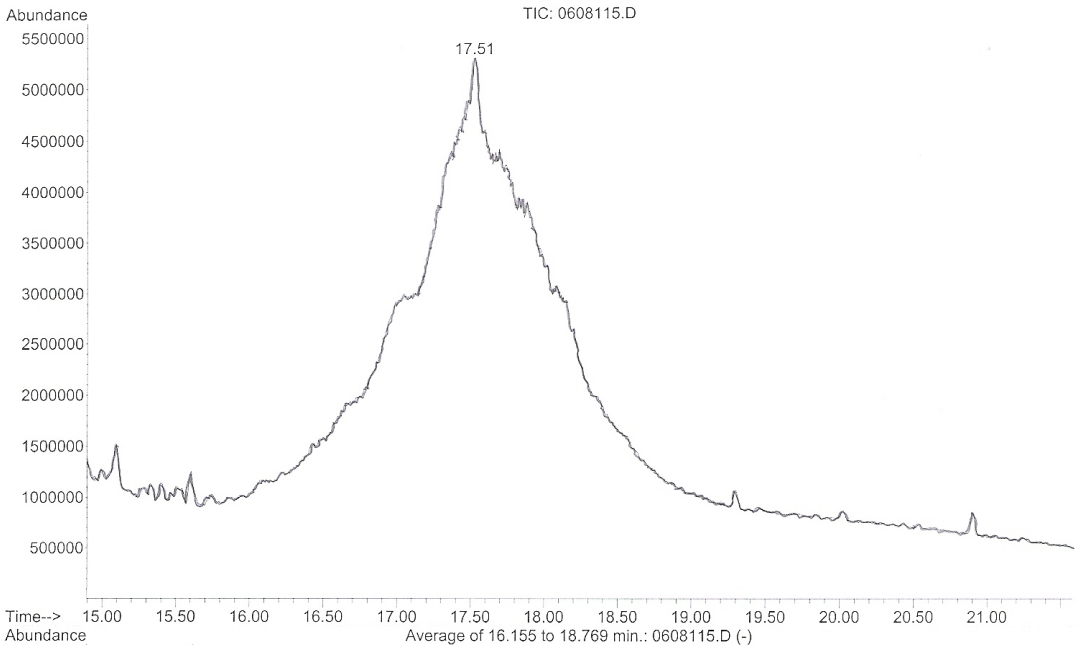

(a)

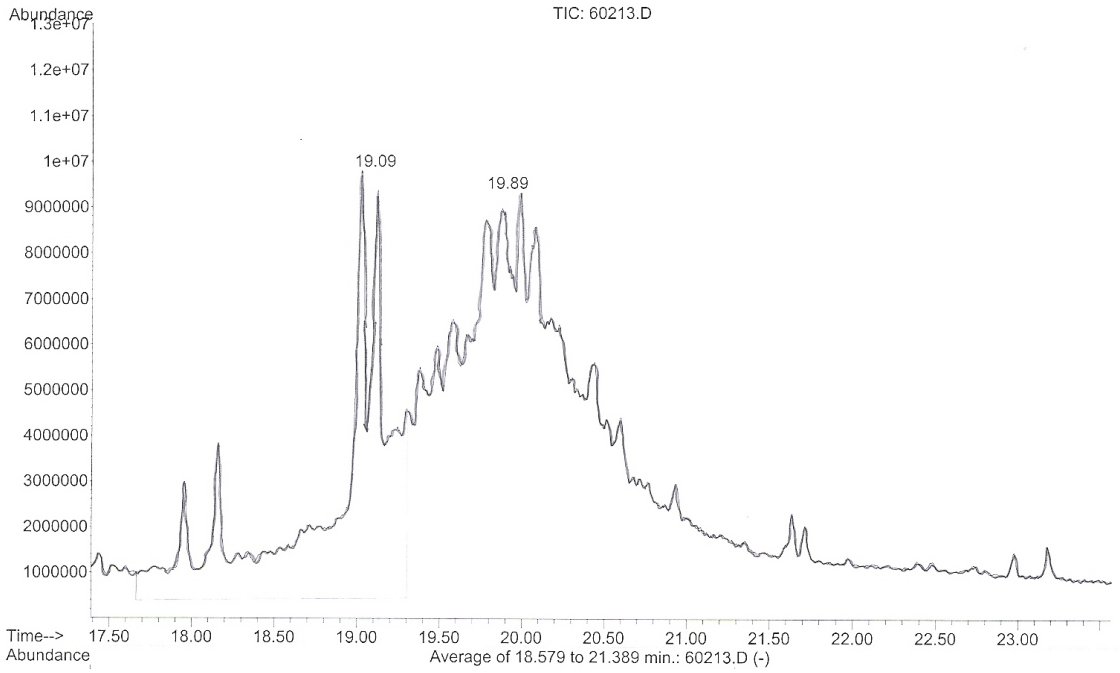

(b)

Figure 3.52 Chromatogram showing (a) the peak for naphthenic acid in underivatized sample (b) the distinct peaks for naphthenic acid in derivatized sample.

3.3.2 Experiments with Produced Water for Large PTFE Membrane Module

The performance of the large module was also studied with simulated produced water containing 45 ppm phenol, 45 ppm cresol, 10 ppm naphthenic acid and 3000 ppm NaCl. It was observed from HPLC analysis (Figure 3.53 and Figure 3.54) that after 30 minutes, concentrations of phenol and cresol on the permeate side were less than 10 ppm at a brine temperature of 110^{o}C.

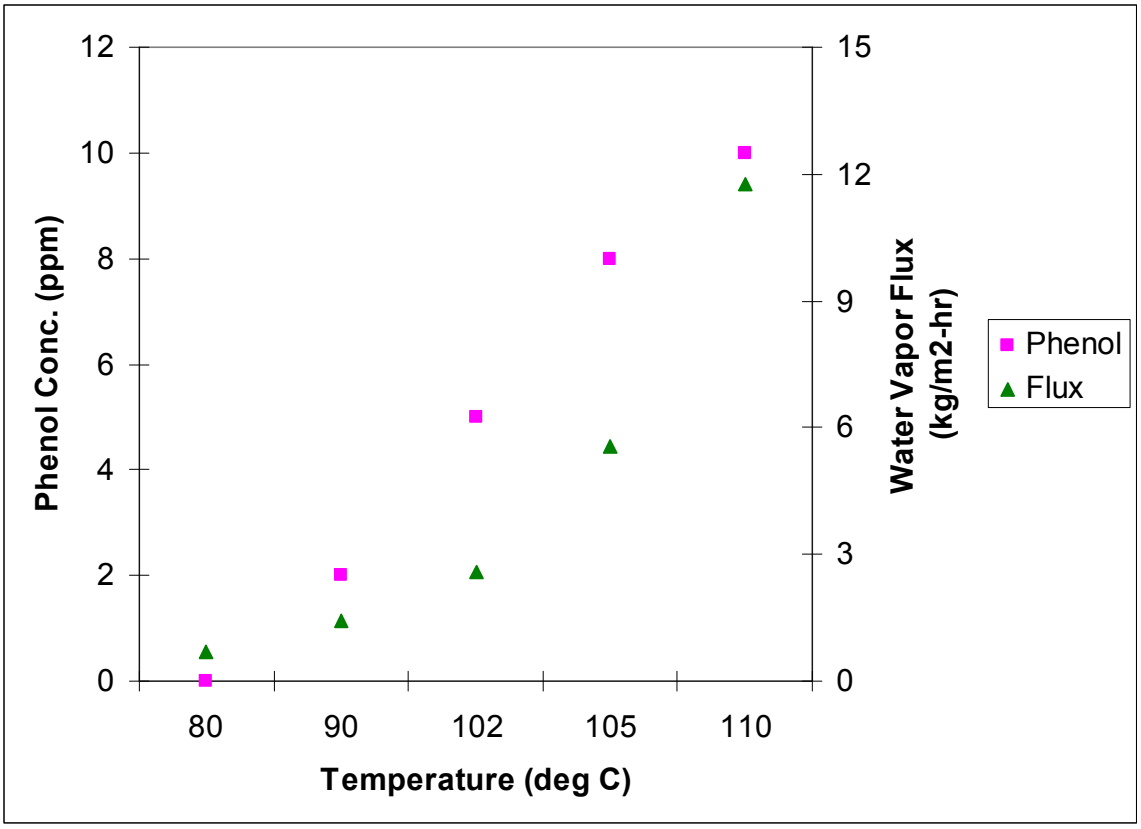

Figure 3.53 Concentration of phenol on permeate side along with water vapor flux at different temperatures of simulated produced water in higher temperature and higher pressure DCMD set up for PTFE hollow fiber-based large module.

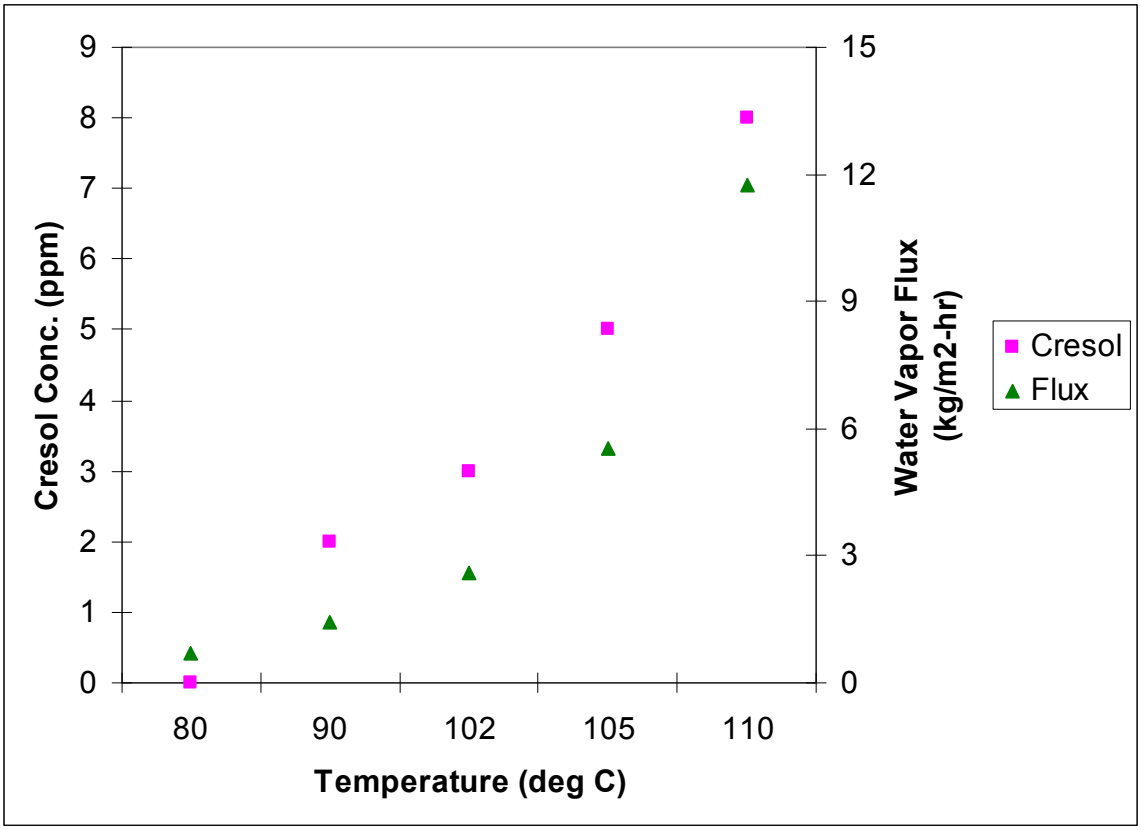

Figure 3.54 Concentration of cresol on the permeate side along with water vapor flux at different temperatures of simulated produced water in higher temperature and higher pressure DCMD set up for PTFE hollow fiber-based large module.

CHAPTER 4

THEORETICAL ANALYSIS OF DCMD RESULTS

Performances of PTFE flat sheet membranes and PTFE hollow fiber were analyzed using Schofield's model for membrane distillation.

4.1 Performances of PTFE membrane for DCMD with 1 % NaCl Solution

The water vapor fluxes achieved by these membranes were analyzed using Schofield's model [9]. The Knudsen number, which is the ratio of mean free path of gas molecules and pore diameter, dictates the transport mode of water vapor through the pores of the membrane. In the experiments described earlier, there was a very large temperature difference across the membrane; therefore the value of the mean free path as well as Knudsen number will change substantially along the pore length. The mean free path and the Knudsen number were calculated for the brine side as well as for the distillate side for all experiments performed with PTFE flat sheet membrane and PTFE hollow fiber membrane modules; these values are given in Tables 4.1, 4.2, and 4.3.

Table 4.1 Values of Mean Free Path and Knudsen Number at Different Temperatures for PTFE Flat Sheet Membrane

Feed Temperature (^{o}C)	Mean Free Path on Brine Side (λ_b) (μm)	Knudsen Number on Brine Side (K_{nb})	Mean Free Path on Distillate Side (λ_d) (μm)	Knudsen Number on Distillate Side (K_{nd})	Average Mean Free Path Along Pore Length (λ_{avg}) (μm)	Average Knudsen Number Along Pore Length ($K_{n\ avg}$)
80	0.082	2.73	0.097	3.23	0.097	3.23
85	0.078	2.60	0.096	3.23	0.096	3.20
90	0.074	2.47	0.097	3.23	0.095	3.17
95	0.070	2.33	0.098	3.23	0.095	3.17
111	0.057	1.90	0.098	3.27	0.089	2.97
117	0.050	1.67	0.098	3.23	0.081	2.70
119.5	0.050	1.67	0.097	3.23	0.072	2.60
120	0.049	1.63	0.096	3.20	0.078	2.60
124	0.050	1.67	0.097	3.23	0.076	2.53
128	0.043	1.4	0.097	3.23	0.076	2.53

Table 4.2 Values of Mean Free Path and Knudsen Number at Different Temperatures for PTFE Hollow Fiber M Membrane

Feed Temperature (^{o}C)	Mean Free Path on Brine Side (λ_b) (μm)	Knudsen Number on Brine Side (K_{nb})	Mean Free Path on Distillate Side (λ_d) (μm)	Knudsen Number on Distillate Side (K_{nd})	Average Mean Free Path Along Pore Length (λ_{avg}) (μm)	Average Knudsen number along pore length ($K_{n\ avg}$)
85	0.079	0.33	0.097	0.40	0.086	0.36
90	0.075	0.31	0.097	0.40	0.084	0.35
95	0.071	0.29	0.097	0.40	0.080	0.33
108	0.057	0.24	0.097	0.40	0.069	0.29
110	0.057	0.24	0.097	0.40	0.054	0.23
112	0.053	0.22	0.098	0.41	0.066	0.28
118	0.047	0.19	0.098	0.41	0.062	0.26

Table 4.3 Values of Mean Free Path and Knudsen Number at Different Temperatures for PTFE Hollow Fiber N Membrane

Feed Temperature (^oC)	Mean Free Path on Brine Side (λ_b) (μm)	Knudsen Number on Brine Side (K_{nb})	Mean Free Path on Distillate Side (λ_d) (μm)	Knudsen Number on Distillate Side (K_{nd})	Average Mean Free Path Along Pore Length (λ_{avg}) (μm)	Average Knudsen Number Along Pore Length ($K_{n\ avg}$)
85	0.078	0.29	0.097	0.36	0.085	0.31
90	0.074	0.27	0.096	0.36	0.083	0.31
95	0.069	0.26	0.097	0.36	0.079	0.29
108	0.057	0.21	0.098	0.36	0.070	0.26
113	0.050	0.19	0.098	0.36	0.066	0.24
118	0.048	0.18	0.098	0.36	0.062	0.23

For PTFE flat sheet membrane having the smaller pore size of 0.03 µm, the values of Knudsen numbers are increasing from brine side to distillate side for all experiments; the values are always greater than one illustrating the dominance of Knudsen flow mechanism during water vapor transport from brine side to distillate side. Similarly, for PTFE hollow fiber membrane modules, Knudsen numbers are increasing from brine side to distillate side but their values were always less than one showing the dominance of Poiseuille flow model for water vapor transport; this follows from much larger membrane pore size of 0.24-0.27 µm. The average of the Knudsen number values at the two membrane surfaces has been plotted at different temperatures of brine feed for PTFE flat sheet membrane and PTFE hollow fiber membrane modules in Figure 4.1. The ratio of the two values reflect the almost ten times larger pore size of the PTFE hollow fiber membranes over those of the flat PTFE membranes.

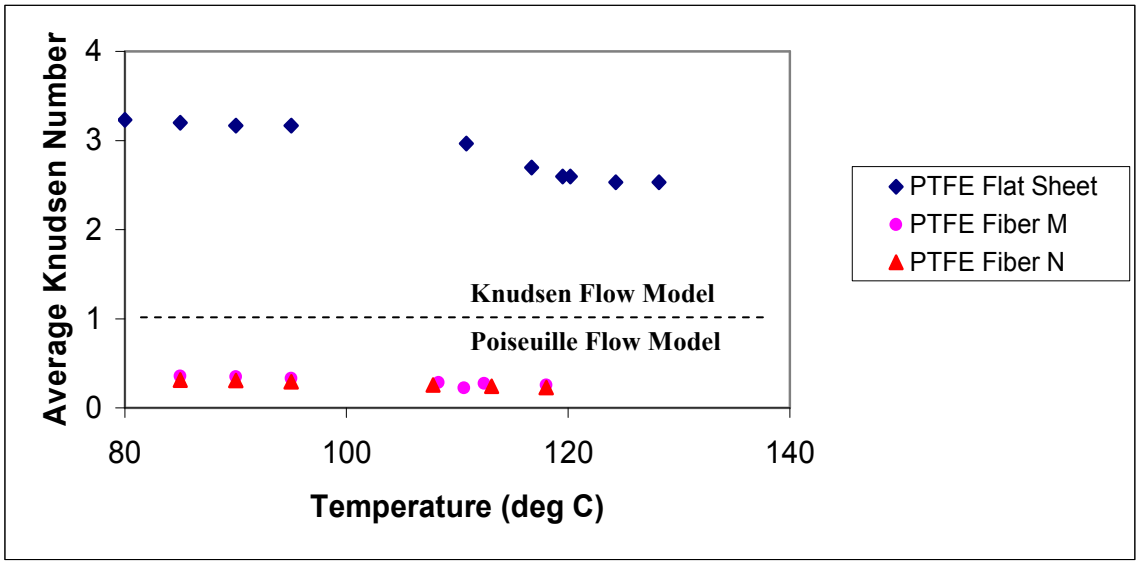

Figure 4.1 Variation of average Knudsen number along the pore of the membrane at different temperatures.

This figure suggests particular transport regimes for particular membranes; for example, Poiseuille flow model is suggested for the hollow fibers. Therefore Poiseuille flow model equation was used to predict the water vapor flux for PTFE fiber M module. The tortuosity factor for fiber M, calculated from equations (2.5) and (2.6) came out to be 2.0 and 4.5, respectively. The fluxes predicted by Poiseuille flow model are slightly higher than the experimental values for $\tau = 2.0$ but significantly lower than experimental values for $\tau = 4.5$, which basically supports the assumption of $\tau = 2.0$ for prediction of water vapor flux in membrane distillation processes [9] (Figure 4.2). This figure suggests that the predicted water vapor fluxes may achieve better agreement with the experimental values if an appropriate tortuosity factor is utilized; it is expected that this value will be slightly higher than 2.

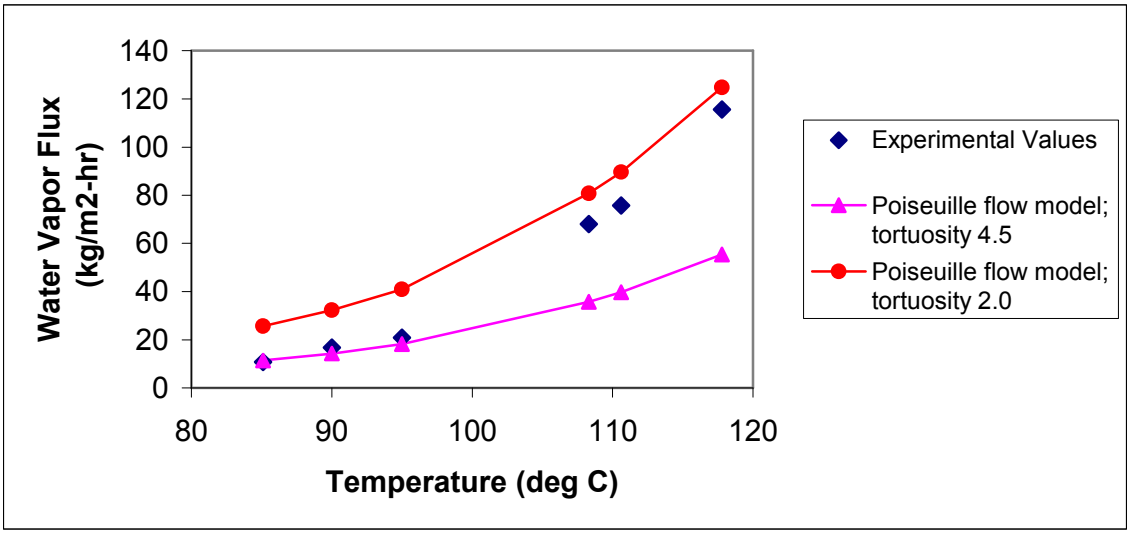

Figure 4.2 Variation of water vapor flux for 1 % NaCl feed solution at different temperatures for PTFE fiber M module along with water vapor flux calculated from Poiseuille flow model for $\tau = 2.0$ and $\tau = 4.5$.

Based on Figure 4.1, Poiseuille flow model was also used to predict the water vapor flux for hollow fiber type N. Figure 4.3 illustrates the water vapor flux calculated from Poiseullie flow model equation (2.3) for tortuosity factors calculated from equations (2.5) and (2.6) along with experimental values at different feed temperatures. The water vapor fluxes predicted for τ = 2.13 and τ = 4.98, are significantly different from experimental values, which suggests that the actual tortuosity will be somewhere between 2.13 and 4.98.

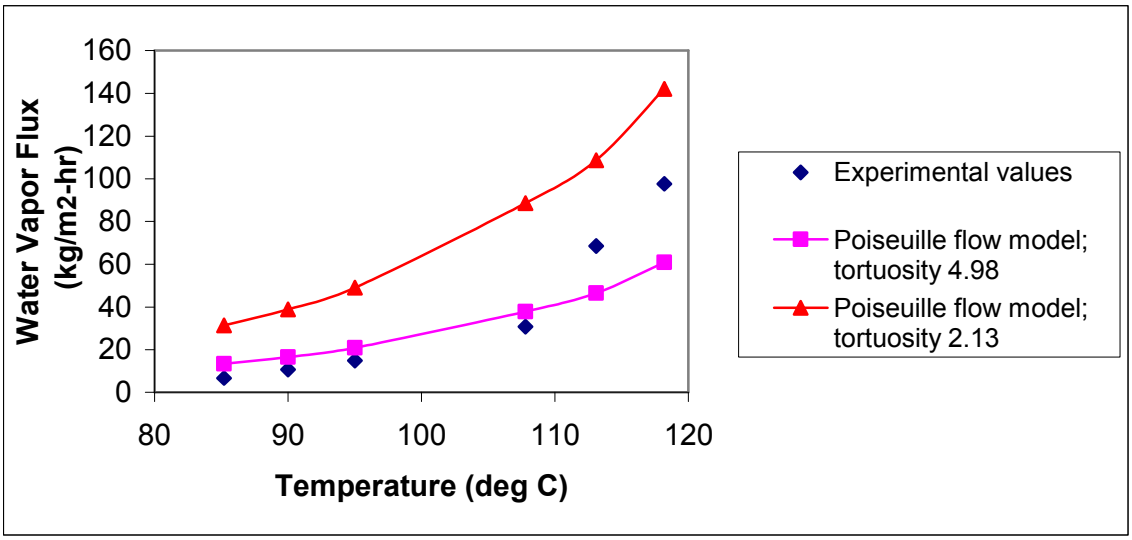

Figure 4.3 Variation of water vapor flux for 1 % NaCl feed solution at different temperatures for PTFE fiber N module along with water vapor flux calculated from Poiseuille flow model for τ = 2.13 and τ = 4.98.

Unlike fiber M, theoretical water vapor flux calculation based on τ = 2.13 is completely in disagreement with the experimental values. It is also clear from the scanning electron micrographs of the cross sections of the fibers in Figures 3.16 and 3.19 that pores in fiber N are more tortuous than those in fiber M. The tortuosity factor for fiber N was also calculated using the value of effective porosity over pore length

determined from nitrogen permeation experiment and the value of porosity from manufacturer; the value of τ comes out to be 3.05. Figure 4.4 shows that the theoretical water vapor flux calculated from Poiseuille flow model for τ = 3.05 is close to experimental values at higher temperatures. The exact predictions of water vapor fluxes depend on accurate values of tortuosity factor of fibers.

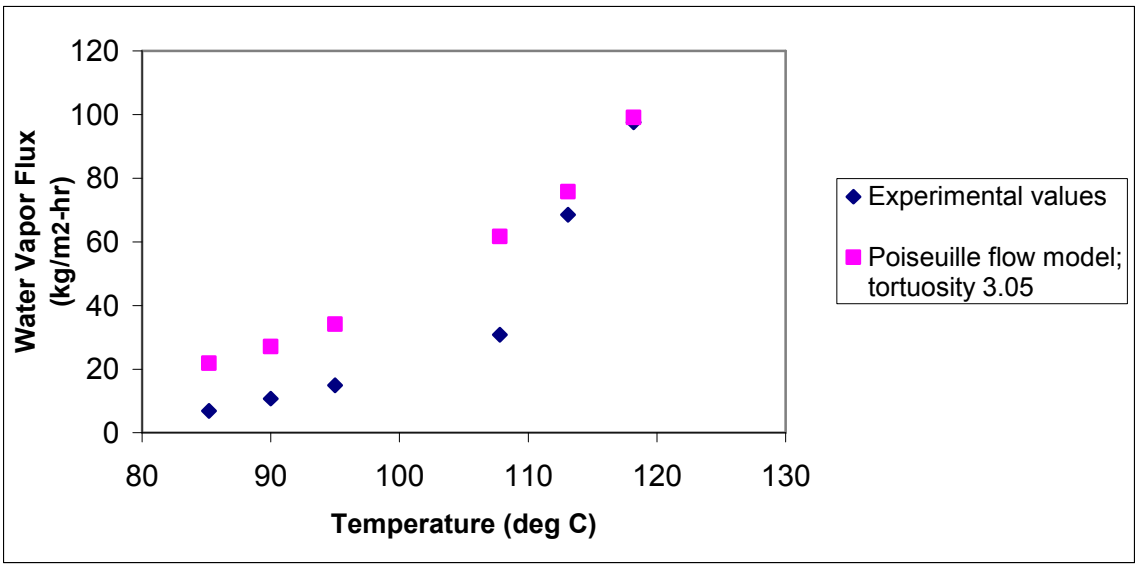

Figure 4.4 Variation of water vapor flux for 1 % NaCl feed solution at different temperatures for PTFE fiber N module along with water vapor flux calculated from Poiseuille flow model for τ = 3.05.

For PTFE flat sheet membranes, Knudsen number is always greater than one illustrating the dominance of Knudsen flow mechanism for water vapor transfer. From Figure 4.5, it is clear that water vapor flux predicted from Knudsen flow model is much higher than the experimental values and at the same time Poiseuille flow model prediction is much lower than the experimental values. It is clear from SEM images of

the PTFE flat sheet membrane that the membrane is symmetric in nature and the wall thickness is much thinner than the PTFE hollow fiber. So, unlike PTFE hollow fiber membranes, tortuosity factor is not responsible for the discrepancies between the theoretical and experimental values; rather the membrane pore size distribution is likely to be the crucial factor. Figure 3.6 shows that many of the pores are larger than 0.2 μm and for these pores Knudsen number is less than one showing the dominance of Poiseuille flow model. Hence it is concluded that for the PTFE flat sheet membrane, a combination of Poiseuille flow model and Knudsen flow model over the pore size distribution of membrane is necessary to model the actual water vapor flux.

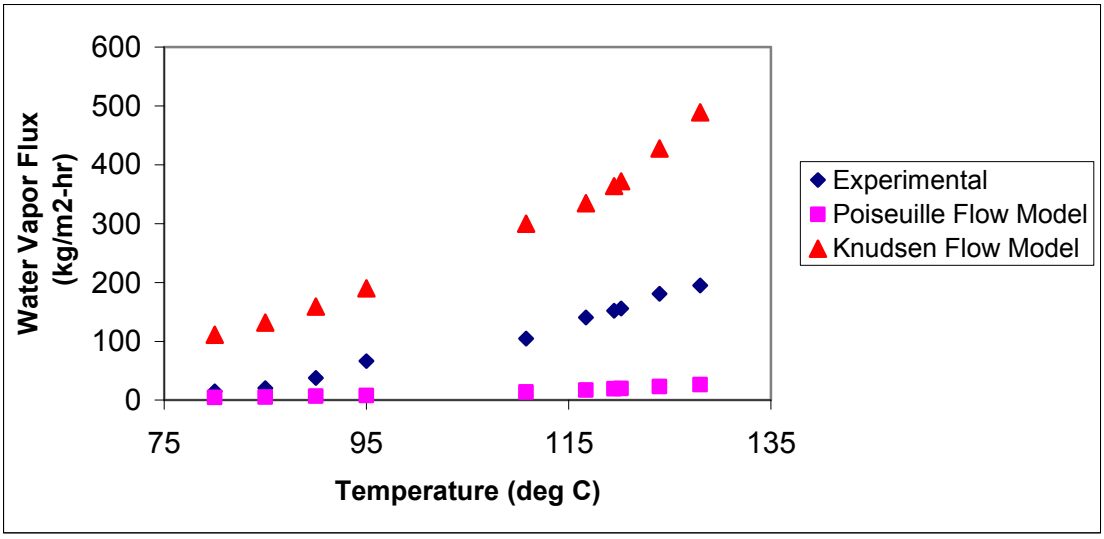

Figure 4.5 Variation of water vapor flux for 1 % NaCl solution at different temperatures for PTFE flat sheet membrane along with theoretical water vapor flux calculated from Poiseuille flow model.

Based on conclusion from Figure 4.5, water vapor fluxes for PTFE flat sheet membrane were analyzed in transition region using Eq. 2.7. It is clear from Figure 4.6 that experimental values are very close to the values predicted in transition region.

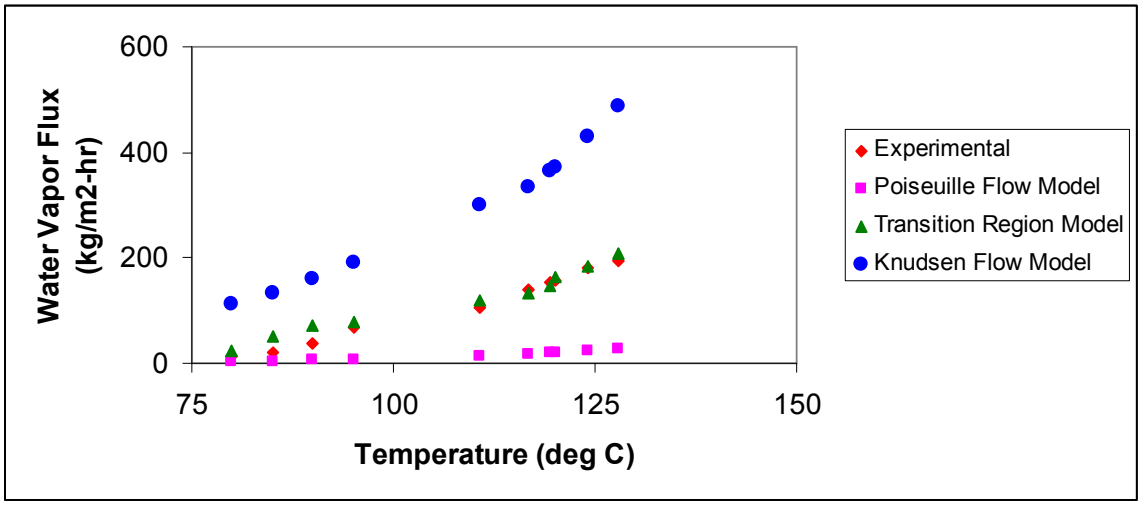

Figure 4.6 Variation of water vapor flux for 1 % NaCl solution at different temperatures for PTFE flat sheet membrane along with theoretical water vapor flux calculated from Schofield's model [48] in transition region.

CHAPTER 5

DESALINATION OF BRINE BY AIR GAP MEMBRANE DISTILLATION

5.1 Introduction

In air gap membrane distillation (AGMD) process [6], a stagnant air gap is maintained between the porous membrane and a condensation surface (Figure 5.1). In this case volatile molecules condense directly over the cold surface near the other side of the membrane. Here conductive heat loss from the brine cannot be totally eliminated; however, unlike that in DCMD, there is no need for a startup distillate stream. Further any cold stream could be used on the other side of the cold surface including the feed brine to be desalted; therefore all heat lost by the hot feed brine via evaporation as well as conduction can be transferred to the cold feed brine to be desalted without a separate heat exchanger.

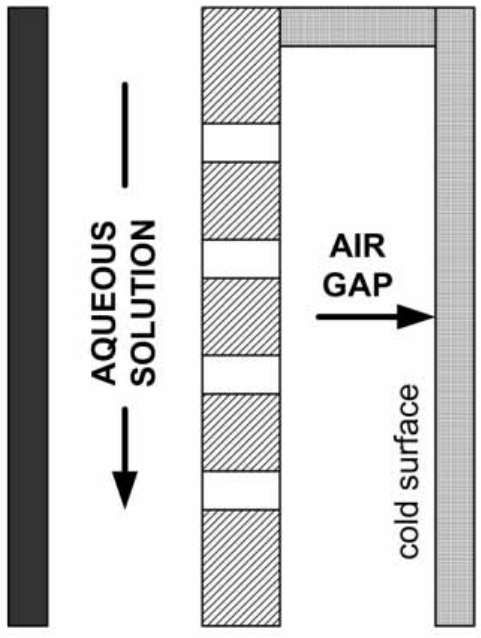

Figure 5.1 Schematic of AGMD process (Taken from [6]).

On the other hand, the module design gets complicated and the footprint becomes quite large. Further the air gap presents significant resistance to water vapor transport and condensation. There exist a number of studies analyzing the heat and mass transfer resistances in AGMD [61-65]. The expression for the mass transfer resistances was developed in air-gap membrane distillation process [62]. The study was concerned to individual mass transfer resistances in the different process domains and their contributions to the total resistances. In AGMD, the distillation process takes place in the following domains shown in Figure 5.2:

- Hot solution (h)
- Membrane (m)
- Air/vapor gap (g)
- Condensate film (f)
- Cooling plate (p)
- Cold fluid (c)

Out of these domains, air/vapor gap domain dominates the mass transfer resistances. The most influential parameters on total mass transfer resistance were air gap width and hot solution inlet temperature as a consequence of their effect on air/vapor gap mass transfer resistance. The next parameter which affects mass transfer resistance was the cold solution inlet temperature but inlet velocities of the hot and cold solutions have very little effect on total mass transfer resistance. The membrane thermal conductivity should be low because of its effect on the permeate flux; however it does not have as much of an effect on thermal efficiency as in DCMD.

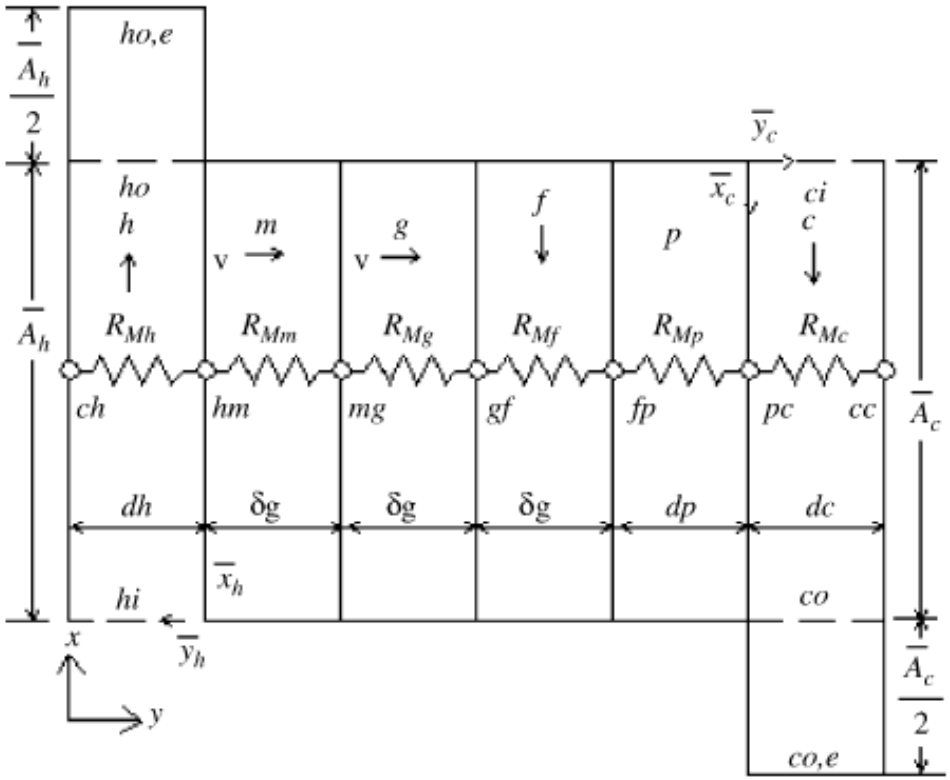

Figure 5.2 Different mass transfer resistance zones in AGMD process (Taken from [62]).

There are a variety of AGMD module designs. A spiral-wound module design was illustrated having three channels: evaporator channel, distillate channel, condensate channel [40]. A single porous hollow fiber was employed in AGMD; through the bore of which hot brine was passed [6, 65]. This hollow fiber was positioned inside a concentric cylindrical annulus on whose outside there was a flow of the cold solution which may be the feed brine. The condensate was obtained from outside the porous hollow fiber. A new type of finned tubular membrane designed especially for flux enhancement in AGMD was demonstrated [64]. Figure 5.3 shows a finned tubular membrane module having a thin air gap in the grooves of a finned copper tube on the outside of which lies the tubular membrane which is a flat-sheet porous PTFE membrane wrapped around the copper tube and heat sealed at the edges. The cooling solution passed through the bore of the hollow copper tube. The proposed module can be easily integrated with external heat source. The performance of the SCARAB system of AGMD process was studied experimentally [66].

It is widely known that modules built with self-supporting hollow fiber membranes can provide a large membrane surface area per unit equipment volume, are simple and are therefore attractive. In an US patent [67] an AGMD module was proposed using two sets of hollow fibers one porous hydrophobic through the bore of which hot brine flows and the other a solid hollow fiber through the bore of which cold solution will flow providing for condensation of the vapor on its outside surface. There has been no experimental demonstration of such a concept; such hollow fiber-based module was numerically modeled and concluded that an increase in module packing density reducing the air gap thickness will enhance membrane productivity [63]. However the highest flux

reported in their calculations for hot brine coming in at 70 ^{0}C and cold water coming in at 25 ^{0}C was around 12 kg/m^{2}-h.

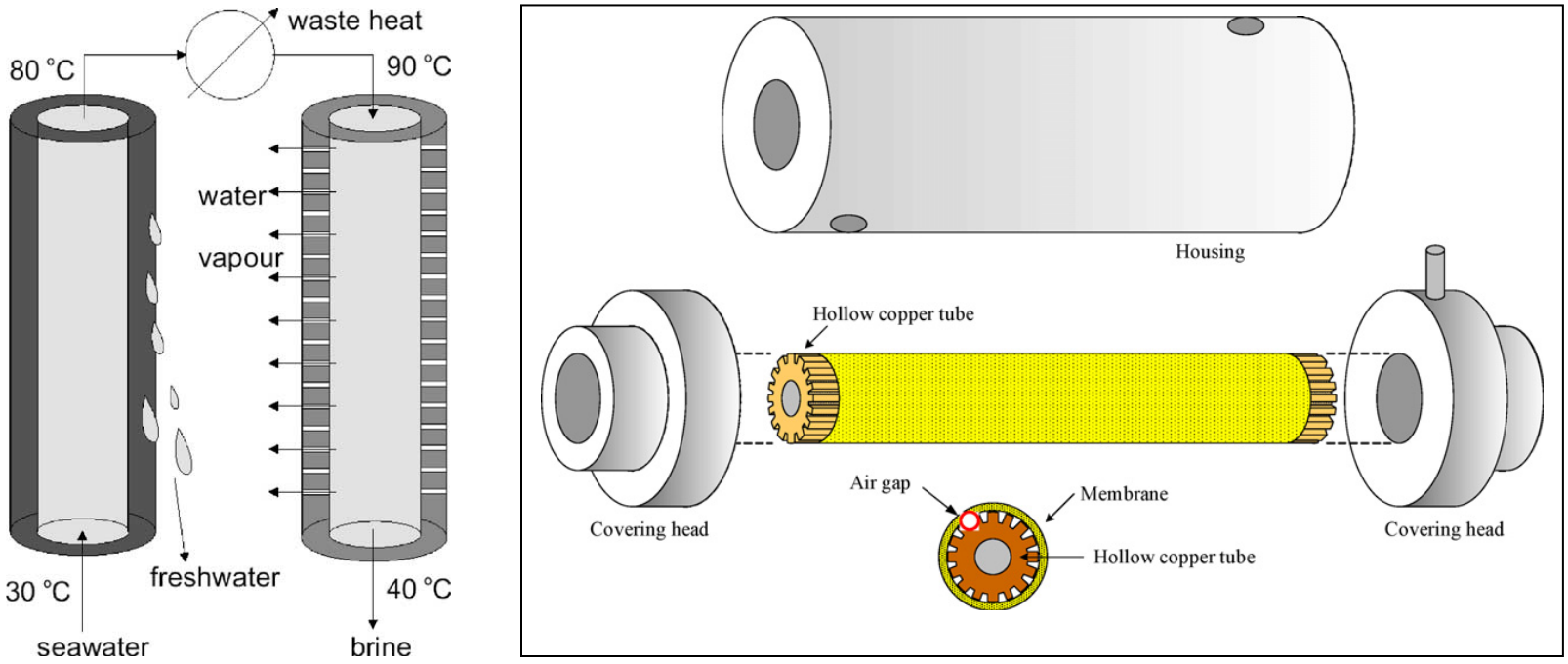

(a) (b)

Figure 5.3 Different modules used in AGMD experiment (Taken from [65] and [64]).

It was proposed and experimentally demonstrated that modules built with solid hollow fine fibers of polypropylene performed extraordinarily well as a heat exchanger [68]. The performance of such heat exchangers large and small was studied in great detail [69]. The concept of hollow fiber modules containing two separate sets of hollow fibers was introduced quite sometime back: two porous hollow fibers for separation via contained liquid membrane (for gas separation, [70]; for liquid separation, [71]); two nonporous hollow fibers for gas separation via internal staging [72]); two porous hollow fibers for synergistic solvent extraction of two separate heavy metals into two separate organic extractants from one aqueous feed solution [73]. Large two fiber set based hollow fiber modules have been built and commercialized following these early studies [74].

Here AGMD using two sets of hollow fine fibers in one cylindrical module kept in a vertical configuration will be illustrated experimentally (Figure 5.4): one set of solid hollow fibers of polypropylene through the bore of which is passed the cooling solution and another set of porous hydrophobic hollow fibers having the hot feed brine flowing through its bore. The water vapor coming out of the pores of this last set of fibers condense on the outside surface of the colder solid hollow fibers and flow downwards; the condensate flowing through the interstices of the two sets of fibers is collected from the bottom of the module. These two sets of fibers are commingled in one module within one cylindrical shell.

Three types of porous hollow fibers were studied; one was porous polypropylene with a porous fluorosilicone coating studied extensively in earlier DCMD studies [12, 14, 36]. The other two were developmental samples of porous PVDF hollow fibers. The solid hollow fibers were always of solid polypropylene. The experiments were carried out over

a range of hot brine inlet temperatures varying between 70^0C and 95^0C as well as hot brine flow rate and cooling water flow rate. The salt concentration in brine was always 1%. The primary item of interest in this experimental study was water vapor flux and the quality of the distillate.

5.2 Experimental Section

5.2.1 Materials and Chemicals

The properties of the porous and solid hollow fibers employed in all hollow fiber membrane modules are listed in Table 5.1. Porous polypropylene hollow fibers having a light porous fluorosilicone coating were obtained from rectangular DCMD modules S/N 1002 [14] used in earlier DCMD research. The substrate fibers were from Membrana, Charlotte, NC and the coating was implemented by Applied Membrane Technology Inc., Minnetonka, MN. PVDF E and PVDF H fibers provided by Arkema Inc., King of Prussia, PA and Hyflux Inc., Singapore, respectively. The chemical used are: NaCl (Sigma Aldrich).

Table 5.1 Details of the Membranes used in AGMD Experiments

Membrane	O.D. of Porous Hollow Fiber (µm)	I.D. of Porous Hollow Fiber (µm)	Wall Thickness (µm)	Pore Size (µm)	Porosity
Polypropylene	630	330	150	0.2	0.65
PVDF E	925	691.7	117	0.2	0.54
PVDF H	1600	900	350	0.693	0.52

5.2.2 Fabrication of Hollow Fiber Membrane Module

Table 5.2 lists the number of modules prepared and their characteristics. A total of 6 membrane modules were fabricated. Each of these modules was prepared using a FEP polymer-based shell having an I.D. of 1.4 cm and two Y-fittings at each end (Figure 5.5).The I.D. of each Y-fitting was 1 cm. Each set of hollow fibers was potted into an epoxy plug located in the bore of each arm of the Y-fitting. The surfaces of the solid hollow fibers were prepared per the procedure described in [68] using a chromic acid solution; their potting procedure with an appropriate epoxy is also described in [68]. These fibers were first potted at one end of the fitting with medical grade highly viscous epoxy. After curing for 12 hours, another epoxy mixture was made with C4 resin and D activator (Beacon Chemicals, Mt. Vernon, NY) in the weight ratio of 4/1. This epoxy mixture was applied to one end of the module and module was clamped in a spinner to make sure that epoxy entered into blank space between the fibers. Once it was cured for 2 days, same potting procedure was followed at the other end of the module.

These modules had varying numbers of two kinds of hollow fibers. In modules #1 to # 4 the number of porous PP fibers was similar to the number of solid hollow fibers; note that their outside dimensions were somewhat comparable. On the other hand the porous PVDF fibers were somewhat larger. Only a few of these fibers with a much larger number of solid hollow fibers were used.

Table 5.2 Details of the Modules used for AGMD Experiments

Membrane	No. of Porous Hollow Fibers	No. of Solid Fibers	Length (cm)	I.D. of Porous Hollow Fiber (µm)	Effective Area of Porous Hollow Fibers (based on I.D.) (cm^2)
Module#1	10	10	15.5	330	16
Module#2	14	14	14.4	330	20.9
Module#3	21	21	14	330	30.35
Module#4	29	29	14.2	330	42.7
PVDF E	7	35	15.5	691.7	23.58
PVDF H	3	35	12.0	900	11.87

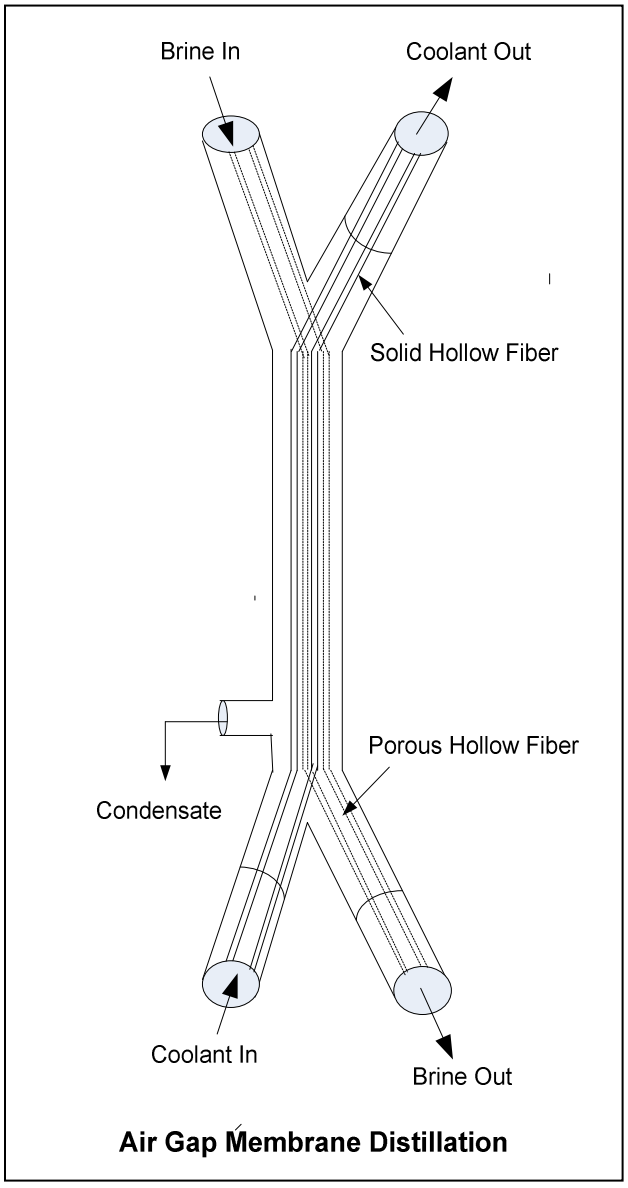

Figure 5.4 Schematic of air gap membrane module.

(a)

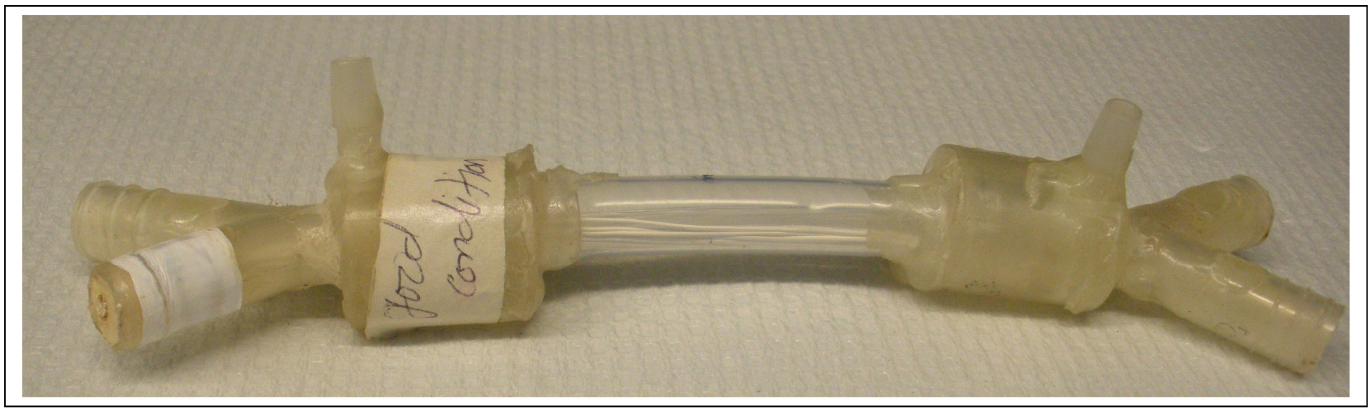

(b)

Figure 5.5 Photograph showing air gap membrane module used in the experiments having shell side opening on (a) one side (b) two side.

5.2.3 AGMD Experiments

AGMD performances were explored in the brine temperature range of 80^{o}C to 95^{o}C in the set up shown in Figure 5.6. Feed brine containing 1% NaCl was pumped through the bores of porous hollow fibers and cold water was introduced into bores of solid hollow fibers by two peristaltic pumps (Masterflex, Cole-Parmer, Vernon Hills, IL). Brine feed solution was heated in a constant temperature bath (A81, HAAKE, Germany). The cold water stream was heated up after passing through the membrane module; cooling of this cold water stream heated up was achieved by a chiller (12920-40, Cole-Parmer, Vernon Hills, IL). The brine reservoir was well covered to prevent evaporation of water to laboratory environment. A filter holder (47 mm, Sterlitech, Washington, contains slits 1 mm x 3 mm long) was placed before the membrane module to avoid any damage to the membrane from larger particles. The liquid level inside the brine beaker was kept constant using two level probes and a level controller which was connected to a peristaltic pump to supply water from the make-up water reservoir.

The inlet and outlet temperatures of the brine and the cold water stream passing through the membrane module were measured by thermocouples (EW-08516-74, Cole-Parmer, Vernon Hills, IL) connected to a data acquisition logger (OM-DAQPRO-5300, Omega Engineering, Stamford, CT). The pressures of brine in and coolant in stream were measured with a digital pressure gauge (DPG1000DAR-15G-1N, Omega Engineering, Stamford, CT) and an analog pressure gauge. The electrical conductivity of the condensate stream was measured by a conductivity meter (Orion 115A^{+}, Thermo Electron Corporation, MA) to monitor for possible leaks of salt into the distillate side. Samples from the condensate side were also analyzed by Atomic Absorption (AAnalyst 400, Atomic Absorption Spectrometer, Perkin Elmer, Norwalk, CT-06859) for sodium

chloride; in addition the conductivity on the condensate side was measured by a conductivity meter (Orion 115A^{+}, Thermo Electron Corporation, MA).

Any experiment under given conditions was run for 6 hours. Steady state was assumed when the brine flow rate, the cold water flow rate and the temperatures of the brine in and brine out as well as the temperatures of the coolant in and coolant out attained constant values. After steady state was reached, the increase in the water level in the condensate tank over a certain time was used for calculation of water vapor flux (N_v) from the following relation:

$$N_v\left(\frac{kg}{m^2.h}\right)=\frac{volume\,of\ water\,transferred\,(L)\,x\ density\,of\ water\,(kg/L)}{membrane\,area\,(m^2)\,x\ time\,(h)} \quad \ldots\ldots\ldots\ldots\ldots(5.1)$$

Here, membrane area is calculated on the basis of inside diameter of the porous hollow fiber.

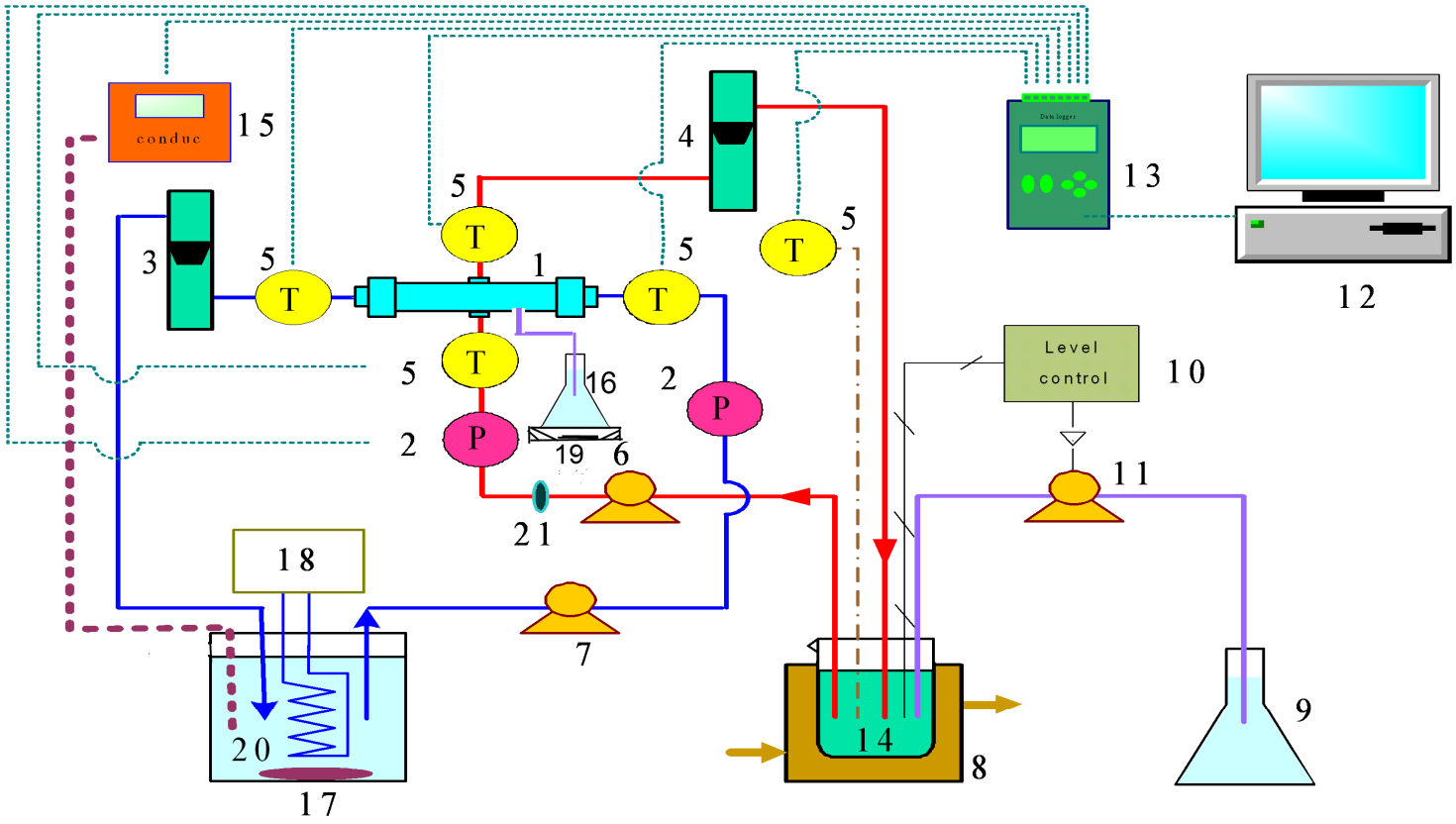

Figure 5.6 Experimental set up for AGMD experiments:
1. Membrane module; 2. Pressure indicator; 3. Coolant flowmeter ; 4. Brine flowmeter; 5. Thermocouple; 6. Hot brine pump ; 7. Coolant pump; 8. Constant temperature bath; 9. Make-up water reservoir; 10. Level controller; 11. Make-up pump; 12. Computer; 13. Data logger; 14. Hot brine beaker ; 15. Conductivity transmitter; 16. Condensate reservoir; 17. Magnetic stirrer; 18. Chiller; 19. Weight balance; 20. Coolant beaker; 21. Filter holder.

5.3 AGMD Experiments with 1 % NaCl Solution at Lower Brine Temperatures

5.3.1 Experiments with PP Porous Hollow Fiber

AGMD was explored with two sets of hollow fibers in a module; one set of solid hollow fiber of polypropylene through which cold water flows acts as a condensing surface and other set of hollow fiber through which hot brine flows is made of porous propylene. The hot vapors coming out from the porous hollow fiber condense on the cold surface of solid polypropylene hollow fibers. The details of the modules are given in Table 5.3.

Hot brine containing 1% NaCl passed through the bores of porous hollow fibers of polypropylene at a flow rate of 75 ml/min. The cooling water was introduced at 20^{o}C at the flow rate of 150 ml/min. Figure 5.7 illustrate the change in water vapor flux with brine temperature for different modules. For module#1, as temperature of the feed brine was increased from 70^{o}C to 85^{o}C, flux increased from 15.12 kg/m^2-hr to 22.92 kg/m^2-hr. For module#2, flux increased from 13.49 kg/m^2-hr to 28.6 kg/m^2-hr as the feed brine temperature was increased from 70^{o}C to 88^{o}C. Water vapor flux increased from 9.49 kg/m^2-hr to 26.11 kg/m^2-hr as feed brine temperature was increased 70^{o}C to 88^{o}C in module#3. Finally, for module#4, flux increased from 9.37 kg/m^2-hr to 22.7 kg/m^2-hr as feed brine temperature was increased from 75^{o}C to 94^{o}C. Each of these modules was prepared using a FEP polymer-based shell having an I.D. of 1.4 cm and two Y-fittings at each end of 1 cm diameter. The air gap between fibers should be minimum for module#4 and correspondingly water vapor flux should be higher for module#4 but experimental results suggest otherwise. It was due to the compact nature of module#4 prohibiting the uniform distribution of fibers in the module. Since outer surface area of solid hollow fiber

is less than the outer surface area of porous hollow fiber, the condensation surface area was decreased, as the number of fibers increased from module#1 to module#4.

Table 5.3 Details of the Porous PP Hollow Fibers and Modules used for AGMD

Membrane	No. of Porous Hollow Fibers	No. of Solid Fibers	Length (cm)	I.D. of Porous Hollow Fiber (µm)	Effective Area of Porous Hollow Fibers (cm^2)
Module#1	10	10	15.5	330	16
Module#2	14	14	14.4	330	20.9
Module#3	21	21	14	330	30.35
Module#4	29	29	14.2	330	42.7

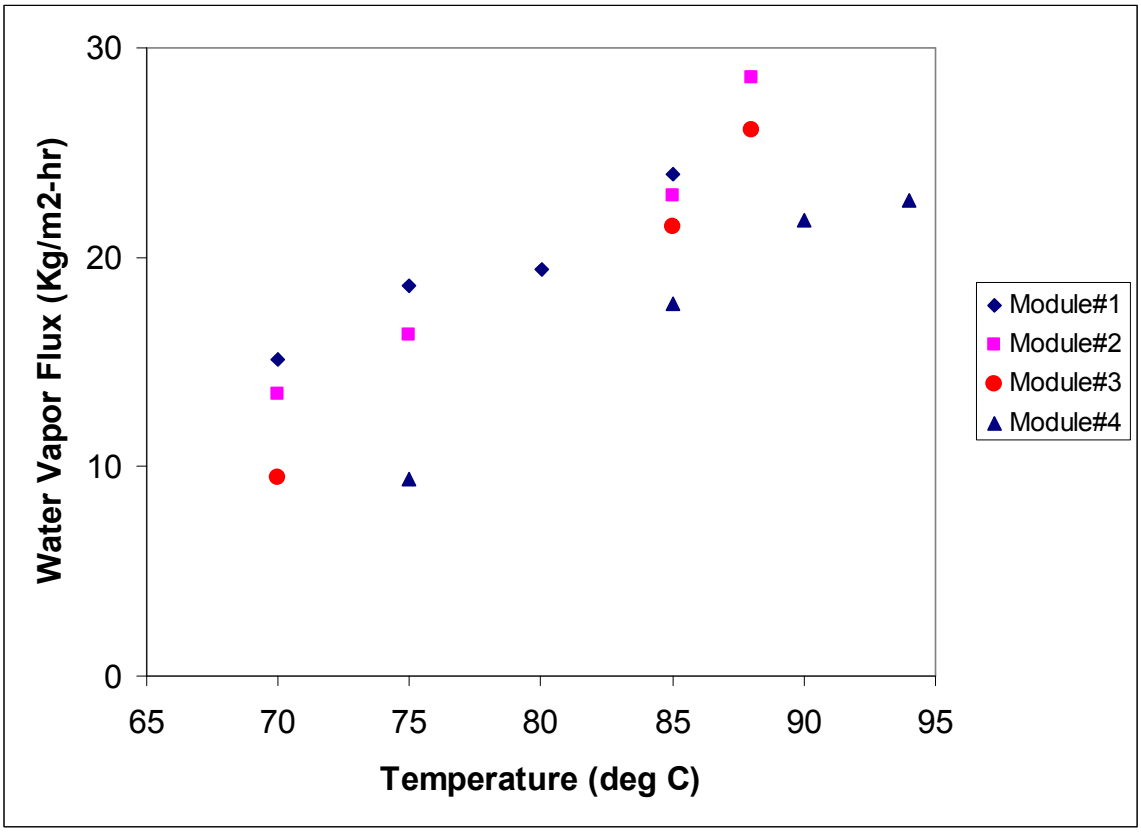

Figure 5.7 Change in water vapor flux with temperatures in AGMD experiments for different PP-based modules.

The effect of brine flow rate on water vapor flux at different brine temperatures was studied for 1 % NaCl solution in module#2. Figure 5.8 illustrates that higher brine flow rate yields higher water vapor flux at different brine temperatures for 1% NaCl solution. It is potentially due to reduction of temperature polarization in the brine at the higher brine flow rate.

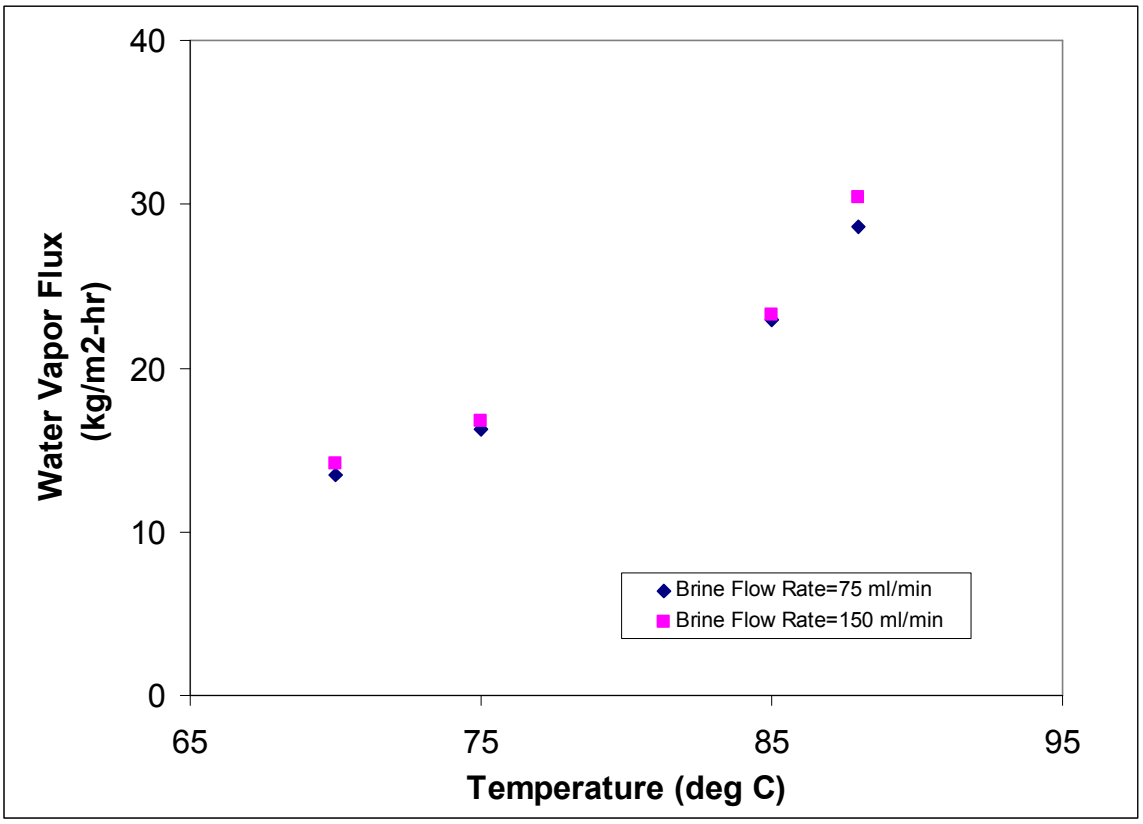

Figure 5.8 Effect of brine flow rate on water vapor flux at different brine temperatures in module # 2 in AGMD.

Higher flow rate of hot brine through the bore of the porous PP fibers leads to significant pressure drop in the brine as shown in Figure 5.9. The inlet hot brine pressure goes upto 20 psig at a brine flow rate of 150 cm^3/min. This increase in brine pressure has

consequences for the very porous PP hollow fibers being used. These fibers have larger pores around 0.65 μm [12] and therefore have a low liquid entry pressure. It is suspected that the larger pores will get wetted and will leak brine into the condensate and raise the permeate/condensate salt concentration. It was noticed that as the brine flow rate increased the salt concentration in the permeate increased; however, the leakage level is quite low for the lowest flow rate studied, 50 ml/min; salt concentration in the condensate was around 3 ppm. At the highest brine flow rate, there is significant salt leakage. The salt concentration is still far lower than the acceptable limit.

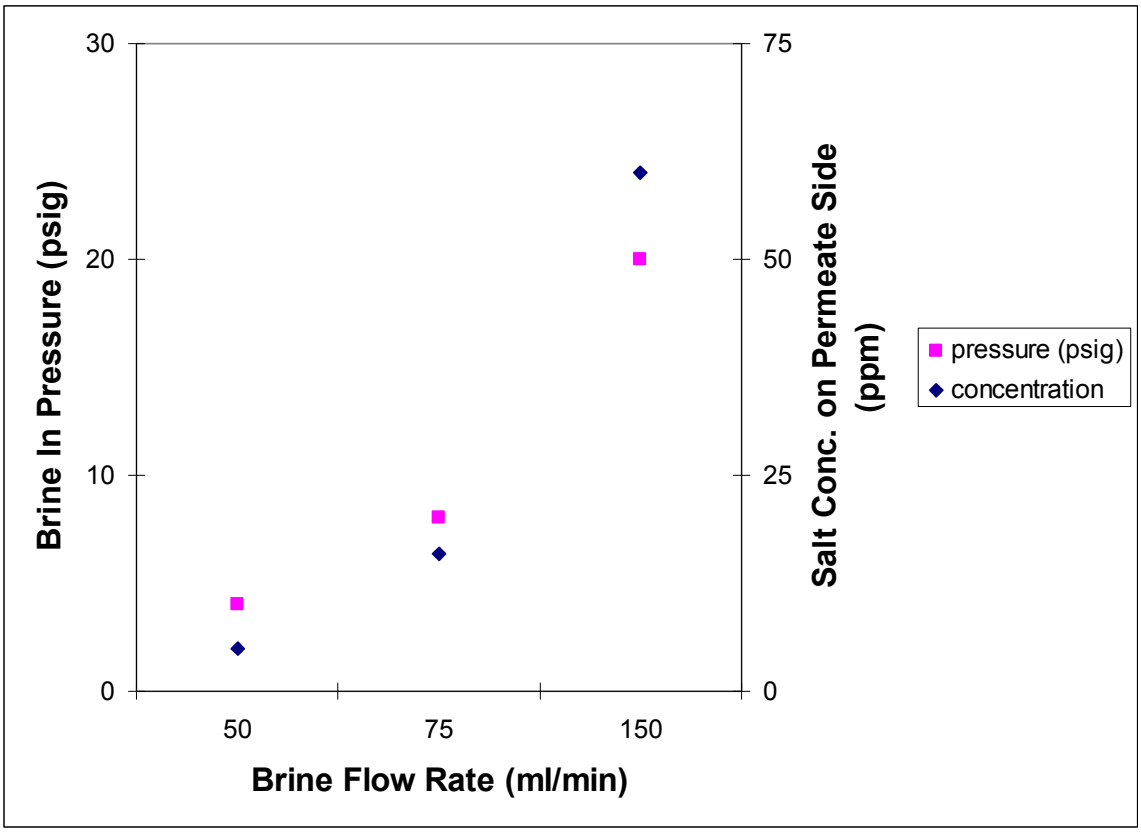

Figure 5.9 Effect of brine flow rate on its pressure drop and salt concentration on permeate side.

The effect of cooling water flow rate flowing through the bores of solid hollow fibers of polypropylene was studied for 1% NaCl solution in AGMD for module#2. It was observed in Figure 5.10 that water vapor flux was increased as the cooling water flow rate increased at different brine temperatures. Higher cooling water flow rate increases the water vapor flux presumably because higher cooling water flow rate increases the cooling water heat transfer coefficient.

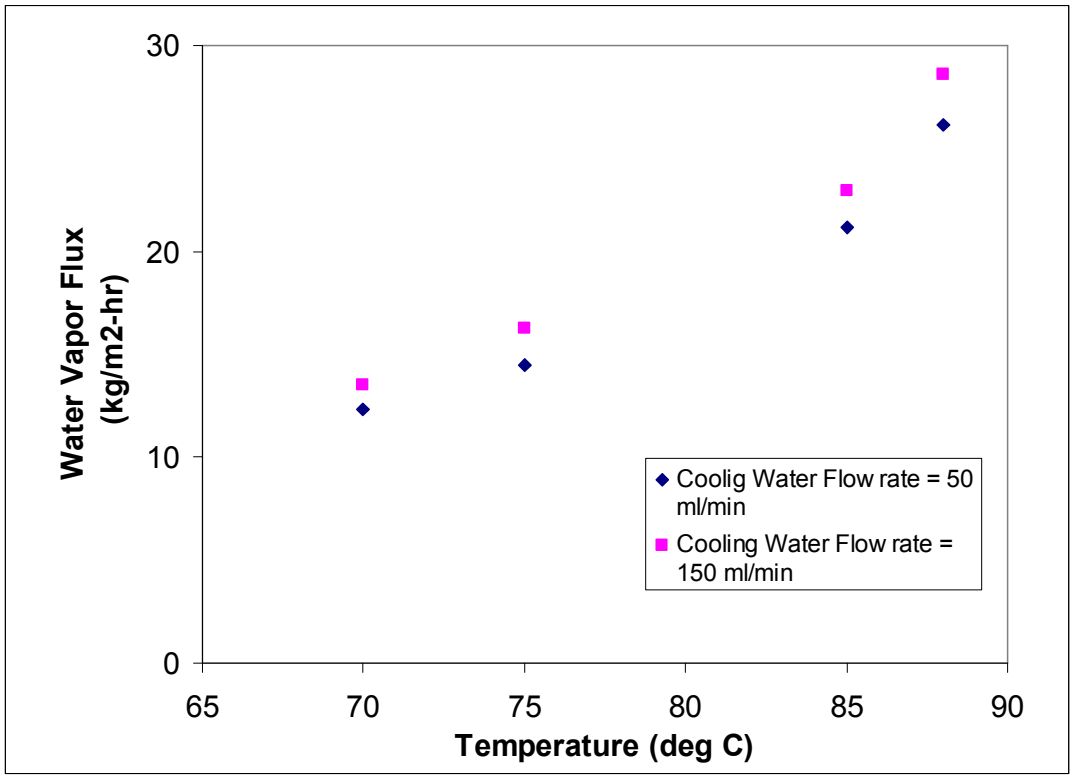

Figure 5.10 Effect of cooling water flow rate on water vapor flux in AGMD.

5.3.2 Experiments with PVDF hollow fiber E and Solid Polypropylene Hollow Fiber

A module was fabricated using a FEP polymer-based shell having an I.D. of 1.4 cm and two Y-fittings at each end (Figure 5.4) having an I.D. of 1 cm. The PVDF E hollow fiber has the following properties: O.D. = 925 μm, I.D. = 691.7 μm, wall thickness = 117 μm,

pore size of 0.2 μm and porosity ~ 0.54. The details of the modules are given in Table 5.4. For all the AGMD experiments, hot 1% NaCl solution was flowing through the bores of PVDF E hollow fibers at the rate of 125 ml/min and cooling water was flowing through the bores of solid polypropylene hollow fibers at the rate of 250 ml/min. Water vapor flux increased from 5.96 kg/m^2-hr to 9.9 kg/m^2-hr as temperature of brine was increased from 80^{o}C to 88^{o}C. The flux values are significantly lower than those in modules with porous PP hollow fibers for the same brine feed containing 1% salt. These fibers are not as porous (porosity~0.54). These PVDF E hollow fibers were also explored with same feed in DCMD at different brine temperatures with brine flowing on the shell side. It is illustrated in Figure 5.11 that the values of water vapor flux were higher than the values obtained in AGMD.

Table 5.4 Details of PVDF Hollow Fiber E and Modules used for AGMD and DCMD Experiments

Process	No. of Porous PVDF E Hollow Fibers	No. of Solid PP Fibers	Effective Length of Module (cm)	I.D. of Porous PVDF E Hollow Fiber (μm)	Effective Area of Porous Hollow Fibers (cm^2)
DCMD	3	-	17.5	691.7	11.41
AGMD	7	35	15.5	691.7	23.58

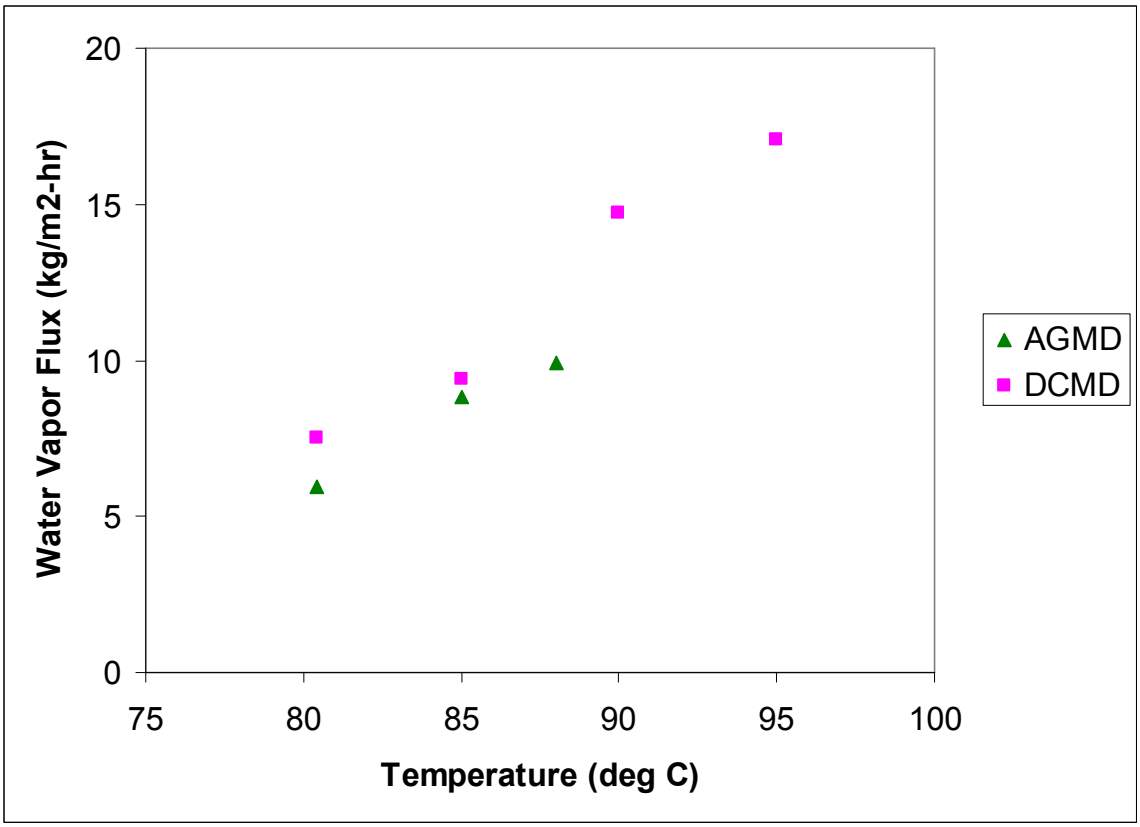

Figure 5.11 Comparison of water vapor flux for PVDF E in DCMD and AGMD.

5.3.3 Investigation of AGMD with Hollow Fibers of Porous PVDF H and Solid Polypropylene

A module was fabricated using a FEP polymer-based shell having an I.D. of 1.4 cm and two Y-fittings at each end (Figure 5.4) having an I.D. of 1 cm. The PVDF H hollow fiber has the following properties: O.D. = 1600 µm, I.D. = 900 µm, wall thickness = 350 µm, pore size of 0.62 µm and porosity ~ 0.50. The details of the modules are given in Table 5.5. For all AGMD experiments, hot 1% NaCl solution was flowing through the bores of PVDF H hollow fibers at the rate of 125 ml/min and cooling water was flowing through the bores of solid polypropylene hollow fibers at the rate of 250 ml/min. Water vapor flux increased from 10.5 kg/m^2-hr to 15.4 kg/m^2-hr as temperature of brine was increased from 82^{o}C to 88^{o}C as shown in Figure 5.12. The flux values are significantly lower than

those in modules with porous PP hollow fibers for the same brine feed containing 1% salt. Like PVDF E hollow fibers, these fibers are also not as porous (porosity~0.50) as PP. These PVDF H hollow fibers were also explored with the same feed in DCMD at different brine temperatures. It is illustrated in Figure 5.12 that the values of water vapor flux were higher than the values obtained in AGMD.

Table 5.5 Details of PVDF Hollow Fiber H and Modules used for AGMD and DCMD Experiments

Process	No. of Porous PVDF H Hollow Fibers	No. of Solid PP Fibers	Effective Length of Module (cm)	I.D. of Porous PVDF H Hollow Fiber (μm)	Effective Area of Porous Hollow Fibers (cm^2)
DCMD	5	-	20.2	900	28.6
AGMD	3	35	14	900	11.87

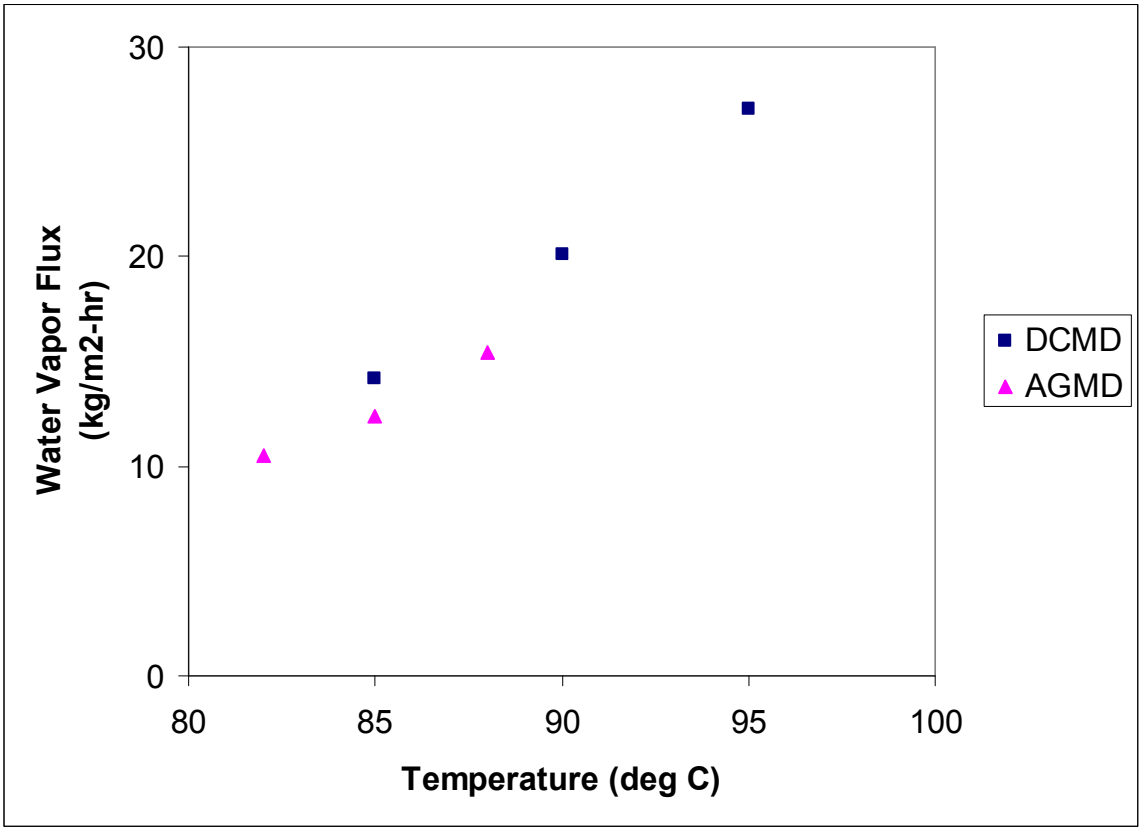

Figure 5.12 Water vapor flux for PVDF H fibers at different temperatures of brine.

It was clear from above experiments that 99.99 % salt rejections were achieved in AGMD for porous PP hollow fiber, PVDF H hollow fiber and PVDF E hollow fiber. Similarly, in DCMD experiments also, 99.99 % salt rejections were observed for PP hollow fiber and PVDF E hollow fiber. However, salt rejections for PVDF H hollow fiber were 96 % for all AGMD experiments shown in Figure 5.13. It is clear from the SEM micrograph (see Figure 3.37) that the sizes of some pores are larger than 5 μm; membrane develops pore wetting due to these defects.

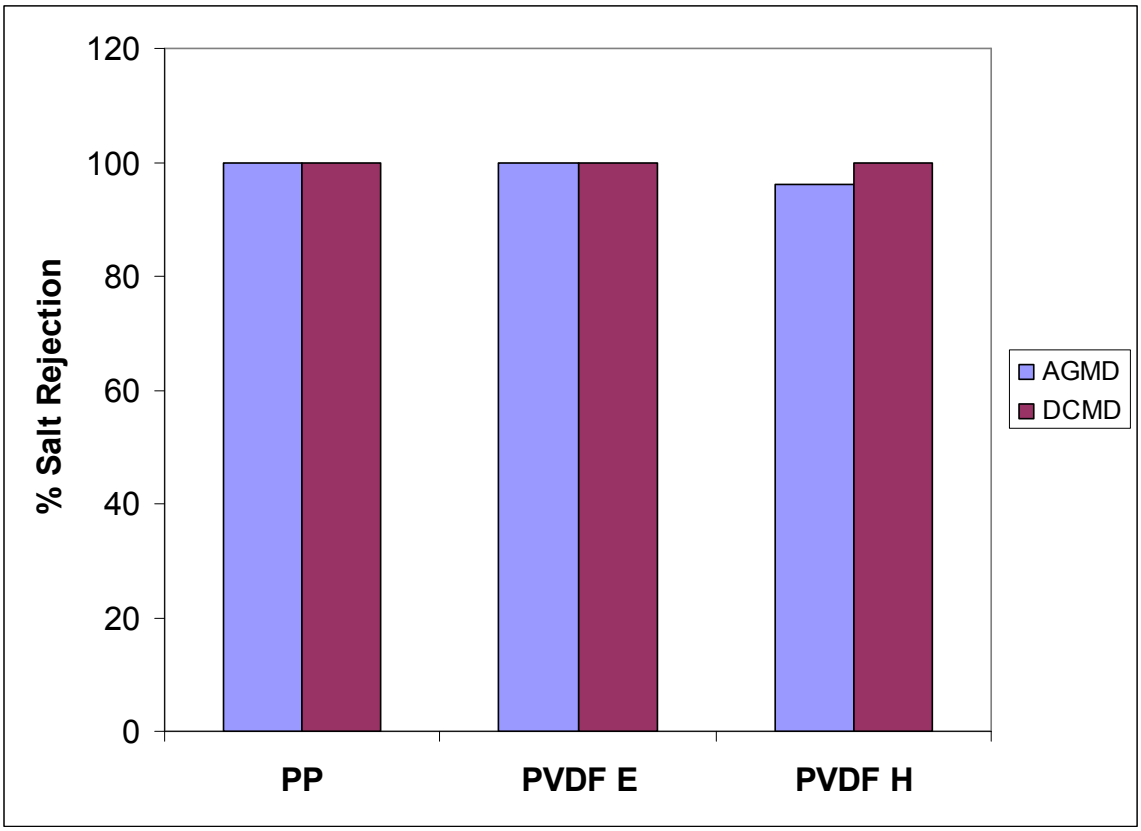

Figure 5.13 % Salt rejection in AGMD and DCMD for different porous hollow fibers.

CONCLUSIONS

In the past, DCMD has been explored for hot brines and other aqueous solutions below 100^{o}C. For feed solutions above 100^{o}C, an experimental setup was designed and successfully tested for different types of membrane materials in different form either in flat sheet or hollow fiber. Porous ceramic disc was successfully hydrophobized for its applications in DCMD experiments. Hydrophobized ceramic tubule was also investigated for DCMD experimnts.

PTFE and PVDF flat sheet membranes were investigated for DCMD experiments at lower as well as higher temperatures. A microporous PTFE flat sheet membrane having a pore size of 0.03 μm was employed in DCMD experiments with 1% NaCl solution at lower brine temperatures as well as higher brine temperatures (>100^{o}C). A simulated feed representing SAGD process produced water containing phenol, cresol, naphthenic acid along with sodium chloride was also investigated. The membrane was characterized by scanning electron microscopy and nitrogen gas permeation test to study surface morphology and its properties. A water vapor flux of up to 195 kg/m^{2}-hr was achieved at 128^{o}C for 1% brine solution, which is around an order of magnitude higher than that for seawater reverse osmosis (RO) processes. Experiments with produced water yielded water vapor fluxes similar to those for 1% NaCl solution. Concentrations of phenol, cresol and naphthenic acid were analyzed successfully by HPLC and GC-EI-MS. It was found that only few ppm (~ 5 ppm) of phenol and cresol passed through the PTFE membrane at very high temperature with no leakage of NaCl. PVDF flat sheet membrane

was also successfully explored with 1 % NaCl solution at lower as well as higher temperatures.

Hollow fiber membranes of PMP, PTFE, PVDF and hydrophobized PEEK were explored for DCMD experiments at lower as well as higher temperatures. It is interesting to note that PMP fibers did not yield any measurable flux in DCMD since, in DCMD, most part of the sensible heat lost by the hot feed brine is transferred by conduction through the very thin solid polymeric wall and the vapor-filled pore space to the cold distillate stream. For experiments with PVDF hollow fiber E in DCMD, water vapor flux increased from 29 kg/m^2-hr to 88.5 kg/m^2-hr as the temperature of the feed brine solution was increased from 105^{o}C to 124^{o}C.

For PTFE hollow fiber M, water vapor flux increased from 68 kg/m^2-hr to 115 kg/m^2-hr as the brine temperature was increased from 108^{o}C to 118^{o}C with constant conductivity on distillate side. Similarly, for PTFE hollow fiber N, water vapor flux increased from 30.8 kg/m^2-hr to 97.6 kg/m^2-hr as temperature was increased from 108^{o}C to 118^{o}C with constant conductivity on distillate side. Experiments were also done with large PTFE hollow fiber module at lower as well as higher temperatures. The water vapor flux increased from 0.43 kg/m^2-hr to 11.76 kg/m^2-hr as the temperature of feed solution was increased from 56^o C to 110^o C. Due to limitations of the experimental setup, the large module performance could be explored only up to 110^o C at a brine flow rate of 1100 ml/min. It is expected that with higher flow rates, the flux will go up considerably.

In general, DCMD has been proved to be very useful process, especially at high temperatures where it can utilize the heat available in the feed. Compared to other

conventional processes like reverse osmosis, it may be economically viable in such cases, because DCMD does not require cooling which reduces additional energy requirements.

For AGMD experiments, two-hollow fiber-set based compact device were developed to investigate with 1 % NaCl solution. The first fiber set consists of porous hydrophobic hollow fibers of either polypropylene (PP) or polyvinylidene fluoride (PVDF). The second set of hollow fibers is of solid PP through the bore of each such hollow fiber the cooling liquid is passed and on the outside surface of which water vapor condensation takes place. For PP porous hollow fibers, it was noticed that as the brine flow rate increased the salt concentration in the permeate increased; however, the leakage level is quite low for the lowest flow rate studied, 50 ml/min; salt concentration in the condensate was around 3 ppm.

For PVDF E hollow fiber in AGMD, water vapor flux increased from 5.96 kg/m^2-hr to 9.9 kg/m^2-hr as temperature of brine was increased from 80^{o}C to 88^{o}C. These PVDF E hollow fibers were also explored with same feed in DCMD at different brine temperatures with brine flowing on the shell side. It was concluded that the values of water vapor flux were higher than the values obtained in AGMD. Similarly, the values of water vapor flux for PVDF H in DCMD were higher than the values obtained for PVDF H hollow fiber in AGMD. For 1 % NaCl feed solution, 99.99 % salt rejection was observed for these porous hollow fibers in AGMD as well as in DCMD experiments at lower flow rate, except for PVDF H hollow fiber in AGMD experiments where the rejection was around 96 % due to the presence of few large pore in the hollow fiber membrane.

APPENDIX A

WATER VAPOR FLUX CALCULATIONS AT LOWER TEMPERATURES

Water Vapor Flux Calculation for PVDF Hollow Fiber H Membrane Module

Effective area of membrane module = 28.62 cm^2

Amount of water collected at 85^o C = 40.7 gm

Time = 1 hr

Water vapor flux = (40.7 x 10^{-3} kg)/(28.62 x 10^{-4} m^2 x 1 hr) = 14.21 kg/m^2-hr.

APPENDIX B

WATER VAPOR FLUX CALCULATIONS AT HIGHER TEMPERATURES

Water Vapor Flux Calculation for PTFE Hollow Fiber M Membrane at 112^{o} C

Effective area of hollow fiber M membrane module = 38.06 cm^2

Distillate in flow rate = 465 ml/min

Distillate out flow rate = 472 ml/min

Change in flow rate = 7 ml/min = 420 ml/hr = 0.42 lt/hr = 0.42 kg/hr

Water vapor flux = 0.42 kg / (38.06 x 10^{-4} m^2 x 1 hr) = 110 kg/m^2-hr

REFERENCES

1. B.R. Bodell, Silicone rubber vapor diffusion in saline water distillation, United States Patent Serial No. 285,032 (1963).

2. E. Findley, Vaporization through porous membrane, Ind. Eng. Chem. Pro. Des. and Dev. 6 (1967) 226-237.

3. M. Khayet, Membranes and theoretical modeling of membrane distillation: A review, Adv. Coll. Inter. Sci. 164 (2011) 56-88.

4. D.W. Gore, Gore-Tex membrane distillation. In proceedings of the 10th Annual Convention of Water Supply Improvement Association, Honolulu, Hawaii, July 25-29, 1982.

5. B. Li, K. K. Sirkar, Novel membrane and device for vacuum membrane distillation based desalination process, J. Membr. Sci. 257 (1-2) (2005) 60-75.

6. C.M. Guijt, G.W. Meindersma, T. Reith, A.B. de Haan, Air gap membrane distillation 1. Modeling and mass transport properties for hollow fiber membranes, Sep. Purif. Technol. 43 (2005) 233-244.

7. C. Feng, K.C. Khulbe, T. Matsuura, R. Gopal, S. Kaur, S. Ramakrishna, M. Khayet, Production of drinking water from saline water by air-gap membrane distillation using polyvinylidene fluoride nanofiber membrane, J. Membr. Sci. 311(1-2) (2008) 1-6.

8. E. Curcio, E Drioli, Membrane distillation and related operations-a review, Sep. and Pur. Rev. 34 (2005) 35-86.

9. R.W. Schofield, A. G. Fane, C. J. D. Fell, Heat and mass transfer in membrane distillation, J. Membr. Sci. 33(3) (1987) 299-313.

10. J. Phattaranawik, R. Jiraratananon, A. G. Fane, Heat transport and membrane distillation coefficients in direct contact membrane distillation, J. Membr. Sci. 212 (1-2) (2003) 177-193.

11. K. W. Lawson, D. R. Lloyd, Membrane distillation II. Direct contact MD, J. Membr. Sci. 120 (1996) 123-133.

12. B. Li, K.K. Sirkar, Novel membrane and device for direct contact membrane distillation-based desalination process, Ind. Eng. Chem. Res. 43 (2004) 5300-5309.

13. L. Song, B. Li, K. K. Sirkar, J. Gilron, Direct contact membrane distillation-based desalination: Novel membranes, devices larger-scale studies and a model, Ind. Eng. Chem. Res. 46 (2007) 5300-5309.

14. L. Song, Z. Ma, X. Liao, P. B. Kosaraju, J. R. Irish, K. K. Sirkar, Pilot plant studies of novel membranes and devices for direct contact membrane distillation-based distillation, J. Membr. Sci. 323 (2008) 257–270.

15. E. Drioli, E. Curcio, G. di Profio, State of the Art and recent progresses in membrane contactors, Chem. Eng. Res. and Des. 83 (3) (2005) 223-233.

16. P. K. Weyl, Recovery of demineralized water from saline waters. U. S. Patent 3,340,186.

17. K. W. Lawson, D. R. Lloyd, Membrane distillation-review, J. Membr. Sci. 124 (1-5) (1997) 1-25.

18. Y. Fujii, S. Kigoshi, H. Iwatani, M. Aoyama, Selectivity and characteristics of direct contact membrane distillation type experiment: I. Permeability and selectivity through dried hydrophobic fine porous membranes, J. Membr. Sci. 72 (1992) 53-72.

19. Y. Fujii, S. Kigoshi, H. Iwatani, M. Aoyama, Y. Fusaoka, Selectivity and characteristics of direct contact membrane distillation type experiment: II. Membrane treatment and selectivity increase, J. Membr. Sci. 72 (1992) 73-89.

20. J. M. Ortiz de Zarate, L. Pena, Ji Mengual, Characterization of membrane distillation membranes prepared by phase inversion, Desalination. 100 (1995) 139-148.

21. M. Tomaszewska, Preparation and properties of flat-sheet membranes from polyvinylidene fluoride for membrane distillation, Desalination. 104 (1996) 1-11.

22. C. Feng, B. Shi, G. Li, Y. Wu, Preliminary research on microporous membrane from F2.4 for membrane distillation, Sep. Purif. Technol. 39 (2004) 221–228.

23. C. Feng, B. Shi, G. Li, Y. Wu, Preparation and properties of microporous membrane from poly(vinylidene fluoride-co-tetrafluoroethylene) (F2.4) for membrane distillation, J. Membr. Sci. 237 (2004) 15–24.

24. M. Khayet, J. Mengual, T. Matsuura, Porous hydrophobic/hydrophilic composite membranes: application in desalination using direct contact membrane distillation, J. Membr. Sci. 252 (2005)101–113.

25. D.Y. Cheng, Method and apparatus for distillation, United States Patent Serial No. 4, 265, 713 (1981).

26. K. Ohta, I. Hayano, T. Okabe, T. Goto, S. Kimura, H. Ohya, Membrane distillation with fluoro-carbon membranes, Desalination. 81(1991) 107–115.

27. Y. Kong, X. Lin, Y. Wu, J. Cheng, J. Xu, Plasma polymerization of octafluorocyclobutane and hydrophobic microporous composite membranes for membrane distillation, J. Appl. Polym. Sci. 46 (1992) 191–99.

28. M. Khayet, T. Matsuura, Application of surface modifying macromolecules for the preparation of membranes for membrane distillation, Desalination. 158 (2003) 51–60.

29. J. Li, Z. Xu, W. Yuan, H. Xiang, S. Wang, Y. Xu, Microporous polypropylene and polyethylene hollow fiber membranes : Part 3. Experimental studies on membrane distillation for desalination, Desalination. 155 (2003) 153-156.

30. S. Bonyadi, T. S. Chung, Flux enhancement in membrane distillation by fabrication of dual layer hydrophilic–hydrophobic hollow fiber membranes, J. Membr. Sci. 306 (2007)134–146.

31. K. Y. Wang, S. W. Foo, T. S. Chung, Mixed matrix PVDF hollow fiber membranes with nanoscale pores for desalination through direct contact membrane distillation, Ind. Eng. Chem. Res. 48 (2009) 4474–4483.

32. M. C. García-Payo, M. Essalhi, M. Khayet, Preparation and characterization of PVDFHFP copolymer hollow fiber membranes for membrane distillation, Desalination. 245 (2009) 469–473.

33. C. Gostoli, G. C. Sarti, Separation of liquid mixtures by membrane distillation, J. Membr. Sci. 41 (1989) 211-224.

34. K. W. Lawson, D. R. Lloyd, Membrane distillation. I. Module design and performance evaluation using vacuum membrane distillation, J. Membr. Sci. 120 (1996) 111-121.

35. M. Khayet, P. Godino, J. I. Mengual, Theory and experiments on sweeping gas membrane distillation, J. Membr. Sci. 165 (2000) 261-272.

36. F. He, J. Gilron, H. Lee, L. Song, K. K. Sirkar, Potential for scaling by sparingly soluble salts in cross-flow DCMD, J. Membr. Sci. 311 (2008) 68-80.

37. F. He, K. K. Sirkar, J. Gilron, Studies on scaling of membranes in desalination by direct contact membrane distillation: $CaCO_3$ and mixed $CaCO_3/CaSO_4$ systems, Chem. Eng. Sci. 64 (2009a) 1844-1859.

38. F. He, K. K. Sirkar, J. Gilron. Effects of antiscalants to mitigate membrane scaling by direct contact membrane distillation. J. Membr. Sci. 345 (2009b) 53-58.

39. G. Zakrewska-Trznadel, M. Harasimowicz, A. G. Chmielewski, Concentration of radioactive components in liquid low-level radioactive waste by membrane distillation, J. Membr. Sci. 163 (1999) 257-264.

40. J. Koschikowski, M. Wieghaus, M. Rommel, Solar thermal-driven desalination plants based on membrane distillation, Desalination 156 (2003) 295–304.

41. H. Kuhn, H. D. Forstering, Principles of Physical Chemistry, Wiley, New York, 2000.

42. R. A. Albert, R. J. Silbey, Physical Chemistry, 2nd ed., Wiley, New York, 1997.

43. E. L. Cussler, Diffusion, Mass Transfer in Fluid System, 2nd ed., Cambridge University Press, New York, 1997.

44. A. F. Mills, Mass Transfer, 2nd ed., Prentice-Hall, New Jersey, 2001.

45. J. S. Mackie, P. Meares, The diffusion of electrolytes in a cation-exchange membrane .I; Theoretical, Proc. Roy. Soc., A232 (1955) 498.

46. T. Kohav., M. Sheintuch, D. Anvir, Steady state diffusion and reactions in catalytic fractal porous media, Chem. Eng. Sci. 46 (1991) 2787-2798.

47. S. B. Iversen, V. K. Bhatia, K. Dam-Johansen, G. Jonsson, Characterization of microporous membranes for use in membrane contactors, J. Membr. Sci. 130 (1997) 205-217.

48. R. W. Schofield, A.G. Fane, C. J. D. Fell, Gas and vapor transport through microporous membranes. II. Membrane Distillation, J. Membr. Sci. 53 (1990) 173-185.

49. E. A. Mason, A. P. Malinauskas, Gas transport in porous media: The Dusty-Gas model, Elsevier, Amsterdam, 1983.

50. M. W. Denny, Air and Water: the biology and physics of life's media, Princeton University Press, Princeton, New Jersey, page 89.1993.

51. T. R. Marrero, Edward Allen Mason, United States. National Bureau of Standards, American Chemical Society and American Institute of Physics, 1972.

52. H. Yasuda, J. T. Tsai, Pore size of microporous polymer membranes, J. Appl. Polym. Sci. 18 (1974) 805-819.

53. K. Li, J. F. Kong, W. K. Teo, Tailor made asymmetric hollow fibers for soluble gas removal, AIChE J. 45(6) (1999) 1211-1219.

54. D. Wang, W. K. Teo, Preparation and characterization of polyvinylidene fluoride (PVDF) hollow fiber membranes, J. Membr. Sci. 163 (1999) 211-220.

55. M. Merlin, S.E. Guigard, P.M. Fedorak, Detecting naphthenic acids in waters by gas chromatography-mass spectrometry, J. Chrom. A. 1140 (2007) 225-229.

56. P. Wayne, St. John, J. Rughani, S. Green, D. Gary, McGinnis, Analysis and characterization of naphthenic acids by gas chromatography-electron impact mass spectrometry of tert.-butyldimethylsilyl derivatives, J. Chrom. A. 807 (1998) 241-251.

57. C. Leger, H. L. Lira, R. Paterson, Preparation and properties of surface modified ceramic membranes, J. Membr. Sci. 120 (1996) 135-146.

58. A. Criscuoli, M. C. Carnevale, E. Drioli, Evaluation of energy requirements in membrane distillation, Chem. Eng. Proc. 47 (2007) 1043-1050.

59. L. Martinez, F. G. Florido-Diaz, Theoretical and experimental studies on desalination using membrane distillation, Desalination. 139 (2001) 373-379.

60. X. Gong, Personal communication, ConocoPhillips, August 04, 2010.

61. H. Lee, F. He, L. Song, J. Gilron, K. K. Sirkar, Desalination with a cascade of crossflow hollow fiber membrane distillation devices integrated with a hollow fiber heat exchanger, AIChE J. 57(7) (2011) 1780-1795.

62. A. M. Alklaibi, N. Lior, Heat and mass transfer resistance analysis of membrane distillation, J. Membr. Sci. 282 (2006) 362-369.

63. Li-Hua Cheng, Ping-Chung Wu, Junghui Chen, Numerical simulation and optimal design of AGMD-based hollow fiber modules for desalination, Ind. Eng. Chem. Res. 48 (2009) 4948-4959.

64. Li-Hua Cheng, Yu-Hung Lin, Junghui Chen, Enhanced air gap membrane desalination by novel finned tubular membrane modules, J. Membr. Sci. 378 (2011) 398-406.

65. C. M. Guijt, G. W. Meindersma, T. Reith, A. B. de Haan, Air gap membrane distillation: 2 Model validation and hollow fiber module performance analysis, Sep. Purif. Technol., 43 (2005) 245-255.

66. J. Walton, et al., Solar and waste heat desalination by membrane distillation, College of Engineering University of Texas at El Paso, 2004.

67. J. H. Hanemaaijer, J. W. Van Heuven, Method for the purification of a liquid by membrane distillation, in particular for the production of desalinated water from seawater or brackish water or process water, US Patent 6,716,355 B1.

68. D. Zarkadas and K. K. Sirkar, Solid hollow fiber cooling crystallization, Ind. & Eng. Chem. Res. 43(22) 7163-7180, 2004.

69. L. Song, B. Li, D. Zarkadas, S. Christian, K. K. Sirkar, Poymeric hollow-fiber heat exchangers for thermal desalination processes, Ind. Eng. Chem. Res. 49 (2010) 11961–11977.

70. S. Majumdar, A. K. Guha, K. K. Sirkar, A new liquid membrane technique for gas separation, AIChE J. 34(7) (1988) 1135-1145.

71. A. Sengupta, R. Basu, K. K. Sirkar, Separation of solutes from aqueous solutons by contained liquid membranes. AIChE J. 34 (1988) 1698-1713.

72. M. Sidhoum, S. Majumdar, K. K. Sirkar, An internally staged hollow-fiber permeator for gas separation, AIChE J. 35(5) (1989) 764-774.

73. Z. Yang, A. K. Guha, K. K. Sirkar, Simultaneous and synergistic extraction of cationic and anionic heavy metallic species by a mixed solvent extraction system and a novel contained liquid membrane device, Ind. Eng. Chem. Res. 35 (1996) 4214-4220.

74. A. Sengupta, Degassing a liquid with a membrane contactor, US Patent +6,402,818,2002.